UiT
THE ARCTIC
UNIVERSITY
OF NORWAY

Faculty of Science and Technology
Department of Geology

# Reconstructions of paleoceanography and ice retreat based on benthic foraminifera, stable isotopes and sedimentological investigations from the northwestern Barents Sea south of Nordaustlandet, Svalbard

**Vårin Trælvik Eilertsen**

*Master thesis in Marine Geology and Geophysics (GEO 3900)*
June 2016

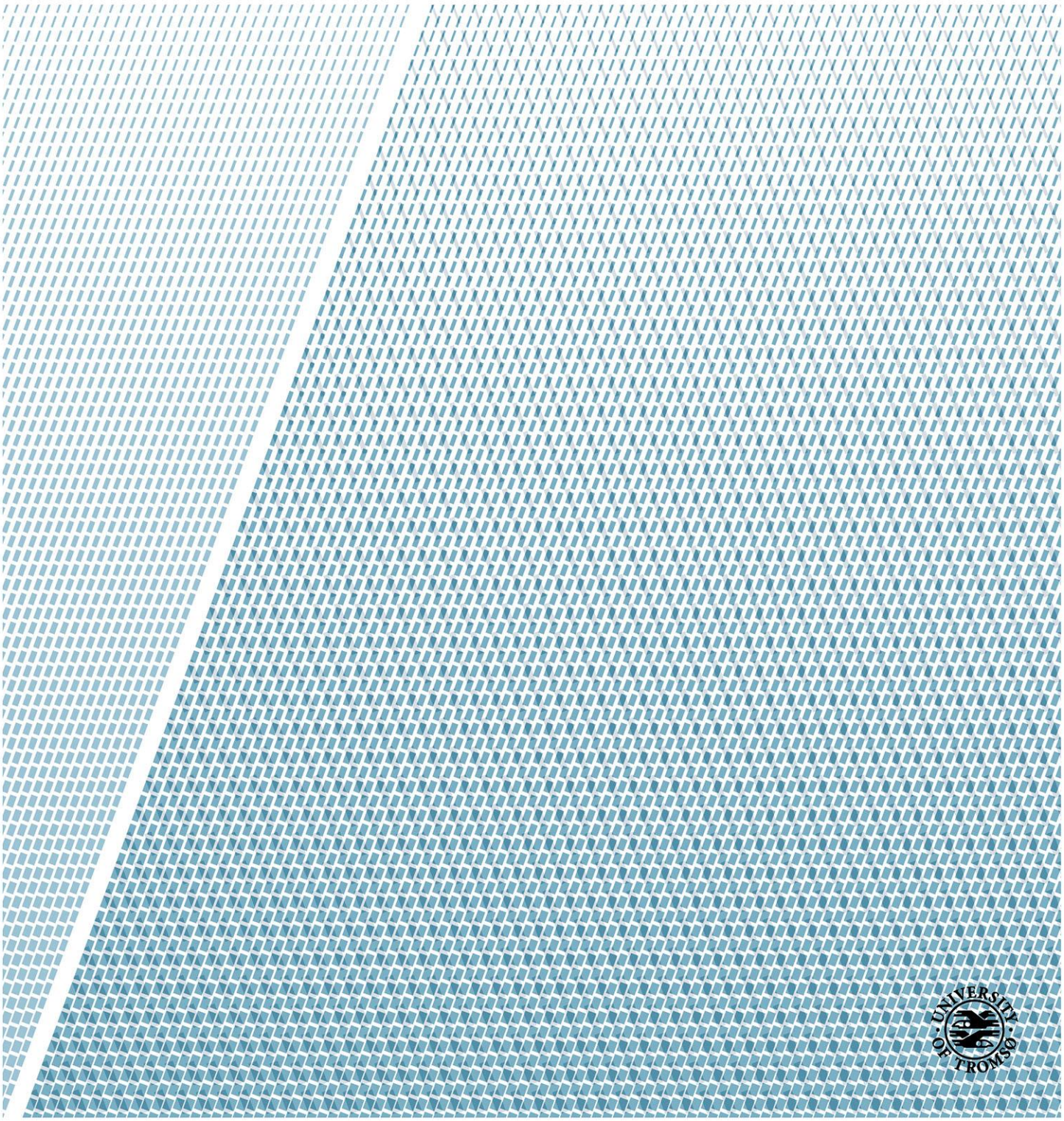

# Abstract

One gracity core NP05–11–49GC was retrieved from a 320 m water depth in the central part of Erik Eriksen Strait, south of Nordaustlandet, northwestern Barents Sea. The core was investigated for benthic foraminiferal distribution patterns, stable isotopes and sedimentological parameters in order to reconstruct the Late Weichselian deglaciation and Holocene paleoenvironment and paleoceanography of the Erik Eriksen Strait. Two additional cores, NP05–11–84GC2 from southwestern Erik Eriksen Strait and NP05–11–51GC2 from the southern head of the Kvitøya Trough, were investigated for sedimentological parameters. The results show that the deglaciation of the Erik Eriksen Strait and Kvitøya Trough was rapid and commenced at 14 100 cal. yr BP. This resulted in the deposition of loose diamicts due to heavy rainout of IRD from released icebergs of the retreating Svalbard-Barents Sea Ice Sheet (SBIS). Continued melting of the SBIS during the Bølling– Allerød interstadials between 14 100 and 12 700 cal. yr BP occurred through the release of sediment-laden meltwater plumes resulting in deposition of laminated sediments. Harsh glaciomarine conditions with increased sea ice cover characterized the Younger Dryas cooling (12 700 –11 950 cal. yr BP). Occasional ice rafting shows that the Erik Eriksen Strait also experienced periods with seasonally open waters during the cooling. The transition to the Early Holocene warming happened in two steps between 11 960 – 11 290 and 11 020 – 10 750 cal yr. BP, interrupted by the Pre-Boreal Oscillation. The glacio-isostatically suppressed sea floor caused an over-deepening of the area and a deeper paleo sea level. Strong inflow of subsurface Atlantic water caused an amelioration of the environmental conditions and very high biological activity. A relatively cool Early Holocene Climatic Optimum characterized the foraminiferal fauna of the Erik Eriksen Strait, which reflected that the east-west climatic gradient observed today also existed in the Early Holocene. An abrupt cooling, along with a decrease of salinity showed a weakening of the Atlantic water inflow at 8300 cal. yr BP until 7600 cal. yr BP. Thereafter, a deterioration of the environment occurred with a stronger dominance of Arctic waters and increased ice rafting. The study show that the high isostatically rebound of the area have affected the inflow of Atlantic water to the northwestern Barents Sea corner and must be considered when reconstructing the areas paleooceanography. The data from Erik Eriksen Strait generally display regional changes that are correlative with studies from the Svalbard-Barents Sea

area. It suggests that an east-west climatic gradient, similar to today, existed between eastern and western Svalbard in the Early Holocene.

# Forord

Først vil jeg rette en stor takk til min hovedveileder Tine Lander Rasmussen som har vært tålmodig og latt meg bruke den tiden jeg trengte. Takk for oppmuntring og at du alltid har vært behjelpelig. Jeg må også takke mine to biveiledere, Liv Plassen og Matthias Forwick, som kom med gode innspill og hjelp.

Takk til damene på laben, Ingvild Hald, Trine Dahl, Karina Monsen og Edel Ellingsen, som alltid var behjelpelig og svarte på alle mulige store og små spørsmål jeg måtte komme med. Takk til Jan P for hjelp til laging av kart

Tusen takk til mine medstudenter og venner som jeg har vært så heldig å bli kjent med gjennom disse årene. Særlig til Carine tag-along Johansen som hjalp meg på laben, og Malin som gav meg en innføring i corel draw. Og ellers bare for at dere er så fine. Tusen takk til snille Mona for støtte og oppmuntring.

Tusen takk Johannes, for din støtte og hjelp med til tider uforståelige matlab. Takk for at du gjorde den siste innspurten mye lettere.

Den aller største takken går til min kjære familie. Mange vil nok si at støtte fra familien er veldig viktig under en mastergradsarbeide, men min mastergrad hadde det aldri blitt noe av uten støtte fra familien min. Kjære mamma, pappa og Venil. Takk for alt dere har gjort for meg over disse årene, og for at jeg nå endelig kan fullføre. Jeg er glad i dere.

Vårin Trælvik Eilertsen

# Table of contents

# 1. Introduction

## 1.1. Objectives

This M. Sc thesis was carried out at the Department of Geology at the University of Tromsø, The Arctic University of Norway, from August 2014 to June 2016. Three gravity cores along with acoustic data from the Erik Eriksen Strait and Kvitøya Trough, Eastern Svalbard, was analyzed and described. The main objectives of this thesis is to take use of marine geological, biological, physical and sedimentological proxies to

1. describe and interpret the benthic foraminiferal assemblages, sedimentary processes and sea floor morphology characterizing the studied area
2. reconstruct the Late Weichselian deglaciation and Holocene paleoenvironment and paleooceanography
3. relate the results to and discuss the causes and rate of climatic and ocean circulation changes in the Erik Eriksen Strait and Kvitøya Trough

## 1.2. Background

The marine and terrestrial record of Eastern Svalbard is scarce and little studied due to an extensive sea ice cover prohibiting access to the area, and a general remote location (Solheim, 1991). The shortage of high-resolution data and well-dated records makes this an interesting area to study to get a better understanding of the glacial activity and paleoenvironment during the Late Weichselian glacial and Holocene interglacial (Kristensen et al., 2013). The lack of larger landmasses in the area, gives the sea floor and the marine record an important role in the goal to acquire this understanding (Dowdeswell et al., 2010).

A strait is a narrow water-way that connects larger bodies of water. During the last glacial, the northwestern corner of the Svalbard-Barents Sea Ice sheet covered the Erik Eriksen Strait and Kvitøya Trough. The strait and the trough functioned as a transportation pathway for ice towards the shelf edge (Dowdeswell et al., 2010; Hogan et al., 2010 a,b, Kristensen et al., 2013). Erik Eriksen Strait and Kvitøya Trough is located close to the northwestern edge of the previous ice sheet (Figure 1.1). The Kvitøya Trough is the northeast continuation of the Erik Eriksen Strait, separated by a shallow sill. The larger St. Anna- and Franz Victoria Troughs are situated further northeast. Hence, the sea floor morphology and lithostratigraphy of the study

area is indicative of the grade of glacier transportation confined to the strait and trough, and the glacial and sedimentary processes taking place during this transport. This can be set in conjunction and compared to other studies from the nearby troughs (Hald et al., 1999; Duplessey et al., 2001, Hogan et al., 2010 a, b; Kristensen et al., 2013).

The study areas proximal location to the edge of the former ice sheet permits a possibility to find the position and extent of the ice sheet margin during the last glacial maximum and deglaciation. An ice dome of the Svalbard- Barents Sea Ice Sheet has been discussed to be located in the study area during the last glacial. The high isostatic rebound of Kong Karls Land, south of Erik Eriksen Strait, indicates an ice dome centered over the archipelago (Salvigsen et al., 1981; 1995; Ingolfsson et al., 1995; Landvik et al., 1998; Forman et al., 1995; 2004). However, new studies of the seafloor suggest a location of the dome further northwest in the southern part of the Hinlopen strait. The absence of landmasses in the area makes the exact pinpointing of the location of the dome difficult (Dowdeswell et al., 2010; Hogan et al., 2010b).

The heat transport to the Svalbard region is very sensitive to changes in both air masses and ocean currents and circulation (Isaksson et al., 2005). Changes in these parameters have been the driving factors behind climatic variations, and hence the buildup and decay of glaciers and the distribution of water masses surrounding the archipelago (Ślubowska-Woldengen et al., 2005; 2008; Schlichtholz & Goszczko, 2006). The build-up and decline of the Svalbard Barents Sea Ice Sheet during the last glacial maximum changed the oceanographic setting. Eastern Svalbard is at present characterized by Arctic surface waters, while the western side is more affected by warm Atlantic water (Gammelsrød et al., 2009). Changes in the distribution of cold and warm surface currents affect the extent of glaciers and ice caps (Ślubowska-Woldengen et al., 2007; Kristensen et al., 2013). A study of the Eastern Svalbard record is important to get an understanding of the relations between glacier growth, changes in ocean circulation and the climate variability in the past. This will give an improved knowledge of the growth and decay of the ice sheet during the last deglaciation in relation with ocean circulation (Kristensen et al., 2013).

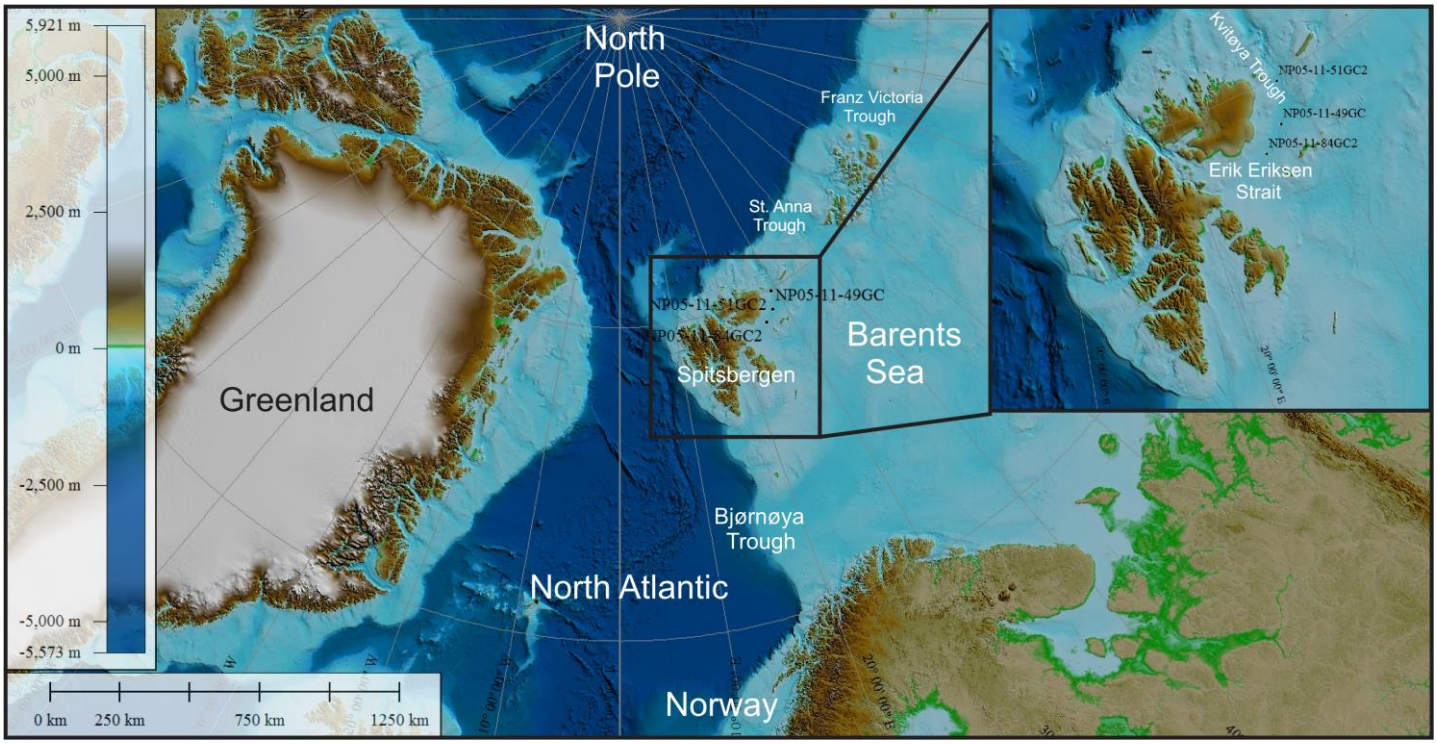


**Figure 1.1:** Overview map of the Arctic region with Svalbard and the study area within black box in right corner. Retrieved cores from Erik Eriksen Strait and Kvitøya Trough are marked by black dots.

### 1.2.1 Glacial history and paleoclimate of the Svalbard-Barents Sea area

Several glaciations have led to an ice sheet build-up across the Svalbard archipelago and the Barents Sea (Mangerud et al., 1992; Elverhøi et al., 1995; Andersen et al., 1996; Mangerud et al., 1998). Advances and retreats of the ice sheet over the last 30 000 years is connected to the flow of Atlantic and Polar water over the Svalbard margin (Jessen et al., 2010).

#### 1.2.1.1 Late Weichselian

During the Late Weichselian glaciation and isotope stage 2, the Svalbard-Barents Sea Ice sheet (SBIS) covered Svalbard and reached out to the continental shelf west and north of Svalbard and across the Barents Sea (Mangerud et al., 1992; Elverhøi et al., 1995; Andersen et al., 1996; Mangerud et al., 1998; Kleiber et al., 2000). Late Weicselian glaciomarine deposits are found over most of the seafloor of the Barents Sea (Landvik et al., 1998). Isostatic modelling suggest a 2000 – 3000 m thick ice sheet and a major ice dome with a center of post-glacial uplift located on southern Hinlopen Strait, easternmost Spitsbergen or between Nordaustlandet and Kong Karls Land (Figure 1.2; Ingolfsson et al., 1995; Salvigsen et al., 1995; Landvik et al., 1998; Dowedeswell et al., 2010).

# 1. Introduction

The Svalbard-Barents Sea ice sheet was characterized by ice masses segmented into faster-flowing ice streams separated by slower flowing ice during the Last Glacial Maximum (LGM; 23 000 to 17 000 cal. yr BP; calendar years before present; Landvik et al., 2005; Ottesen et al., 2005; Ottesen & Dowdeswell, 2009; Jessen et al., 2010). The slower flowing areas, referred to as inter-ice stream areas, were fed by a much smaller ice-sheet drainage basin compared to the faster flowing ice streams (Ottesen & Dowdeswell, 2009).

Faster-flowing ice streams have resulted in major troughs forming off the fjord systems like Is-, Kongs-, Van Keul- and Van Mijenfjorden after the deglaciation of Spitsbergen (Landvik et al., 1998, 2005; Ottesen & Dowdeswell, 2009). Sedimentation during the LGM was restricted to submarine trough mouth fans located at the end of faster-flowing ice streams at the shelf edge (Andersen et al., 1996, Landvik et al., 1998; Ottesen et al., 2005). The inflow of Atlantic water to the region was relatively weak during the late glacial, conditions were cold and the deposition of Ice Rafted Debris (IRD) were widespread (Ślubowska-Woldengen et al., 2008; Jessen et al., 2010)

A distinct ice rafted debris pulse, dated to c. 18 000 cal. yr BP in the Franz Victoria Through, reveal the timing of the disintegration of the northern Svalbard Barents Sea Ice Sheet (Kleiber et al., 2000). The deglaciation and retreat of the Svalbard–Barents Sea ice sheet started around c. 20 500 cal. yr BP through massive iceberg discharge and calving within the deeper troughs in the Barents Sea (Andersen et al., 1996; Landvik et al., 1998; Jessen et al., 2010). In addition, large amounts of melt water were released during the retreat which cooled the surface waters and led to a widespread formation of sea-ice. The retreat was characterized by several halts and re-advances that lead to an erosion of shelf banks (Elverhøi et al., 1995; Andersen et al., 1996; Landvik et al., 1998; Mangerud et al., 1998).

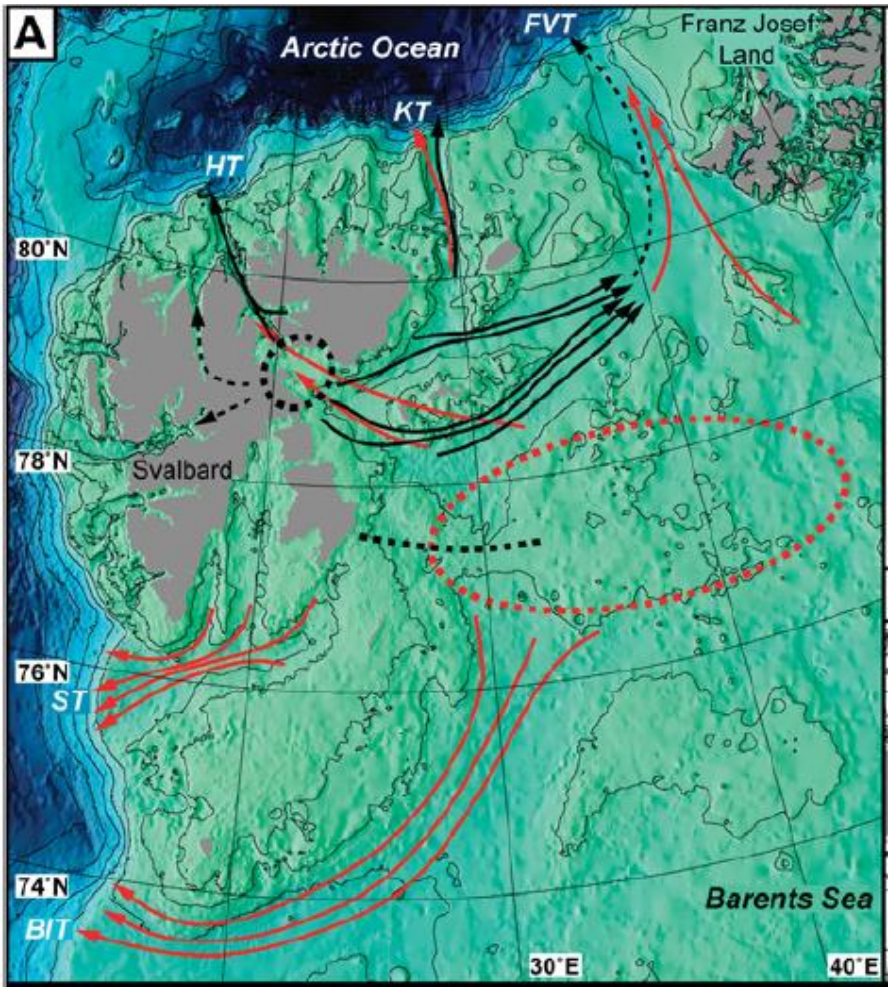


**Figure 1.2:** Reconstruction of ice-sheet drainage pattern and location of Svalbard Barents Sea Ice Sheet domes between Franz Josef Land and Svalbard. Arrows display ice flow. Dotted lines show position of ice domes and ice crest. FVT- Frans Victoria Trough, KT- Kvitøya Trough, HT- Hinlopen Trough, ST- Storfjorden Trough, BIT- Bear Island Trough (From Dowdeswell., 2010).

#### 1.2.1.2 Bølling-Allerød

Bølling–Allerød (14 500 – 13 500 cal. yr BP) is a time that is recorded as warm interstades in the Greenland ice cores (Rasmussen et al., 2007). The period was characterized by a relatively strong inflow of Atlantic Water, however still as a subsurface layer (Figure 1.4). This relatively warm period resulted in a rapid ice sheet retreat into the fjords (Figure 1.3) with turbid meltwater plumes causing a high sedimentation rate, and the deposition of laminated fine clays (Rasmussen et al., 2007; Ślubowska- Woldengen et al., 2008; Jessen et al., 2010). Low amounts of IRD in the Barents Sea and Nordic Seas is recorded for the Bølling–Allerød (Ślubowska- Woldengen et al., 2008).

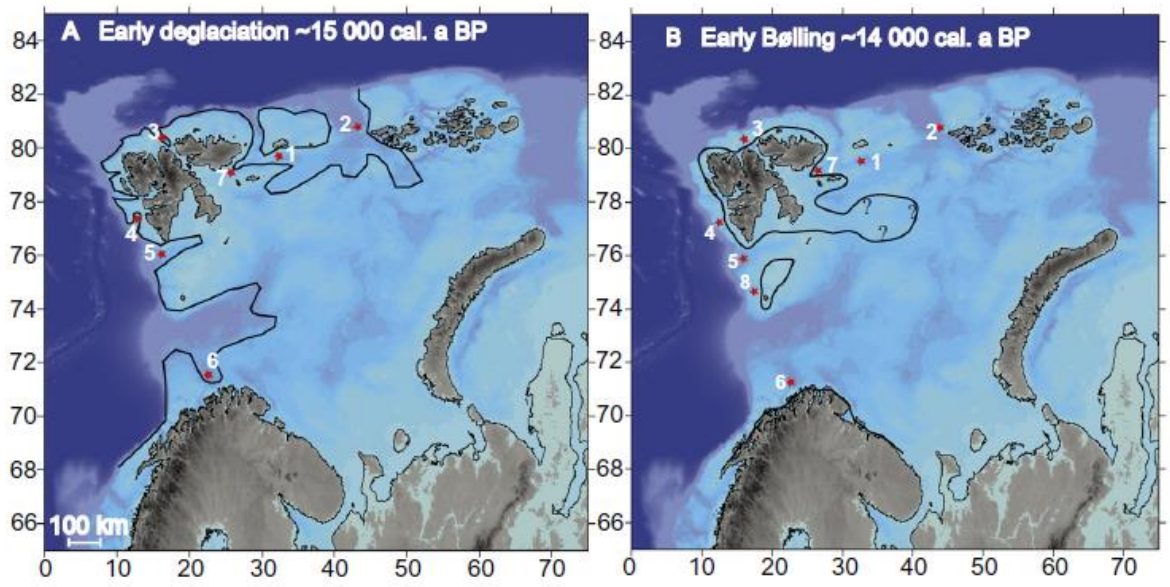


**Figure 1.3:** (**A**) Reconstrucion of the Svalbard region ice-margin extent during the early Deglaciation (c. 15 000 cal. yr BP. (**B**) Reconstruction of ice-margin extent during the early Bølling (c. 14 000 cal. yr BP). Red dots mark the position of cores and obtained data in various studies used for the reconstruction. 1- Kristensen et al. (2013), 2- Lubinski et al. (2001), 3- Koç et al. (2002), Ślubowska-Woldengen et al. (2007), 4-Ślubowska-Woldegen et al. (2007), 6- Aagaard-Sørensen et al. (2010), 7- Hogan et al. (2010a), 8- Rüther et al. (2012) (From Kristensen et al., 2013).

### 1.2.1.3 Younger Dryas

The Younger Dryas (YD; 12 500 – 11 500 cal. yr BP), a period associated with cooling and glacial advances at the end of the Late Weichselian glaciation, has been difficult to identify on Svalbard (Mangerud & Landvik, 2007; Ślubowska- Woldengen et al., 2008; Forwick & Vorren, 2009). In contrast to mainland Europe, glaciers on Spitsbergen were smaller during the Younger Dryas compared the Late Holocene cold event, the Little Ice Age. Starvation of precipitation may have resulted in a retarded or missing glacial re-advance during the Younger Dryas (Mangerud & Landvik, 2007). Proof of reduced iceberg rafting and increased sea-ice formation might be a reflection of this Younger Dryas cooling (Forwick & Vorren, 2009). A record showing stable relative sea level on western Spitsbergen during the Younger Dryas indicates a renewed glacial loading, possibly only in the eastern part of Svalbard or the Barents Sea (Forman et al., 1987, Lehman & Forman, 1992).

The Younger Dryas was also characterized by a reduced inflow of Atlantic water as a subsurface layer, which was fresher and colder compared to the Bølling–Allerød interstades (Figure 1.4; Rasmussen et al., 2007; Ślubowska- Woldengen et al., 2008). Surface conditions

at high latitudes were cold both prior to the period and after, which may cause it to be difficult to detect (Rasmussen et al., 2007).

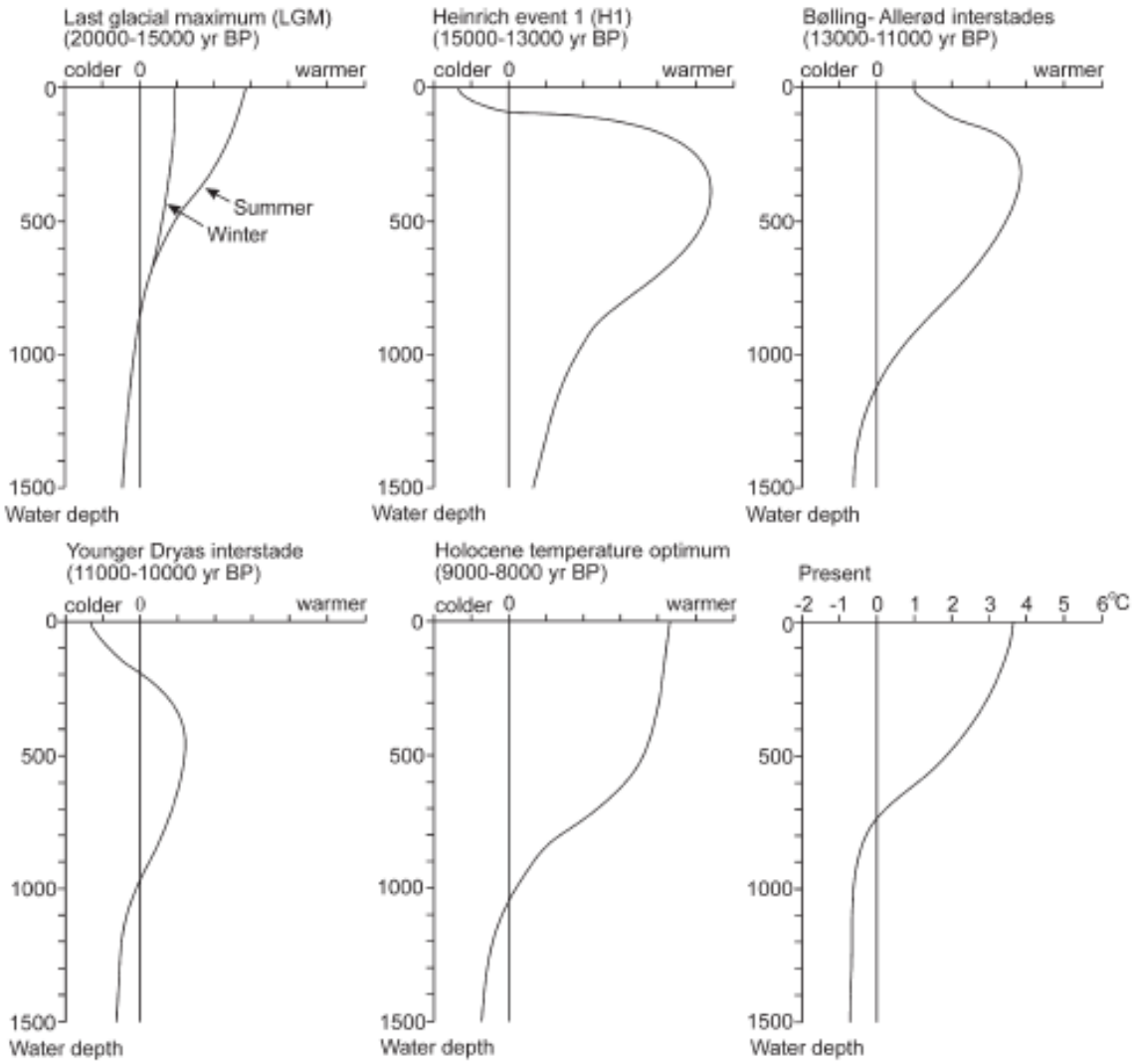


**FIgure 1.4:** Reconstruction of summer sea paleotemperature profiles for the southeastern Svalbard margin based on planktic and benthic foraminifera distribution along with $\delta^{18}O$ values and abundance of IRD for: a-Last Glacial Maximum (LGM), b- Heinrich event H1, c- Bølling–Allerød, d- Younger Dryas, e- Holocene Temperature Optimum (From Rasmussen et al., 2007).

#### 1.2.1.4 Holocene

The Holocene interglacial period followed the cooler Younger Dryas (Ślubowska et al., 2005). Warm and saline Atlantic water reached the coast of Svalbard and the Barents Sea as the ice sheet melted away which contributed to further melting of the remnants of the ice sheet.

Increased solar insulation also contributed the higher temperatures and melting (Ślubowska-Woldengen et al., 2007).

The Holocene is often divided into three intervals, the early-, middle- and late Holocene time intervals (Ślubowska et al., 2005; Ślubowska-Woldengen et al., 2007;2008; Rasmussen et al.,2007; 2012;2014). In this chapter, the dating of the different intervals is taken from Rasmussen et al., (2014).

The Younger Dryas–Holocene transition (11 700 – 10 500 ca. yr BP) was a two- step warming divided by the Preboreal Oscillation (PB; 11 300 – 11 150 cal. yr BP). The Preboreal Oscillation was a cool and humid event characterized by ice re-advances, increased precipitation and a slow-down of the themohaline circulation (Björck et al., 1997; Ślubowska et al., 2005; Rasmussen et al., 2007). The warming was first recorded in the benthic environment, before the planktic environment also reflected surface warming and the retreat of polar waters (Rasmussen et al., 2007). A deterioration of the climate by the return of the Polar Front, related to the Preboreal Oscillation, was observed in the Hinlopen Strait north of the Erik Eriksen Strait (Koç et al., 2002).

The early Holocene (10 500 – 8200 cal. yr BP) was characterized by an average of 2.5 °C warmer temperatures during summer north of 70 °N, due to an 8 % higher summer solar insulation at 80°C N, compared to today (Kutzbach & Guetter, 1986; Svendsen & Mangerud, 1997). This warming with a significantly warmer climate than at present is widely registered along the Norwegian coast and the western Barents slope and is referred to as the Holocene Climatic Optimum (Figure 1.4; Svendsen & Mangerud, 1997; Ślubowska- Woldengen et al., 2007). Sea surface temperatures (SST) in the western Barents Sea were possibly 4 °C higher that today (Santhein et al., 2003b). There was a strong inflow of saline and chilled Atlantic Water along the western and northern shelves of Svalbard and the northern Barents Sea shelf (Ślubowska-Woldengen et al., 2008). The Arctic front was located close to the western Svalbard shelf and the Polar front close to the northern shelf (Ślubowska-Woldengen et al., 2008). An increase of Atlantic Water is seen by the increase of the abundance of benthic foraminifera and the decrease of IRD to a minimum, which points to a higher organic productivity and a further glacier front retreat (Ślubowska-Woldengen et al., 2008; Rasmussen et al., 2014). Bottom

water temperatures increased on the northern North Sea shelf (Kristensen et al., 2001). The IRD count was mostly low throughout the Holocene (Dowdeswell, 1989). However, a pronounced peak implying increased ice rafting due to the collapse of the northern Svalbard-Barents Sea ice sheet is observed around 10 000 cal. yr BP (Landvik et al., 1998; Duplessey et al., 2001; Ślubowska et al., 2005). After the Holocene temperature optimum, a gradual cooling followed into and through the middle and late Holocene (Koç et al., 2002; Ślubowska et al., 2005; Rasmussen et al., 2007).

The middle Holocene (c. 8200–4000 cal. yr BP) was characterized by conditions approaching modern and harsher conditions with more extensive sea ice. The abundance and diversity of benthic foraminifera decreased (Rasmussen et al., 2007; Kristensen et al., 2013). Several studies from the Svalbard - Barents Sea show a cold event around 8 200 cal. yr BP suggested to have been triggered by a discharge of water from ice-dammed Northern American lakes (Duplessey et al., 2001; Hald & Korsun 2008; Kristensen et al., 2013). The amount of IRD was low, which suggest reduced glacier cover and hence ice rafting (Ślubowska-Woldengen et al., 2008). Northern Norwegian fjords showed a development from ice-distal to more ice-proximal conditions in the middle Holocene (Hald & Korsun, 1997).

The late Holocene (c. 4000 cal yr BP – to present) was characterized by further cooling of the Svalbard – Barents Sea area and glacier growth (Svendsen & Mangerud, et al., 1997). The foraminiferal record became more heterogeneous (Ślubowska et al., 2005). A cooling and freshening of the bottom waters, suggesting a decrease in the inflow of Atlantic water, was recorded in the St. Anna Trough (Hald et al., 1999). The concentration of IRD increased, which is indicative of advance of glaciers (Rasmussen et al., 2007; 2014). The last 1100 years of the northern Svalbard margin was more environmentally unstable with an inflow of Atlantic bottom waters and a decrease in IRD (Ślubowska et al., 2005). Glacier growth in central Spitsbergen culminated 500 cal. yr BP during the cold event the Little Ice Age (Svendsen & Mangerud, 1997).

### 1.2.2 Previous studies

Submarine landforms in the Kvitøya Through, located between Nordaustlandet and the Franz Victoria Through east of Spitsbergen (Figure 1.1), was described by Hogan et al. (2010a). Detection of streamlined landforms indicated warm based glacial activity, probably during the glacial peak when the Svalbard - Barents Sea ice sheet extended all the way out to the shelf edge. Meltwater channels and channel cavity system incised into bedrock were found, which was indicative of the presence of melt water during the last glaciation. There was little evidence of still stands during ice retreat. This, in addition to many iceberg scours, indicated a rapid retreat mainly caused by calving. Hogan et al. (2010) concluded that the Kvitøya Through was submerged by a warm based ice stream during the Late Weichselian glacial peak. This ice stream was probably small due to the fact that most of the ice was led into the much larger Franz Victoria Through further east.

Another article from Hogan et al. (2010b) published results from a submarine survey of the seafloor surrounding Kong Karls Land. Three troughs were studied: Olga Strait, Erik Eriksen Strait and an unnamed deep northeast of Kong Karls Land Streamlined landforms and subglacial till evidenced that grounded ice from the Svalbard Barents Sea ice sheet overrun the area during the Late Weichselian glaciation (Figure 1.5). Small still-stands or re-advances indicated by recessional moraines were observed. Laminated mud deposited from meltwater plumes suggested meltwater-derived ice loss, in addition to iceberg discharge in the transition from glacial to interglacial conditions.

Unconsolidated glaciomarine sediments found by Kristensen et al. (2013) indicated an ice sheet margin located west of the Kvitøya Trough. Kristensen et al. (2013) found that the retreat was rapid and sediment-laden plumes resulted in the deposition of a fine grained, laminated layer. The foraminiferal record from marine cores taken in the unnamed trough northeast of Kong Karls Land by Kristensen et al. (2013) revealed a start of strong inflow at c. 14 600 cal. yr BP of relatively warm Atlantic water during the Bølling-Allerød interstadials (Figure 1.3). Reduced inflow occurred in the Younger Dryas, during the Holocene between

8600 and 7600 cal. yr BP and after c. 6000 cal. yr BP. The inflow increased significantly between 11 000 and 6000 cal. yr BP. The Younger Dryas also showed a heavy sea ice cover.

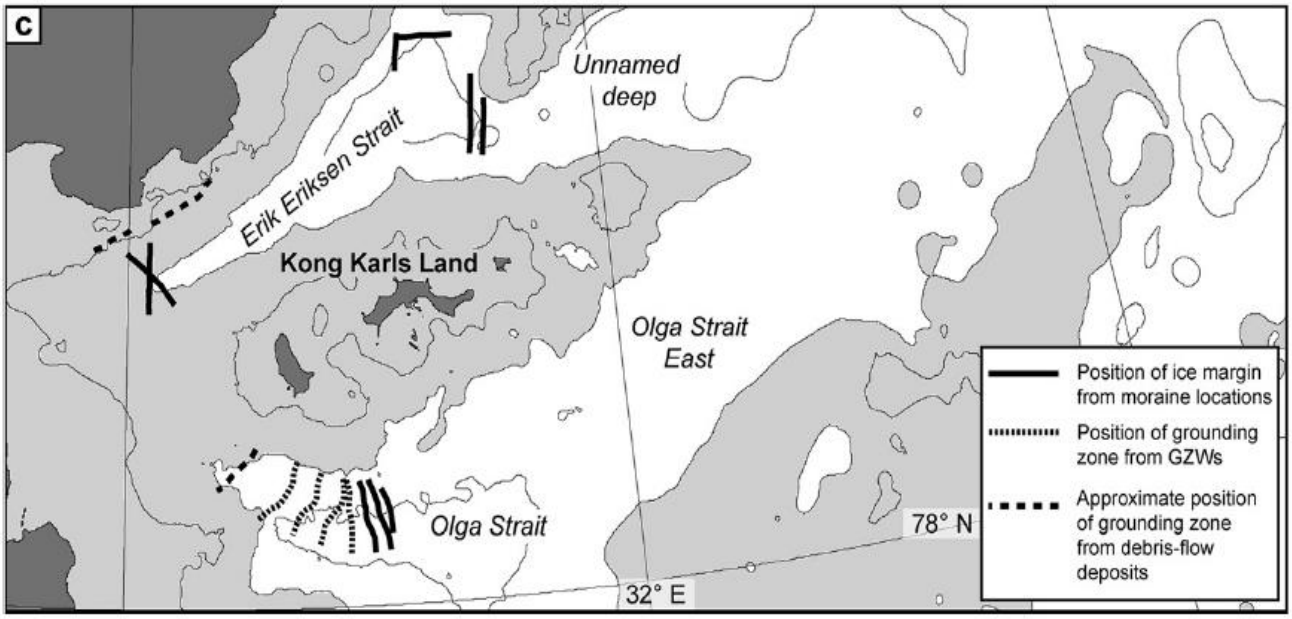


**Figure 1.5:** Location of Grounding zone wedges, ice margins and debris flow deposits in grounding zones in Erik Eriksen Strait, Olga Strait and Unnamed deep (From Hogan et al., 2010b).

# 1. Introduction

# 2. Study area

## 2.1 Physiographic setting

The Svalbard archipelago is situated in the high Arctic between the Norwegian, Greenland, Arctic and Barents Sea (74°N- 81°N and 10°E-35°E (Figure 2.1). Spitsbergen, the largest island, comprise over half of Svalbard's total area. It is characterized by mountain ranges with summits reaching 1000 m above sea level, strandflats, glacially eroded sounds, fjords and cross-shelf troughs (Landvik et al., 2003). Other large islands are Nordaustlandet, Edgeøya, Barentsøya, Kvitløya, Kong Karls Land, Hopen and Bjørnøya.

The Erik Eriksen Strait (78°80'N – 79°86'N and 23°44'E – 30°36'E) is a SE-NW oriented waterway located west of Spitsbergen. The strait is found in the northwest corner of the epicontinental Barents Sea, which is one of the widest and broadest continental shelves in the world. It is bounded between Svenskøya and Abeløya on Kong Karls Land in the south and Bråsvellbreen and Italiaodden on Nordaustlandet in the north (Figure 2.1). The strait is approximately 130 km long, between 60 and 100 km wide and have a present-day water depth of up to 400 m (Hogan et al., 2010b).

North of the southern end of the strait lies the NW- SE oriented Hinlopen Strait with a sill boardering the Erik Eriksen Strait (Solheim, 1991). The islands Edgeøya and Barentsøya are situated southwest of the strait. A sill at the south end of the Kvitøya trough boarders the Erik Eriksen strait's northeast corner. Further south, the strait continues eastwards into another unnamed trough flanked by Abeløya and Kvitøya (Hogan et al., 2010b). South of Kong Karls Land lies the SE-NW oriented Olga Strait. The unnamed trough and the Olga Strait consolidate into another deep depression and continue northeast in to the Franz Victoria Trough. Shallow banks, with typical water depths of 50 – 150 m, separate the troughs (Hogan et al., 2010b).


**Figure 2.1:** Map of the Svalbard archipelago and the investigated Erik Eriksen Strait and Kvitøya Trough. Retrieved cores are marked in red (Map modified from npolar.no).

## 2.2 Geomorphology

Glaciations during the Quarternary have caused a build-up and decline of ice sheets. This activity is responsible for major erosion and transport of sediment to the continental shelf break and slope (Vorren et al., 1989; Dowdeswell et al., 1998). The seafloor sediment record

and features is indicative of the dimensions and dynamics of ice sheets after they have withdrawn to their interglacial position (Ottesen & Dowdeswell, 2009).

Until now, the focus of study has mainly evolved around the faster-flowing ice streams, resulting in troughs after deglaciation, and the areas between, referred to as inter-ice stream areas, has been studied less (Ottesen & Dowdeswell, 2009). A study from the northwestern most part of Svalbard concludes that the seafloor on continental shelves located in an inter-ice stream area have landforms oriented mainly transverse to the ice flow of the ice sheet. Which differentiate from areas influenced by faster flowing ice streams, where the landforms are oriented in the same direction as the ice flow (Figure 2.2; Ottesen & Dowdeswell, 2009).

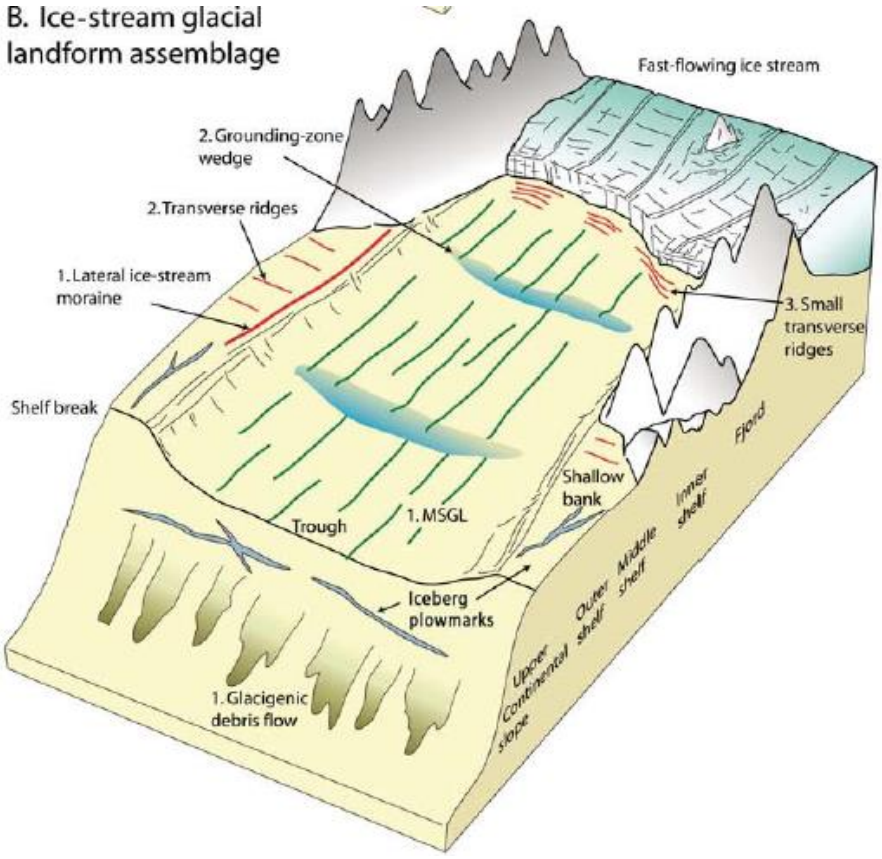


**Figure 2.2:** Typical landforms formed by a glacial ice- stream (Ottesen & Dowdeswell, 2009).

Geomorphic features were studied on the seafloor of the Erik Eriksen Strait and described in Hogan et al (2010b). No features, except iceberg scours, were found below 215 m water

depth. The southern part of the trough had lineations oriented in a NW-SE direction. Overriding them were W-E oriented lineations interpreted to be Mega Scale Glacial Lineation (MSGL). MSGL are curvilinear submarine features elongated in the direction of the long axis of troughs. They are the result of the deformation by fast flowing ice on soft-sediment (Ottesen et al., 2007). A pair of low relief drumlins were found overlying dome-shaped grounding-zone features. Smoothened seafloor with a subtle sinous character and transverse ridges were also observed in the southern part. The deepest part of the strait, found south of the sill separating the Kvitøya Trough from Erik Eriksen Strait, were characterized by transverse ridges on the flanks and the absence of MSGL. Hill-hole pairs, related to glacitectonic trusting under grounded ice, and channels interpreted to have been eroded by subglacial meltwater, were also found in the northern part of the trough. Multiple lobe formed deposits, interpreted to be debris flow deposits, overlay other features and were interpreted to be deposited after glacial retreat. A surface drape of up to 4 m, interpreted to be of Holocene age, were observed overlying the features throughout the trough. The drape was interpreted to be the result of settling suspended sediments in a distal glacimarine environment.

## 2.3 Bedrock geology

Outcrops on Kong Karls Land, south of the Erik Eriksen Strait (Figure 2.3), reveal a bedrock composed of Late Triassic and Early Cretaceous clastics and limestones, which is overlain by Tertiary basaltic lavas and terrestrial sediments (Solheim, 1991). North of the strait, the southern part of Nordaustlandet, the bedrock is made up by Early Palaeozoic limestones and dolomitic limestones with a high chert content and silicified sediments (Antonsen et al., 1991). The boundary between the Early Paleozoic carbonates on southern Nordaustlandet and the Late Triassic and Early Creataceous clastic rocks and limestones on Kong Karls Land is hypothetically placed along the central part of the Erik Eriksen Strait (Antonsen et al., 1991; Solheim, 1991). The area close to Kvitøya comprises crystalline rocks of the Hekla Hoek Formation (Antonsen et al., 1991).

West of the study area, on Barentsøya and Edgeøya, the bedrock consists of Triassic and Early Jurassic poorly consolidated shales, siltstones and sandstones (Solheim, 1991; Salvigsen et al.,

1995). Outcropping of Triassic clastic rocks and Mesozoic doleritic intrusions are found northwest of the study area on Olav V Land and on Wilhelmøya and Kiepertøya in the Hinlopen Strait (Solheim, 1991). The Olga basin and the Storbanken high southeast of Kong Karls Land consists mainly of late Jurassic to early Cretaceous sandstones (Antonsen et al., 1991).

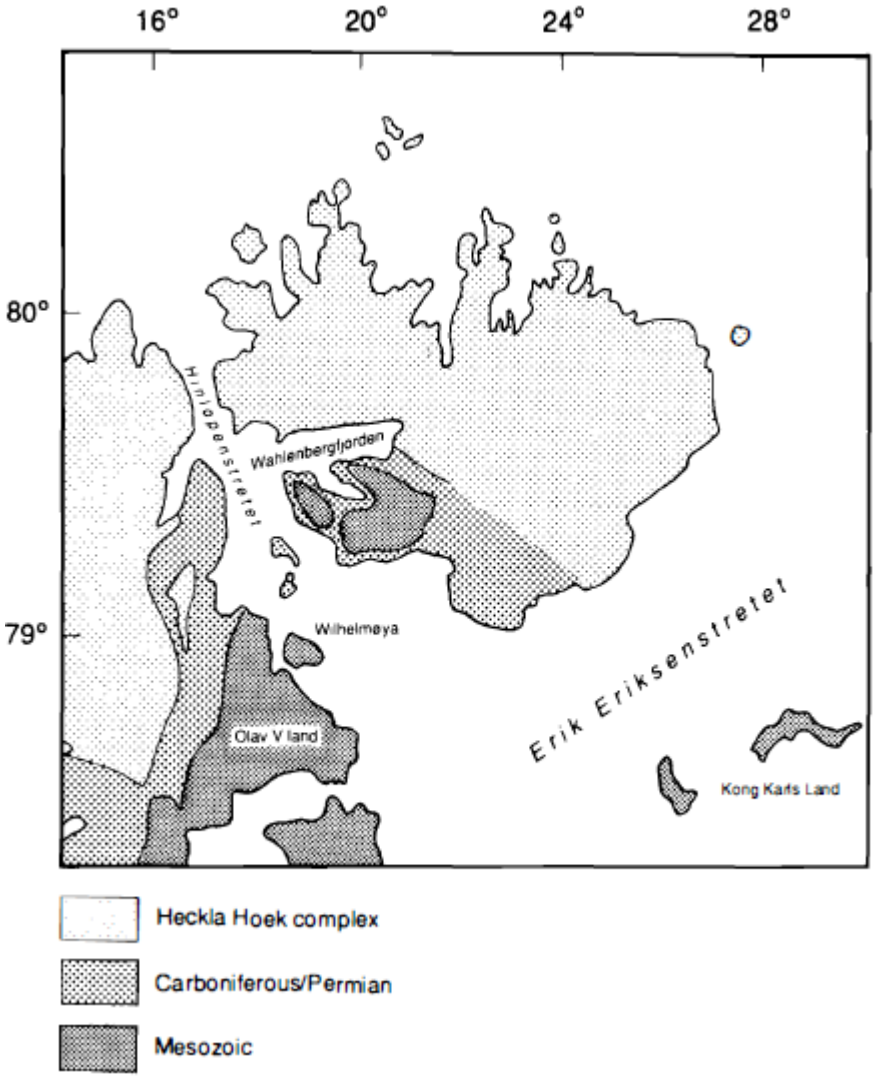


**Figure 2.3:** Bedrock geology of Nordaustlandet, Kong Karls Land and Eastern Spitsbergen (Solheim, 1991).

## 2.4 Oceanography

The thermohaline circulation is mainly driven by the water masses' differences in density caused by temperature and salinity differences (Broecker, 1991). Mainly three types of water masses determine the physical conditions of the ocean surrounding Svalbard: Coastal water, Arctic water and Atlantic water (Figure 2.4; Loeng, 1991).

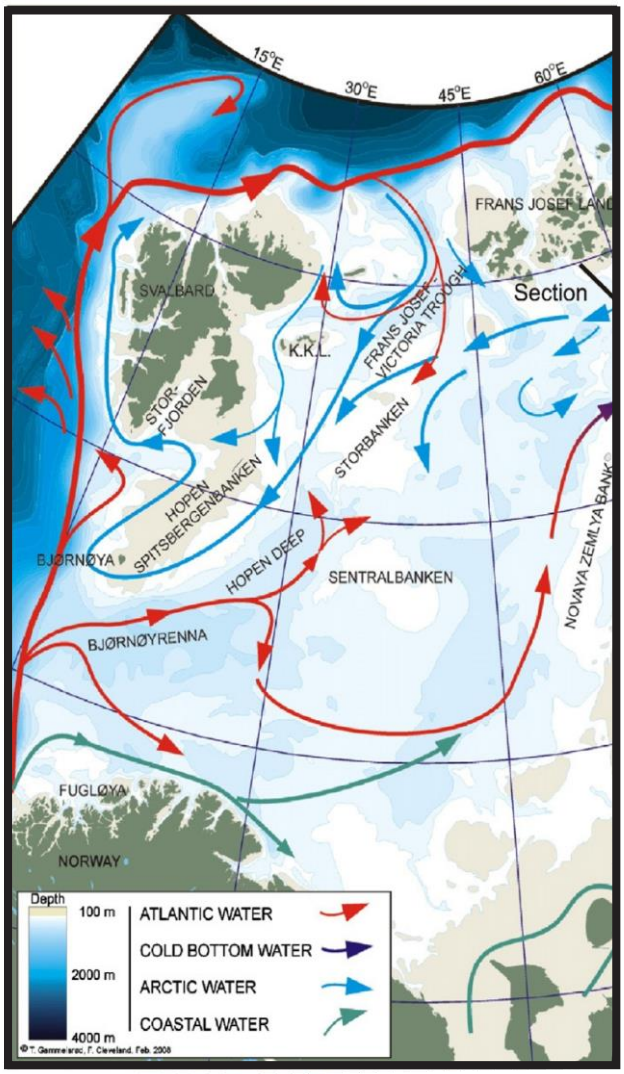


**Figure 2.4:** Current system of the Barents Sea and Svalbard margin. Dark blue represent the deepest water masses. Red is 2nd from bottom. Green is 3rd from bottom. Light blue is closest to the surface (modified from Gammelsrød et al. 2009).

The relatively warm and saline Atlantic water, called the Atlantic Layer, has a temperature >2°C and salinity >34.9 psu. It is transported into the Nordic and Barents Seas by the North Atlantic Current and is considered an important source for heath and salt to the Arctic Ocean (Schlichtholz & Goszczko, 2006). The North Atlantic Current transports the Atlantic Water northward mainly along the Norwegian coast as the Norwegian Atlantic Current (Ślubowska-Woldengen et al., 2007).

The Atlantic Layer is found as surface and bottom layers of the water column at water depths of 50–500 m at the western and northern Svalbard slope (Koç et al., 2002) and at 120–200 m depths of the Barents Sea (Duplessy et al., 2001). One branch of the Norwegian Atlantic Current flows into the Barents Sea as the North Cape Current. The Atlantic water enters the Barents Sea via the Barents Sea Opening between Fugløya and Bjørnøya. It is effectively modified by cooling and mixing, and loses heat on its way to the Arctic Ocean (Drange et al., 2005; Gammelsrød et al., 2009). The northern extension of the North Atlantic Current follows the bathymetry of the Eurasian continental plate and is named the West Spitsbergen Current (Aagaard et al., 1975; Ślubowska-Woldengen et al., 2007). The current flows north along the western and northern Svalbard slope and provides the Svalbard region with warm and saline Atlantic water (Broecker, 1991; Ślubowska et al., 2005; Rasmussen et al., 2007). As the warm Atlantic water flows northwards, it loses heat directly to the atmosphere and probably also to the melting of sea ice and mixing with colder surrounding waters. It submerges therefore under less saline and cold Arctic surface water at approximately 78°N, and continues as a subsurface layer confined to the upper part of the continental slope (Aagaard et al., 1975; Saloranta & Haugan, 2004). The current braches into tree subcurrents at approximately 79°, where one, named the Svalbard branch, enters the Arctic Ocean through the Fram Strait, continues around the northern part of Spitsbergen and is guided southward into the Hinlopen trough (Ślubowska- Woldengen et al., 2007).

The east coast of Svalbard is highly affected by the cold and Arctic surface waters from the East Spitsbergen Current (Skogseth et al., 2005). This results in conditions along the northern Barents Sea shelf east of Svalbard, standing in stark conditions to the western side (Gammelsrød et al., 2009). The current flows around the south tip of Spitsbergen and then north along the western Svalbard margin, now named the Coastal Current (Loeng, 1991; Skogseth et al., 2005; Ślubowska- Woldengen et al., 2007).

Atlantic water follows the continental slope and penetrates into the Barents Sea from north via the Franz Victoria and St Anna troughs. It continues west as a subsurface layer and enters the Kvitøya through from the south (Gammelsrød et al., 2009). Cold Polar surface water forms in the Arctic Ocean under the influence of freshwater discharge from Siberian rivers, low solar radiation balance and perennial sea-ice cover (Steinsund et al., 1994). The cold surface waters

also flow in through the troughs and occupies approximately the top 40 m of the water column in the Franz Victoria Trough. The lower part mixes with inflowing Atlantic water which forms a warm and saline intermediate water mass (Duplessey et al., 2001). The bottom of the trough is occupied with outflowing more saline and colder Barents Sea bottom water. This water layer is formed in the Barents Sea and controlled by factors like surface cooling, sea-ice cover, polynia activity and brine formation (Steinsund et al., 1994; Duplessey et al., 2001; Gammelsrød et al., 2009).

The interaction between the Atlantic water brought north by the Norwegian Atlantic Current and Polar derived water creates a strong hydrological front called the Arctic Front (Swift et al., 1986; Loeng, 1991; Steinsund et al., 1994; Piechura & Walczowski, 1995; ). The inflow of Atlantic water controls the position of the Arctic front and the sea-ice limit (Duplessy et al., 2001). The contact zone between Polar and Arctic water is termed the Polar Front (Swift et al., 1986; Piechura & Walczowski, 1995). During colder periods, like the Younger Dryas, the Polar Front retreated northward (Koç et al., 2002; Ślubowska et al., 2005). The most productive areas are associated with the frontal systems and small changes are recorded in the distribution of benthic foraminifera assemblages (Ślubowska-Woldengen et al., 2008). Sea-ice melting during the spring generate nutrition rich water and consequently an algal bloom at the ice edge (Steinsund et al., 1994; Wassmann et al., 1999). In the northern and eastern parts of the Barents Sea, sea-ice is formed. The pack ice extends to 74°N and has its maximum extent in March and April (Hald & Steinsund., 1992).

## 2.5 Climate

The Svalbard archipelago is geographically located in a climatically sensitive area where cold air from the northeast meet warm air masses from the southwest. The variation between mild air arriving from southwest causing relatively high temperatures during winter (Figure 2.6), and a weather type causing cold easterly and northeasterly winds characterize the Svalbard weather (Isaksson et al., 2005). The climate can be termed ‘continental’ in periods of abundant sea ice with cold and dry air, or ‘maritime’ in periods with little sea ice with relatively warm and humid air (Førland et al., 2009). The relatively small land area occupied by the archipelago and its location near the southern limit of polar ice pack and the northernmost branches of

the warm North Atlantic Current causes the Svalbard local climate to be very affected by even small changes in these factors (Humlum et al., 2003).

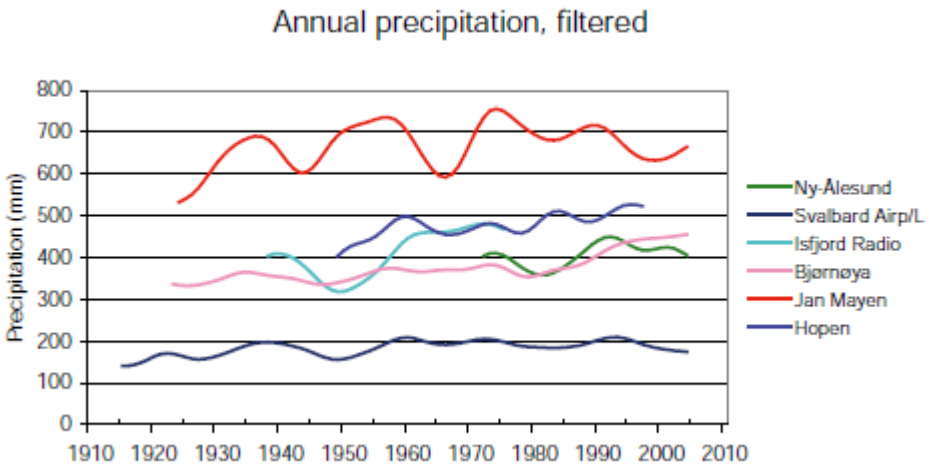


**Figure 2.5:** Annual precipitation at the high-Arctic stations: Ny-Ålesund, Svalbard airport, Isfjord Radio, Bjørnøya, Jan Mayen and Hopen (From Førland et al., 2009).

A temperature gradient of about 2.5°C per degree latitude from south to north exists during the winter. Cold polar air causes the northern and eastern parts of Svalbard to be colder (Isaksson et al., 2005). The annual precipitation of the Svalbard region is low. A northeast-southwest gradient in precipitation exists, with higher values in the southwest, due to the fact that easterly winds brings most of the precipitation that reaches the Svalbard Archipelago (Hisdal, 1998; Førland et al., 2009; Figure 2.5). The climate has changed over the past two decades resulting in a temperature increase of approximately 1°C, glacier and snow cover retreat and permafrost thaw (Comiso & Parkinson, 2004).

## 2.6 Glaciology

At present, 60 % of Svalbard's areal is covered with ice caps and glaciers (Ślubowska et al., 2005). Glaciers growth and size are greatly affected by the temperature and precipitation gradients between east and west on Svalbard (Day et al., 2012). The surrounding islands of the Erik Eriksen Strait are either occupied by glaciers or show evidence of earlier glacier activity. The higher parts of Edgeøya is covered by the ice cap Edgeøyjøkulen with outlet glaciers in surrounding valleys. One tidewater glacier is located on the southeastern shore (Nagy, 1984). An ice cap named Barentsjøkulen covers Barentsøya. The ice cap has several

outlet tidewater glaciers that are known to surge (Dowdeswell & Bamber, 1995). No glaciers exist on Kong Karls Land (Ingólfsson et al., 1995). Nordaustlandet, located north of Erik Eriksen Strait, is covered by an ice cap where Austfonna is the largest glacier. Bråsvellbreen occupies the southern part of Nordaustlandet and boarders the Erik Eriksen Strait. The glacier surged 12–15 km along a 30 km wide front between 1936 and 1938 (Solheim, 1991).

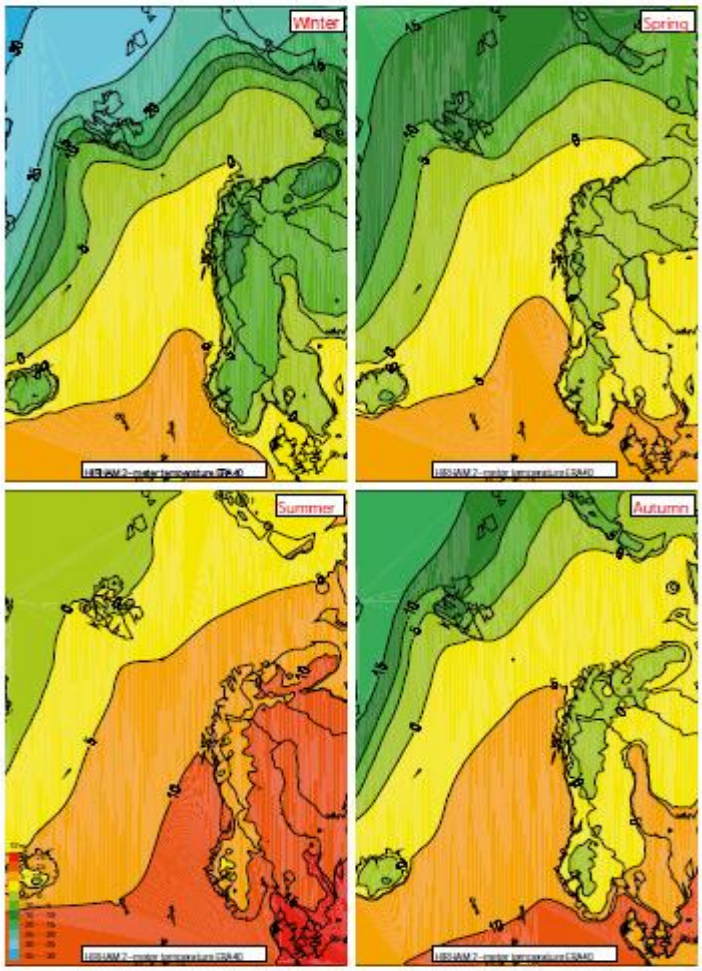


**Figure 2.6:** Mean temperature (°C) over the Nordic sea, Svalbard region and Barents Sea from 1961–2000. Upper left- winter, upper right-spring, lower left-summer and lower right-autumn (from Førland et al., 2009).

# 3. Material and method

Data from core analysis and acoustic data provide the basis for the study. Three gravity cores were taken in a transect from the inner part to the outer part of the Erik Eriksen Strait along with several 3.5 kHz and sparker profiles. The gravity cores were analysed with focus on the 3 m long core NP05-49GC from the central part of the street.

**Table 3.1:** Specifics of studied sediment cores.

| Station/Core | Date | Latitude | Longitude | Water Depth | Length | Type |
|---|---|---|---|---|---|---|
| | | (N) | (E) | (m) | (m) | GC |
| NP05-11/49GC | 17.08.2005 | 79°22,4' N | 27°49,8'E | 320 | 293 | GC |
| NP05-11/51GC2 | 17.08.2005 | 79°55,5' N | 29°05,3'E | 327 | 176 | GC |
| NP05-11-84GC2 | 24.08.2005 | 79°05,25' N | 25°50,1'E | 215 | 231 | GC |

## 3.1. Sediment cores

Three sediment cores were collected in August in 2005 on the NP05–11 cruise to the north-western corner of the Barents Sea by the research vessel of the Norwegian Polar Institute, R/V Lance (Table 3.1). The cores were retrieved with a gravity corer that is used to retrieve long cores of the seafloor sediments.

The gravity corer consists of a steel barrel, core cutter, core catcher and a replaceable plastic liner, with an outer diameter of 11 cm, within the barrel. The steel barrel is 6 metres long and has a 1600 kg weight attached at the top. The core cutter at the bottom enables the barrel to cut into the sediments, while the weight aids the barrel to penetrate the sea floor further. A core catcher is fitted inside the barrel to minimize the loss of sediment once the barrel is elevated with a steel wire. The plastic liner, containing the sediment, is removed from the barrel on deck and cut into 1 m long sections. Each section is labelled and sealed by plastic caps and bags before put into a 4 °C cooled storage room to prohibit drying.

## 3.2. Seismic profiles

High resolution seismic data were acquired during the NP05–11 cruise to the north-western corner of the Barents Sea. The data was collected using a hull-mounted O. R. E penetration echo sounder with a sampling frequency of 10 kHz. Three profiles displaying each of the three core sites were supplied by the Norwegian Polar Institute. The profiles, displaying the subsurface, are included to get an overview of the local subsurface sedimentology (Figure 3.1).

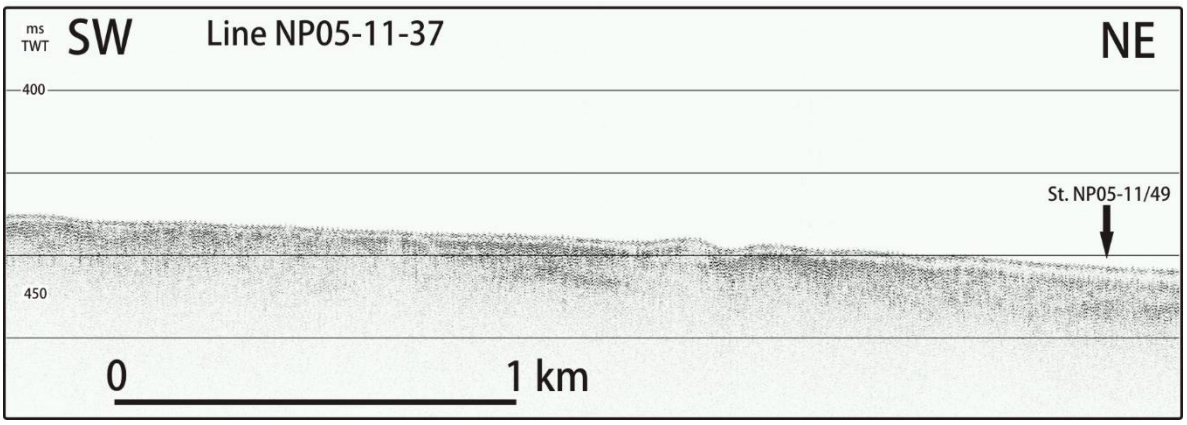


**Figure 3.1:** Seismic profile of line NP05–11–37 from Erik Eriksen Strait displaying location of core NP05–11–49GC by black arrow (for location see Figure 5.1).

## 3.3. CTD

Conductivity-Temperature-Depth (CTD) profiles were retrieved from the core stations during the research cruise. To profile the salinity and temperature of the water column, a probe continuously measures the temperature and conductivity of the water masses as the CTD-instrument is lowered down from the sea surface. The conductivity is later calculated to get the salinity.

## 3.4. Laboratory work

The laboratory work on the three cores were carried out on and off over the course of one year between August 2014 and Jan 2016. Except the measurements of physical properties, which were done in November and December 2005. The work took place in the laboratory of the Geology department of University of Tromsø, The Arctic University of Norway. The

foraminiferal distribution, other physical parameters and grain size analyses and distribution were determined.

### 3.4.1. Physical properties

The physical properties such as magnetic susceptibility, wet bulk density, P-wave velocity and amplitude of the sediment were measured using a GEOTEK Multi Sensor Core Logger (MSCL; Figure 3.2). The MSCL is a versatile core measurement system with the ability to measure multiple parameters simultaneously. Core sections were placed upon a belt and pushed past an array of stationary sensors, which collect data when the core pauses at a measurement point. The properties were measured before opening the core sections.

Complete cores were logged in a continuous process and measurements were taken at spatial intervals of 1 cm with a 10 seconds measuring time. The cores were left in room temperature overnight. This is done as temperature differences can disrupt the measurement and the result of for instance the measured sediment velocity (GEOTEK, 2014a)

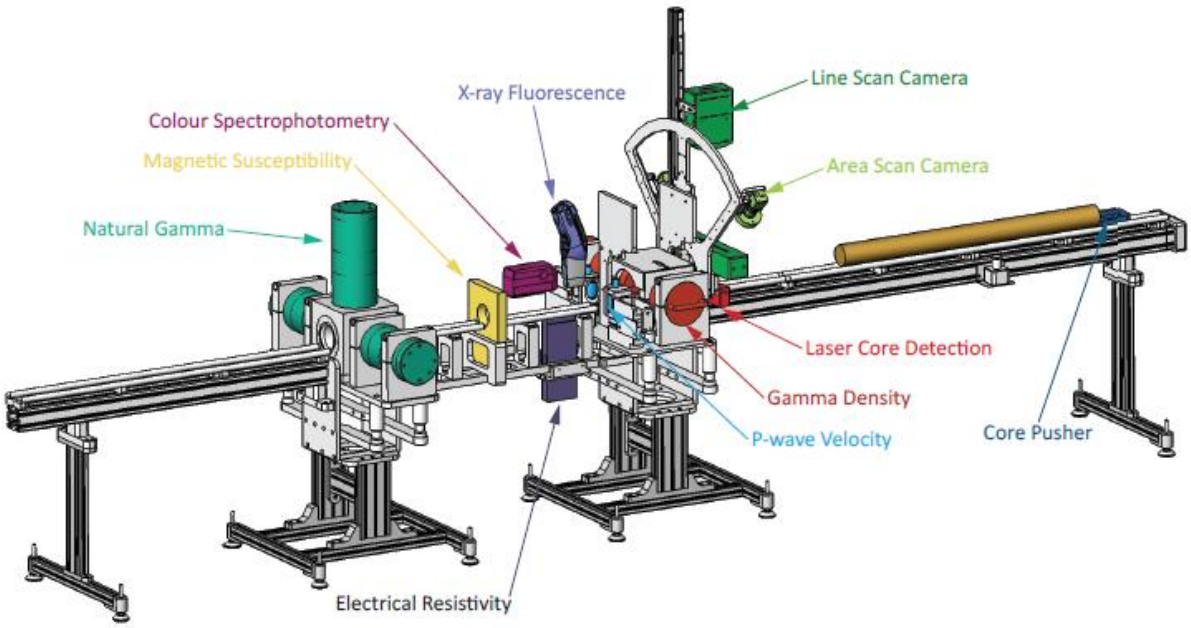


**Figure 3.2** Principal sketch of the GEOTEK Multi Sensor Core Logger (GEOTEK, 2014a).

#### 3.4.1.1. *γ* -ray attenuation (wet-bulk density)

The density of a material is given by the ratio of its mass to its volume. Bulk density is a measurement of how densely packed sediments are, and is defined as the mass of particles of a material divided by the total volume they occupy. The mineral composition of the sediments and the degree of packing affect the bulk density.

A gamma density sensor system mounted on the MSCL is used to detect the bulk density of the core. The gamma source emit a narrow beam of $_{137}$C photons, which pass through the core sections and are detected by detectors on the other side of the core. Electrons in the core cause the photons to scatter with a partial energy loss. Measurement of the number of photons that pass un-attenuated through the core determines the density of the core material. The sediments were wet and the obtained density is therefore the wet bulk density (GEOTEK, 2014a)

Handling can disrupt the degree of packing and hence be a potential factor of error when measuring the bulk density. Poor measurements can also be the result of a core not completely filled with sediment.

#### 3.4.1.2. P-wave velocity

P-waves are longitudinal waves, which compress and dilate the material they propagate through in the direction of propagation. An ultrasonic P-wave system consisting of transducers placed on each side of the MSCL core logger (Figure 3.1) measure the P-wave velocity as the core sections move between the transducers. A transmitter transducer produces an ultrasonic compressional pulse at 230 kHz, which propagates through the core and is detected by a transducer receiver. The distance travelled, the thickness of the core liner and travel time are measured to calculate the P-wave velocity with a resolution of 1.5m/s (GEOTEK, 2014 a).

The P-wave amplitude, which is related to the intensity of the signal, was also measured. Low measurements indicate poor contact between the transducers, liner and sediment (GEOTEK, 2014 a). Water was used to moisturize the liner to ensure direct contact with the transducers.

#### 3.4.1.3. Acoustic impedance and fraction porosity

The product of the P-wave velocity and the wet bulk density can be used to calculate the acoustic impedance with the formula Z=V*p, where Z is the acoustic impedance, V is P-wave velocity and p is density. Porosity can be calculated directly from sediment density when the mineral grain density and the fluid density is known (GEOTEK, 2014a).

#### 3.4.1.4. Magnetic susceptibility

The magnetic susceptibility is how magnetized a material becomes when subjected to a magnetic field. It indicates the magneto-mineral content and can therefore be an indication of the mineralogy and origin of the sediments (Pirrung et al., 2002). The magnetic susceptibility is negative and the field is weakened in the presence of a diamagnetic material. Para-, ferro-, ferri- or antiferromagnetic materials causes a strengthening of the magnetic field and a positive susceptibility (GEOTEK, 2014a).

A Bartington loop sensor (MS2C) mounted on the core logger was used to find the variation of the magnetic susceptibility throughout the cores. The sensor is mounted a part from other instruments to avoid interference from other magnetic or metallic components (Figure 3.1). An oscillator circuit in the loop produces a low intensity magnetic field of 0,565 kHz. The core sections pushed through the loop causes change in the oscillator frequency, which is converted into information about the magnetic susceptibility (GEOTEK, 2014a). The magnetic susceptibility is used to create a time scale for changes in the sedimentary environment and correlation between cores.

### 3.4.2. Sedimentological description and logging

A circular saw, spatula and a thin wire were used to cut the plastic liner and the sediments in the core sections in half, along the long axis of the liner. One part was wrapped and archived in a 4°C cooled storage room. The other was marked ‘work’ before it was logged and sampled.

The sediment surface was cleaned and smoothed with a thin plastic card upon logging. The sections were investigated for approximate grain size and clast distribution, sedimentary structures, clear layers, boundaries, texture, bioturbation, macrofossils and other visible

variations. The Munsell Soil Colour Chart was used to determine colour and name. Lithological logs, created using Corel Draw, with attached colour images present the results (Figure 5.8, 5.11 and 5.13).

### 3.4.3. Grain size analysis

#### 3.4.3.1. Sampling

The core sections marked 'Work' was cut into 1 cm slices and put into pre-weighed plastic bags for counting of foraminifera, IRD and grain size analysis. An osmotic knife and a spatula was used to obtain the sediments. The edges were avoided due to a possible sediment disturbance during the coring process.

#### 3.4.3.2. Freeze-drying

The samples were weighed before they were put into a freezer. The frozen sediment samples were afterwards freeze-dried using the Christ Alpha 1–4 freeze-dryer. This process takes approximately 25 hours, depending on the amount of water. The process of sublimation is considered to be more gentle on the foraminiferal tests as opposed to drying in an oven. The dried samples were again weighed to obtain the water content for each sample.

#### 3.4.3.4. Grain size distribution

The distribution of grain sizes are found by calculating the percentages of the fractions 0–63 µm, 63–100 µm, 100µm – 1 mm and > 1mm to the total sediment volume. The grain size range of each fraction is chosen based on the division used in the GRADISTAT program (Blott & Pye, 2001).

#### 3.4.3.3. Sieving

Three sieves with mesh sizes of 1 mm, 100 µm and 63 µm were used to carefully wet sieve the samples. Distilled water was used to remove the remaining sediments in the sieves into filters. The sieves were carefully cleaned between each sample with running water, a brush and compressed air to avoid contamination. An oven of 40 °C was used for drying. The dried

samples were weighed and put into small glass jars, sealed and labelled. The weight of the samples make up the basis for finding the grain size distribution.

### 3.4.4. Foraminifera analysis

The >100 µm size fraction from core NP05-11-49GC was used to count the distribution of foraminifera. Every other sample was counted between 155 and 185 cm. Every 4$^{th}$ sample was counted in the rest of the core, making up a total of 79 samples. A splitter was used to divide large samples in half or more before picking. The splitter was thoroughly cleaned with compressed air before and after use. The residue from the sieving was evenly distributed over a metal tray with 45 squares. Every foraminifera in a randomly picked square was counted until at least 300 specimens of benthic foraminifera was reached. This is required to get a complete assemblage for statistically comparability between samples (Lowe & Walker, 1997). A collecting tray underneath was used to gather the picked specimens. The binocular microscope Leica CLS 150X - MZ12.5 was used.

A division between calcareous and agglutinated benthic forms was done and the percentages of each form was calculated. The benthic forms was also identified down to species level and the percentages for each species were calculated relative to total foraminifera amount (agglutinated and calcareous specimens) in a sample. Planktonic forms were counted, but not identified.

### 3.4.5. Ice Rafted Debris (IRD)

The amount of IRD was calculated in the > 1.0 mm fraction as number of grains per gram dry weight sediment. The sediments of this fraction was evenly distributed over a picking tray and all the grains were counted underneath a binocular microscope. The lithology of the grains can be used for tracing the origin and source of the IRD and enhance the insight to the processes involved in the IRD transportation (Solheim, 1991; Jessen et al., 2010).

### 3.4.6. X-ray photographs

X-ray photographs were taken of the half core sections using the Philips Macrotank. The photographs are shadow images showing differences in density. Darker areas are low in density, whereas brighter areas are high. Features and structures, unseen to the eye, such as clasts bioturbation, molluscs, boundaries and stratification can be easier to detect when looking at x-rays.

### 3.4.7. Colour photography

A Jai L-107CC 3 CCD RGB Line Scan Camera (70µm resolution) attached to the Avaatech XRF core scanner was used to take colour photography of the different core sections of the archive half of the core. The sediment surfaces were cleaned and smoothened with a thin plastic card prior to photographing. The cores were additionally left in room temperature for a while to enable evaporation of surface water and prevent reflections.

### 3.4.8. Isotope analysis of benthic foraminifera

The oxygen isotope method is used to investigate paleotemperatures of the earth's surface. Estimating the changes in isotopic composition of the oceans is also done to approximate the extent of Northern Hemisphere glaciations (Shackleton, 1974). Variations of $\delta^{18}O$ in benthic foraminifera reflect also hydrological bottom water changes and the temperature, which the foraminifera grew in (Duplessy et al., 2001). The study of foraminiferal assemblages and stable isotopes provide a valuable record of understanding the change of inflow of Atlantic and fresh surface water into the Barents Sea during deglaciation and the Holocene, as water mass changes are likely to be recorded by the foraminiferal species and isotopic compositions (Duplessy et al., 2001).

Stable isotope analysis on oxygen and carbon isotopes was performed on the benthic species *Nonionellina labradorica, Cibicides lobatulus* and *Melonis barleeanus*. The measurements were done in a total of 60 samples in the upper 185 cm of core NP05–11–49GC to create a

stable isotope record for the core. The isotope record was compared with other proxies of the core (see *Discussion and correlations*).

### 3.4.8.1 The sampling

A minimum of seven specimens were picked for each sample under a binocular microscope. *N. labradorica* was sampled between 3 and 75 cm, *M. barleeanus* between 59–169 and *C. lobatulus* between 165–185 cm. An overlap was ensured to achieve a continuous stable isotope record. The samples were weighed and put into centrifuge tubes. The tubes were sealed and sent to at the University of Bergen.

### 3.4.8.2 The method

Isotope analysis were conducted at the Department of Earth Science's mass spectrometry laboratory, University of Bergen, Norway. To remove sediment from the foraminifera shells, methanol was used to clean the samples. The samples were dried and put into glass vials. A MAT Carbo Kiel III preparation line was used to add three drops of $H_3PO_4$. The Finnigan MAT 253 mass spectrometer was used to measure the stable isotope ratios. The laboratory's external error is based on replicate measurements of carbonate standards, which is ± 0.06 for $\delta^{18}O$ and ± 0.03 for $\delta^{13}C$ versus the PeeDee Belemnite after calibration with the NBS19 standard (Coplen, 1996). The oxygen isotopic record was corrected for isotopic disequilibrium with seawater between the different species (Table 3.2) Global continental ice volume changes during the deglaciation and early and middle Holocene causes variations in $\delta^{18}O$ (Duplessy et al., 2001). A 10 m change of sea level, leads to a 0.11‰ change of $\delta^{18}O$. The samples were global sea-level corrected with a 0.011‰ per meter rise in global sea level (Fairbanks, 1989).

**Table 3.2:** Corrections of vital effects for *Nonionella labradorica, Melonis barleeanus* and *Cibicides lobatulus*

| Species | $\delta^{18}O$ correction | Reference |
|---|---|---|
| *Nonionellina labradorica* | -0.2 | Shackleton, 1974 |
| *Melonis barleeanus* | +0.4 | Smalley et al., 1986 |
| *Cibicides lobatulus* | +0.64 | Duplessy et al., 2005 |

## 3.4.9. Radiocarbon dating

The chronology of the key core NP05–11–49GC is based on four dated levels, where sufficient biogenic material was available. Two bivalve shells of the genus *Nucula* were sampled from 87 and 127 cm. At least 900 specimens of the foraminifera species *Cassidulina reniforme* and *Cassidulina neoteretis* were sampled from 35 and 181 cm. The four samples were sent to $^{14}$CHRONO Centre at Queen's University of Belfast, UK for radiocarbon dating using the AMS-method.

### 3.4.9.1. Principle

Carbon has three naturally occurring isotopes, $^{12}$C and $^{13}$C, which are stable, and $^{14}$C which is unstable and known as radiocarbon. Radiocarbon is continually being formed in the upper atmosphere by the interaction of neutrons produced by cosmic rays with nitrogen atoms. It quickly forms carbon dioxide with oxygen and mixes in the atmosphere and the oceans. Through the photosynthesis, it enters the biosphere and thus calcareous marine organisms. After death, the exchange with the biosphere stops, and the unstable radiocarbon starts to decay with a half- life of 5730 years (Bowman, 1990).

### 3.4.9.2. Accelerator Mass Spectroscopy (AMS)

The AMS method measures the number, or a proportion of a number, of $^{14}$C atoms in a sample compared to the number of $^{12}$C and $^{13}$C atoms. C-ions from the sediment samples are accelerated and subjected to a magnetic field, which causes them to deflect from a straight path. Particles of dissimilar mass deflect differently, and heavier particles deflects the least. Detectors at different angles receive the particles, making it possible to identify and obtain the amount of $^{14}$C (Bowman, 1990).

### 3.4.9.3. Marine reservoir effect and calibration

Several different factors, including radioactive decay, contribute to the concentration of $^{14}$C in animals and plants. Factors such as the variation of the formation of $^{14}$C in the atmosphere due to fluctuations in earth's magnetic field and sunspot activity, natural changes due to glaciations and human activity like burning of fossil-fuel, known as the Suess effect, and

nuclear-weapons testing (Bowman, 1990). This has led to a need for calibration between radiocarbon years and calendar years before present (cal. Yr. BP).

Radiocarbon is mixed into the ocean at the ocean-atmosphere interface. This gives surface waters and the atmosphere similar concentration of radiocarbon. Mixing rates in the subsurface and deep oceans are slow. This results in a more isolated layer of deeper water and little compensating for the decay of $^{14}C$ with mixing of fresh surface waters. Marine organisms, using carbon to build for instance tests and shells, incorporate this lower amount of $^{14}C$ (Bowman, 1990). This gives an apparent older radiocarbon age and is called the marine reservoir effect R(t), which varies over time and is defined as the difference between $^{14}C$ age of samples grown in the sea and the $^{14}C$ age in samples grown the atmosphere contemporaneously (Stuiver et al., 1986). To compare a radiocarbon age of a marine organism with ice-core and terrestrial records, it is important to correct for a marine reservoir effect (Bondevik et al., 2006).

Local and lateral differences in water masses also needs to be accounted for (Bowman, 1990; Mangerud et al., 2006), and a regional offset from a global mean reservoir age R(t) is referred to as ΔR (Stuiver et al., 1986; Bard et al., 1994). A regional difference is due variations in sea-ice cover, wind speed and upwelling of poorly ventilated subsurface waters (Bard et al., 1994).

# 4. Benthic foraminifera

## 4.1. Introduction and ecology

Benthic foraminifera are protists or prokaryotes with calcareous, organic or agglutinated tests. The tests are either single chambered or multi-chambered separated by septae. They are in- or epifaunal and live mainly in marine environments. Foraminiferal remains deposited and incorporated in the seabed sediments after death are dominated by benthic forms in most inshore waters and shelf areas (Lowe & Walker, 1984).

Poor preservation of the foraminiferal tests, reworking and re-deposition of sediments may lead to a misinterpretation of the faunal composition and hence the paleoenvironment. The studied core NP05-11-49GC appear undisturbed – with homogenous hemipelagic sediments and occasional bioturbation.

Benthic foraminifera is the most abundant microfossil group in the sediments of the Barents Sea and the understanding of their modern Arctic assemblages are important for reconstructing marine environments (Steinsund et al., 1994). The ecology, the relationship between the living organism and the environment, of benthic foraminifera is studied to find the distribution pattern and dynamics of communities and environment. This distribution pattern of foraminifera is controlled by their feeding strategies and microhabitat preferences on the one hand, and by climate, ocean circulation, sea-ice and water mass properties on the other hand (Steinsund et al 1994; Murray, 2001). Important controlling factors are studied to reconstruct the paleoecology and paleoceanography are therefore salinity, oxygen, temperature, turbidity, bottom current activities, alkalinity and the grain size of sediments (Murray, 2001)

## 4.2. The ecological preference of dominating species

The ecology of eight dominating species from the core NP05-11-49GC are presented in this chapter. Less dominating species are briefly described as they display short episodes of high

relative abundance, or their appearance could give an indication of the paleoenvironment. Samples under 185 cm contained less than 25 benthic calcareous specimens and have therefore been excluded to avoid biased results.

### 4.2.1. *Buccella spp*

This group consists mainly of *B. frigida* and a smaller proportion of *B. tenerrima. They are* epifaunal or shallow infaunal (Rosoff & Corliss, 1992).

*Buceclla spp* prefers a cold, polar environment within areas influenced by seasonal sea ice, suggesting that the group take advantage of algal bloom at the ice edge (Hald & Steinsund, 1996; Polyak et al., 2002). Temperatures between 0-1 degrees, salinity between 33-34 ‰ and water depths of 100-200 m are preferred (Steinsund et al,. 1994). *Buccella spp*. is recorded in river-affected areas from the Ob estuary in the Kara Sea (Polyak et al., 2002). It is typically found around Franz Josef Land in relative shallow areas with slightly sandy sediments (Steinsund et al., 1994; Hald & Seinsund, 1996). Faunas dominated by *Elphidium excavatum* and *Cassidulina reniforme* in modern arctic fjords are typically accompanied by *Buccella frigida* and *Buccella tenerrima* (Jennings et al., 2004).

### 4.2.2. *Elphidium excavatum* forma *clavatum*

*Elphidium excavatum* comprises four ecophenotypes, where *Elphidium excavatum* forma *clavata* is the arctic form commonly found on the east and west coast of Spitsbergen (Feyling-Hanssen, 1972). Rare occurrences of *Elphidium excavatum* forma *selseyensis* from the studied sediment core is possible (cf. Kristensen et al., 2013), but here all forms registered are *Elphidium excavatum* forma *clavata*, referred to as *Elphidium excavatum* in this thesis.

*Elphidium excavatum* is an opportunistic and infaunal species, which is found in a wide sediment depth range (Corliss, 1991; Steinsund et al., 1994). The species is widespread on Arctic shelves and is extensively distributed in marine deposits of Quaternary age (Steinsund et al 1994; Hald & Korsun 1997; Polyak et al., 2002,). It clearly dominates in a pure arctic environments with presence of sea-ice and high turbidity and high sedimentation rates

(Steinsund et al 1994; Hald & Steinsund, 1996; Hald & Korsun, 1997). It is mainly distributed in Arctic and shallow waters characterized by rapid changes in temperature and salinity, typical for glacier proximal environments (Feyling-Hanssen, 1972; Osterman, 1984; Hald & Vorren, 1987; Steinsund et al., 1994). It is both a salinity and temperature indicator, and prefers low temperatures under 1°C and/or reduced salinities between 30 and 34 psu (Hald & Vorren, 1987; Steinsund., et al 1994).

The species strongly dominates the bottom of laminated muds, with general low diversity, commonly found in glaciomarine deposits proximal to a retreating glacier (Vorren & Hald, 1987; Hald & Korsun, 1997). It is almost exclusively confined to Arctic waters in the Barents and Kara Sea (Steinsund et al., 1994). The southward distribution of *Elphidium excavatum* in the Barents Sea is limited by the winter sea-ice and temperatures above 4°C due to competition from species thriving on more stable feeding (Polyak et al., 2002). The species is related to brackish water in the Kara Sea (Hald & Korsun, 1997) and is related to in riverine effected near-shore waters at lower latitudes (Feyling-Hanssen, 1972).

### *4.2.3. Nonionellina labradorica*

*Nonionellina labradorica* is a deep infaunal species associated with high productive environments and high food supply to the bottom (Corliss, 1991; Polyak & Mikhailov, 1996; Zajaczkowski et al., 2010). It is common in glaciomarine environments and prefers low temperatures of <1°C and reduced salinities of 33-34‰ (Cedhagen, 1991; Steinsund et al., 1994). *Nonionellina labradorica* is associated with the Polar front, with rapid changes and high organic production. It is commonly found in moderate water depths and in slightly sandy sediments (Steinsund et al., 1994; Jennings et al., 2004). *Nonionellina labradorica* is related to Atlantic water and dominate the deeper, middle and outer part of fjords (Hald & Korsun et al., 1997). It is found in more dynamic environments affected by iceberg activity with temperate, saline and oxygenated water masses (Vorren et al., 1984). It is found at intermediate distances from rivers (Polyak et al., 2002). The species is capable of surviving prolonged starvation, however it prefers environments with at least seasonally elevated concentrations of food supply (Cedhagen, 1991, Polyak et al., 2002). It thrives on buried organic matter (Corliss,

1991), and a low supply of phyto-detritus to the sediment surface may result in a low abundance of *Nonionellia labradorica* (Zajaczkowski et al., 2010).

### 4.2.4. Cassidulina reniforme

*Cassidulina reniforme* is commonly found in cold bottom waters in areas with seasonal sea ice cover. It is the second most important species in glaciomarine environments (Polyak & Solheim, 1994; Hald & Korsun, 1997; Polyak et al., 2002). It prefers temperatures below 2°C and salinities above 30 psu (Polyak et al., 2002). Laminated muds are often dominated by *Cassidulina reniforme* (Steinsund et al., 1994) and it is typically found in areas affected by Atlantic water and is associated with the warmer interstadials, where it indicates a distal glaciomarine environment (Hald & Vorren, 1987; Polyak & Solheim, 1994). It is associated with local water and occupies fjord mouths in Svalbard today (Hald & Korsun, 1997).

### 4.2.5. Cassidulina neoteretis

*Cassidulina neoteretis* is an epifaunal or shallow infaunal species that reflect organic fluxes to the seabed (Jennings et al., 2004). This species flourishes at very low temperatures and are rarely found at salinities <32‰. It has a preference for finer sediments and follows the same distribution as planktic foraminifera (Steinsund et al., 1994). A high abundance of *Cassidulina neoteretis*, occasionally together with abundant planktonic specimens, suggests a period with inflow of mainly subsurface Atlantic water, which could promote ice melting (Polyak & Solheim, 1994). ). In Greenland Fjords it is abundant in Atlantic Intermediate Water with a temperature >0 degree C (Jennings and Helgadottir 1994?). It is therefore an indicator of modified Atlantic water and its distribution is controlled by the supply of seasonal foodfalls (Steinsund et al., 1994). *Cassidulina neoteretis* is most commonly found between 626 and 1500 m water depth (Rosoff & Corliss, 1992).

### 4.2.6. Cibicides lobatulus

*Cibicides lobatulus* is an epifaunal suspension-feeding species that can attach to stones, sponge skeletons, algae and other objects (Hald & Vorren, 1984; Steinsund et al., 1994, Hansen et al., 1995). This gives an elevated habitat existence in addition to the top centimetre

of the sediment habitat (Corliss, 1991). *Cibicides lobatulus'* plano-convex form and sessile nature, enables it to cling on to the hard substrate and survive environments exposed to winnowing and high current activity (Hald & Vorren, 1984; Hald & Korsun, 1997). This explains why *Cibicides lobatulus* is recorded to often dominate together with *Trifarina angulosa* in sand facies (Hald & Vorren, 1984). In Svalbard today, it is commonly observed in the outer parts of fjords in high energetic environments with coarse sediments close to the fjord terminus (Hald & Korsun, 1997). A low sedimentation rate is associated with high occurence of *Cibicides lobatulus* and it prefers salinities mostly above 32‰, but can survive in a wider salinity range also (Steinsund et al., 1994). Bioturbation and survival inside polychaete tubes can result in a deep penetration into the sediment for *Cibicides lobatulus*, which probably happens when the substrate available is too soft for it to cling on (Ivanova et al., 2008).

### 4.2.7. Islandiella norcrossi

The two forms *Islandiella norcrossi* and *Islandiella helenae* can be challenging to distinguish, especially when preservation is poor and the shell is opaque instead of clear and transparent. Henceforth, these two forms are not distinguished and will be termed *Islandiella norcrossi*.

*Islandiella norcrossi* is an epifaunal or shallow infaunal species. The distributions pattern is similar to *Buccella spp*, but Islandiella norcrossi prefers finer sediments and larger water depths of 200-400 m (Steinsund et al., 1994). *Islandiella norcrossi* is often found in glacier-distal settings together with *Nonionellia labradorica* in Svalbard fjords (Hald & Korsun 1997; Korsun & Hald, 2000). It is typically observed in marine mud and glaciomarine sediments with ice rafted debris (Hald & Korsun, 1997). The species reflects high organic fluxes to the seabed (Jennings et al., 2004). Large concentration of the species have been found in troughs or depressions filled with winter bottom water with slow sedimentation rates (Steinsund et al., 1994; Jennings et al., 2004). Areas with seasonal sea ice cover is also favourable for this species, as it possible takes advantage of ice-edge algal blooms (Steinsund et al., 1994).

### 4.2.8. Melonis barleeanus

This species is an intermediate infaunal species that is found in the upper 4 cm of the sediment package on the seafloor (Corliss, 1991). The search for a more favourable microhabitat, can

result in a penetration down to 8-10 cm below the sediment surface (Ivanova et al., 2008). *Melonis bareeanus* is related to high sedimentation rates and fine sediments with high and steady rates of partlydegraded organic carbon (Mackensen et al., 1985; Caralp, 1989; Steinsund et al., 1994). In the Barents Sea, the species is found in troughs with chilled Atlantic water with temperatures between 3–4.5 °C and normal salinities with usually more than 32 ‰ (Hald & Steinsund, 1992). It is commonly found on the eastern flanks on the northern troughs in the Barents Sea, where it feeds on organic debris transported by winter bottom waters (Steinsund et al., 1992). *Melonis barleeanus* has the same feeding strategy and thermohaline preferences as *Pullenia bulloides* (Corliss, 1991). Due to high adaptability, *Melonis barleeanus* change to an epifaunal habitat depending on food supply (Linke & Lutze, 1993).

## 4.3. The ecological preference of secondary species

### *4.3.1. Elphidium subarcticum*

*Elphidium subarcticum* is an opportunistic and epifaunal species. Similar to *Elphidium excavatum,* it prefers glacier proximal environments, sea ice cover, low temperatures of less than 1°C and decreased salinities of 33–34‰. It is typically found in areas with coarse sediments and on slopes of the Spitsbergen and Central Banks (Steinsund et al., 1994). This species is widely occurring on both high and temperate latitude shelves. It tends to prefer river distal environments (Polyak et al., 2002).

### *4.3.2. Stainforthia loeblichi*

*Stainforthia* species are opportunistic and commonly found in areas of high seasonal productivity (Gustavsson & Nordberg, 2001). This species is common at bank slopes subjected to cold waters at approximately 0°C. It is typical within areas covered by seasonal sea-ice and show a similar distribution pattern as *Nonionellina labradoricum* (Steinsund et al 1994).

### 4.3.3. Pullenia bulloides

*Pullenia bulloides* is an intermediate infaunal species found in the upper 4 cm from the sediment surface on the seafloor (Corliss, 1991). The species prefer fine-grained sediments, which are typically found in troughs influenced by chilled Atlantic water like the Franz Victoria through. It prefers a narrow salinity interval close to 35‰ and a temperature interval between 2 and 4 °C (Steinsund et al., 1994).

### 4.3.4. Astrononion gallowayi

*Astrononion gallowayi* thrives in low temperatures of <1°C and high salinities of >30‰, mostly > 33‰. It is found in shallow areas with coarse sediments influenced by stronger bottom currents and are often accompanied by *Cibicides lobatulus* (Steinsund et al., 1994; Wollenburg and Mackensen, 1998).

### 4.3.5. Trifarina fluens

*Trifarina fluens* is a shallow infaunal species (Corliss, 1991). It is typically found on bank slopes covered by sandy sediments, and is an important paleoenvironmental indicator due to a specific thermohaline preference. It thrives in highly productive mixing zones between Arctic and Atlantic waters, like the Polar front, with temperatures of 1-3°C and salinity of 34-35‰ (Steinsund et al., 1994).

### 4.3.6. Miliolids

*Miliolids* are generally epifaunal and most common in the top centimetre of the seafloor sediments. They have a decreasing abundance with increasing sediment depth (Corliss, 1991). Several species belong to the *Miliolinella* genera, which show an unclear distribution pattern probably due to several individual ecological preferences (Polyak et al., 2002).

### 4.3.7. Agglutinated species

Agglutinated foraminifera disintegrate easily after death often resulting in varying amounts and high fractionation of the tests in the sediment (Steinsund et al., 1994). They are most common in the upper 0.5 cm of the seafloor sediments (Corliss, 1991). The number of agglutinated species can be an indicator if increased water turbidity (Zajaczkowski et al., 2010). *Reophax scorpiurus* is the most common species from the investigated sediment core. This foraminifera correlate well with the amount of organic carbon in the surface sediments and is found in colder bottom waters of 2-4°C (Hald & Steinsund., 1992). Brine formation, associated with acidic bottom waters, is well tolerated by *Reophax scorpiurus* (Rasmussen & Thomsen, 2014).

# 5. Results and interpretation

## 5.1. Seismostratigraphy

This subchapter present a brief seismic data analysis of the subsurface characteristics of the three core sites from Erik Eriksen Strait and southern Kvitøya Trough. The three collected sediment cores were taken along three transects, going SW-NE along the long-axis of the Erik Eriksen Strait and E-W along the short-axis at the southern head of the Kvitøya Trough (Figure 5.1). The three lines are included in order to obtain an overview of the bathymetry, acoustic layers penetrated by the cores and sub bottom sedimentary record characterizing the three core sites, and correlate this with the obtained sediment cores (See 5.2 *Lithostratigraphy*).

Line NP05–11–69, includes core location of core NP05–11–84GC2 in western Erik Eriksen Strait

Line NP05–11–37, includes core location of core NP05–11–49GC in middle Erik Eriksen Strait

Line NP05–11–42, includes core location of core NP05–11–51GC2 in southern Kvitøya Trough

Two-way-travel time (TWT) is displayed along the y- axis in seconds. The mean P-wave velocity obtained from core NP05–11–49GC and NP05–11–51GC2 is 1480 m/s. However, the retrieved P-wave amplitude is mostly zero. The obtained P-wave velocity is therefore disregarded (see 3.4.1.2 *P-wave velocity*). An acoustic velocity of 1700 m/s was chosen for the post-glacial deposits of Andfjorden and Vågsfjorden (Plassen & Vorren, 2002). An average acoustic impedance of 1600 m/s is typically used for sediments of Spitsbergen fjords (Elverhøi et al., 1995; Plassen et al. 2004; Forwick et al., 2011). The acoustic velocity of water is 1500 m/s. Due to the softness of the sediments, a chosen velocity of 1600 m/s was used to convert the TWT into sediment thickness (m).

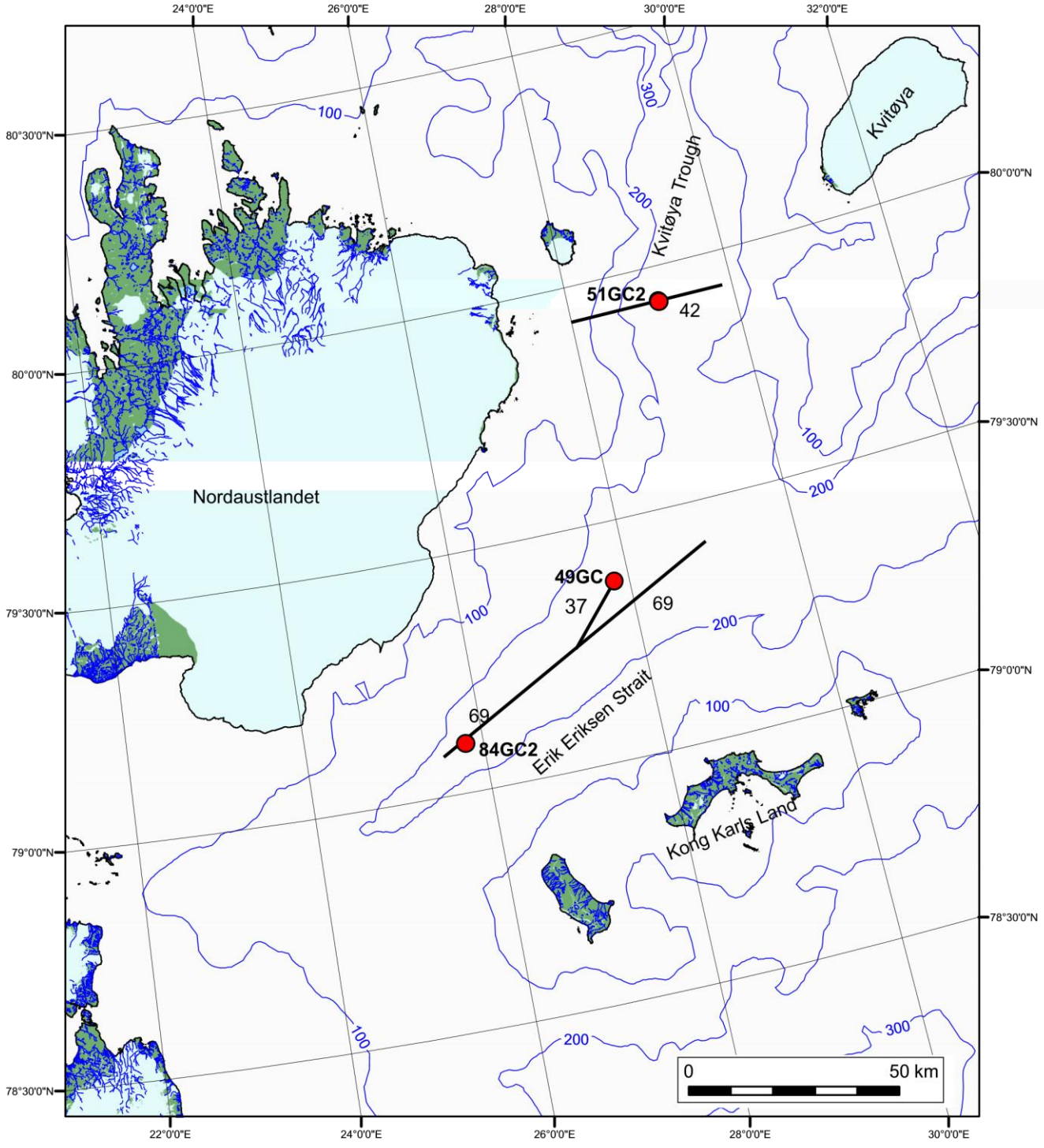


**Figure 5.1:** Map of Erik Eriksen Strait and Kvitøya Trough displaying obtained seismic lines and core location with red dots.

## 5.1.2 Core site NP05–11–84GC2 – S-W Erik Eriksen Strait

### 5.1.2.1. Description

The core was retrieved from an acoustically transparent wedge-form. (Figure 5.2). East of the wedge, the seabed is smooth and deepening, with an overlying 30 – 60 cm surface drape. Approximately 1.2 km further east, a hummocky seabed with an underlying undulating acoustically transparent layer with subtle morphological features are observed.

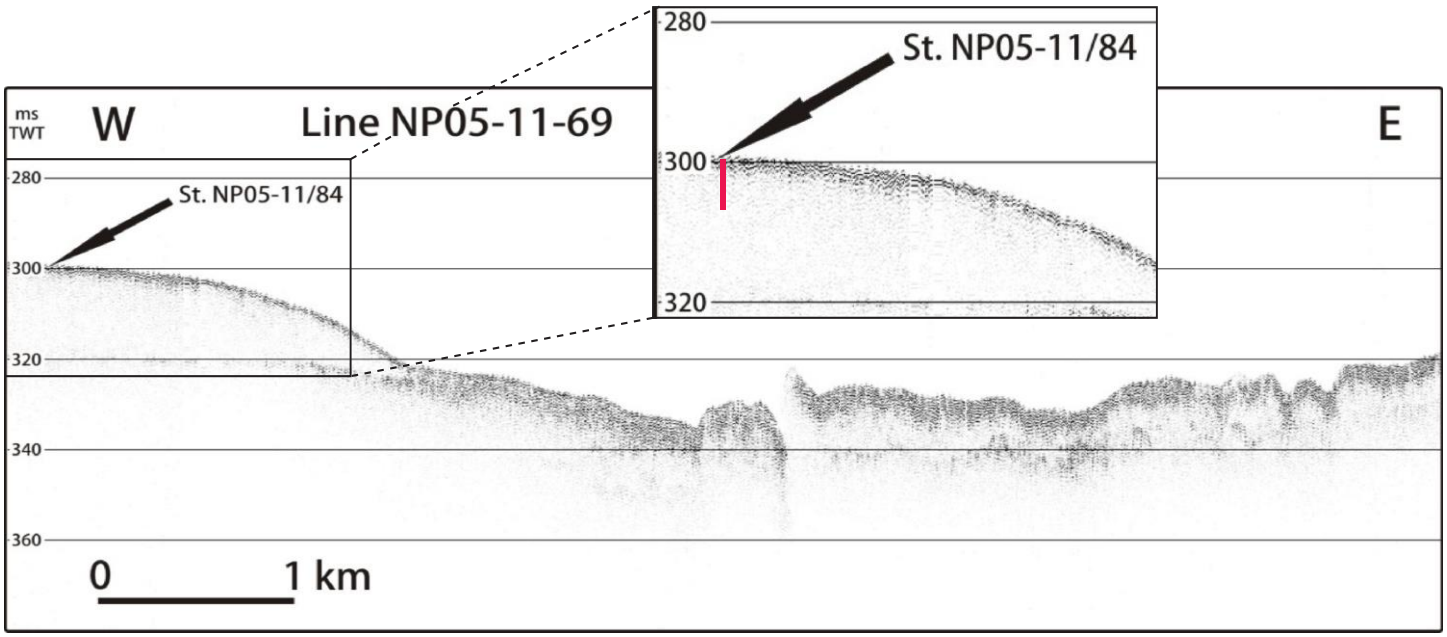


**Figure 5.2:** Seismic line NP05–11–69 from western Erik Eriksen Strait displaying location for core NP05–84–GC2 showing acoustically transparent Grounding zone wedge with proximal subtle morphological feature overlain by a thin post-glacial surface drape Approximate position and length of core is indicated by red line.

### 5.1.2.2. Interpretation

An acoustically transparent sediment layer were described by Hogan et al. (2010b) from the Erik Eriksen Strait. The layer was subdivided into lobate deposits or discrete accumulations of sediment. The lobate deposits, up to 15m high, were interpreted to be grounding zone wedges. Grounding zone wedges are mainly transparent or chaotic on seismic profiles and are formed by advection of till towards the glacier front in a still-stand of a retreating glacier during deglaciation (Dowdeswell et al.,2008; Hogan et al., 2010b; Dowdeswell & Fugelli, 2012).

The acoustically transparent and approximately 10m thick wedge from Erik Eriksen Strait is therefore probably such a grounding zone wedge. Subtle morphological features, observed situated further east of the wedge-form, were described from Erik Eriksen Strait by Hogan et al. (2010b) as transverse ridges formed during glacier still-stand or readvance during retreat. The subtle morphological feature observed east of the wedge-form can be such ridges, however more extensive seismic analysis are needed for determining the origin of the hummocky seafloor. The acoustically homogenous surface drape is interpreted to be post-glacial accretion of sediments through the water column. Similar surface sediments of up to 4 m were described from Erik Eriksen Strait by Hogan et al. (2010b).

## 5.1.3. Core site NP05–11–49GC – Middle Erik Eriksen Strait

### 5.1.3.1 Description

The core was retrieved from homogeneous sea floor with a slight deepening towards northeast (Figure 5.3). The top layer is a 1.5 to 2 m acoustically homogenous surface drape. The core penetrates into the underlying layer, which is laterally extensive with a relatively smooth and distinct upper reflector.

### 5.1.3.2. Interpretation

The observed surface drape is correlative with the top acoustic facies of Erik Eriksen Strait interpreted by Hogan et al. (2010b) to have accumulated through post-glacial rainout from the water column. The underlying laterally extensive layer is correlative with a diamictic facies interpreted by Hogan et al. (2010) to reflect subglacial deposition.

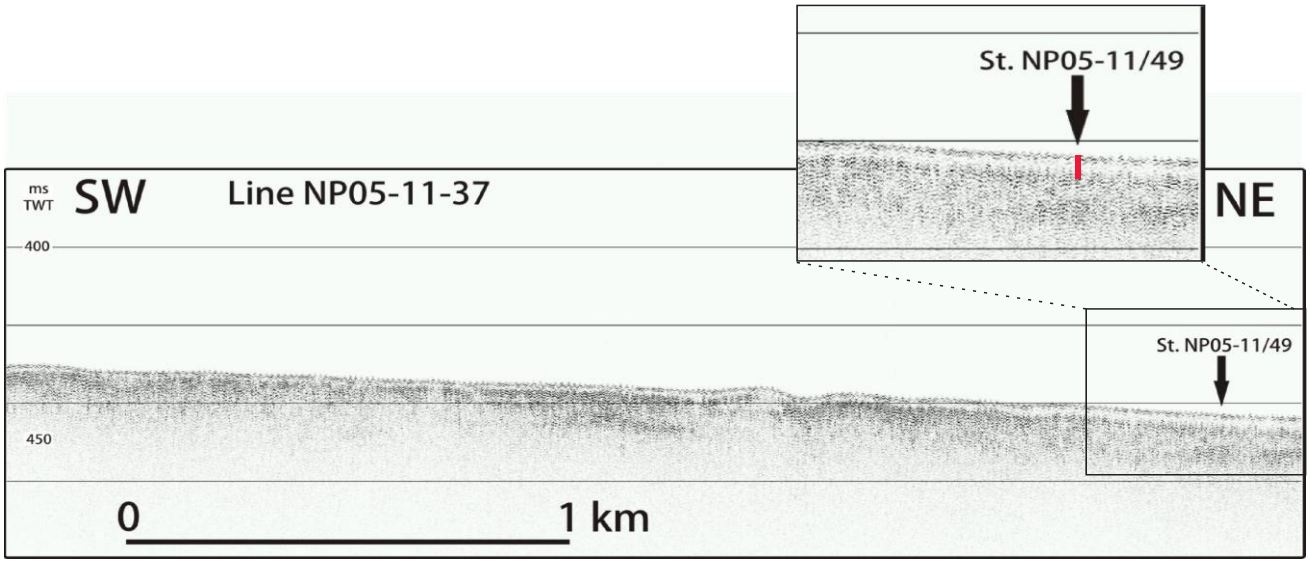


**Figure 5.3:** Seismic line NP05–11–37 from middle Erik Eriksen Strait displaying location for core NP05–11–49GC showing laterally extensive layer of varying thickness overlain by a thin post-glacial surface drape. Approximate position and length of core is indicated by red line.

## 5.1.4. Core site NP05–11–51GC2 – Southern Kvitøya Trough

### 5.1.4.1. Description

The core was retrieved from homogeneous sea floor in close proximity to the Nordaustlandet bank (Figure 5.4). The top layer is a 0.5 to 1.8 m acoustically homogenous surface drape. The core penetrates slightly into the underlying layer that is also acoustically homogenous, with an upper relatively smooth and distinct reflector.

### 5.1.4.2. Interpretation

The observed surface drape is correlative with a thin and widespread draping unit observed by Hogan et al. (2010a) from the Kvitøya Trough, interpreted to be accumulation of post-glacial sediment-rainout from the water column. The underlying lateral layer is correlative with an unlithified sediment unit interpreted to represent thin subglacial deformation till, or a diamictic layer representing a transitional facies and ice-proximal deposition from a retreating glacier front during deglaciation.

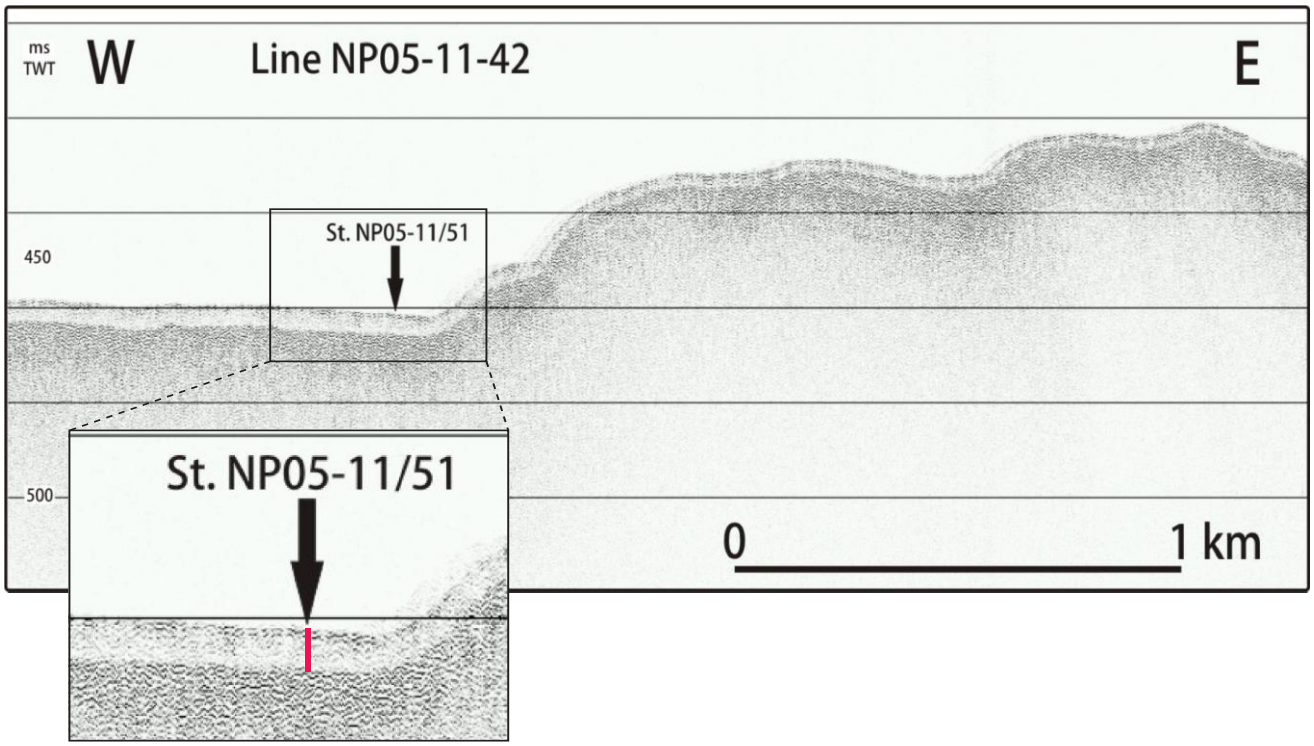


**Figure 5.4:** Seismic line NP05–11–42 from southern Kvitøya Trough displayin location for core NP05–49–GC showing laterally extensive layer of varying thickness overlain by a thin post-glacial surface drape. Approximate position and length of core is indicated by red line.

## 5.2. Lithostratigraphy

### 5.2.1. Introduction

Three sediment cores from Erik Eriksen Strait and Kvitøya Trough make up the basis for the lithostratigraphy. The cores were analysed using the methods described in Chapter 3 in order to understand and reconstruct the depositional environment of the strait. The results of the analysis is presented below along with an interpretation of each proxy. The thesis is mainly built on the results obtained from core NP05–11–49GC. Two more cores, NP05–11–51GC2 and NP05–11–84GC2, are included for lithostratigraphical purposes and to attain an understanding of the different sedimentological processes during the deposition of the different units. The latter cores are divided into a deglacial and post-glacial unit, as dating of biogenic material is needed for further division. The chronology is therefore based on the results from core NP05–11–49GC, which had sufficient biogenic material for dating

### 5.2.2. Visual description and lithofacies

Visual description of the sediment surface along with a study of X-ray photos was done to create lithological logs of the cores. Colour photography's of the cores are shown next to the logs. Sections with the different units, lithofacies codes, colour of the sediment surfaces and the amount of bioturbation are created and displayed along with the log. The lithofacies codes are based on the classification of diamictic and sorted sediments from Krüger & Kjær (1999; Figure 5.1). Diamictic (D) sediments are separated into general appearance, granulometric composition of matrix, clast/matrix relationship and the consistence when moist. The sorted sediments are separated into gravel (G), sand (S) and fines or mud (silt and clay), and whether the laminas or the bedding is horizontal (h), planar (p) or massive (m). The scale and ranges of grain size fractions are based on the division used in the GRADISTAT program (Blott & Pye, 2001). Some of the subdivisions are excluded to simplify the scale. Matrix-supported units, beds and pockets dominated by mud with an obvious sand component are termed, based on visual description and the obtained grain size distribution, sandy mud or muddy sand.

### 5.2.3. Introduction physical properties

The measured physical properties for core NP05–11–49GC and NP05–11–51GC2 are water content (%), wet bulk density ($g/cm^3$), magnetic susceptibility ($10^{-5}$ SI), acoustic impedance ($g*m*cm^{-2}*s^{-1}$) and fraction porosity. A presentation of the physical properties plots are included for each of the cores. Table 5.1 include the physical properties mean, maximum and minimum values for each core. The obtained P-wave amplitude for the two cores are mostly zero. Low P-wave amplitude measurements (see *3.4.1.2 P-wave velocity)* is indicative of poor contact between transducer, liner and sediment contact. The P-wave velocity measurements are therefore rejected. The magnetic susceptibility is measured for core NP05–11–84GC2.

### 5.2.4. Grain size distribution

The grain size distribution is presented in continuous plots relative to depth for the cores NP05–11–49GC and NP05–11–51GC2 (Figure 5.8 and 5.13). Calculations of the percentages of

the total sediment volume for the fractions 0–63 µm, 63–100 µm, 100 µm – 1 mm and > 1mm is done. The 0-63 µm fraction, consisting of clay and silt, is referred to as fines or mud.

**Table 5.1:** Minimum, mean and maximum values for measured physical properties.

| Physical properties | NP05–11–49GC | NP05–11–51GC2 | NP05–11–84GC2 |
|---|---|---|---|
| **Magnetic susceptibility (10^(-5) SI)** | | | |
| Minimum | -0.1 | 2.1 | 10.6 |
| Mean | 21.9 | 22.8 | 61.2 |
| Maximum | 42.4 | 67.8 | 85.2 |
| **Wet bulk density (g/cm^3)** | | | |
| Minimum | 0.8 | 1.2 | |
| Mean | 1.6 | 1.6 | |
| Maximum | 2.1 | 2.2 | |
| **Acoustic impedance (g*m*cm^-2*s^-1)** | | | |
| Minimum | 1287 | 1726 | |
| Mean | 2405 | 2355 | |
| Maximum | 3183 | 3483 | |
| **Fraction porosity** | | | |
| Minimum | 0.4 | 0.3 | |
| Mean | 0.7 | 0.6 | |
| Maximum | 1.1 | 0.9 | |

### 5.2.5. Ice rafted debris

Ice rafted debris (IRD) from the 1 mm fraction was picked for core NP05–11–49GC. Minerogenic grains was picked, leaving out any authigenic material. Continuous plots relative to depth present the IRD-distribution.

### 5.2.6 CTD (Conductivity, Temperature, Depth) description

CTD- profiles from core sites of the the investigated cores NP05–11–49GC and NP05–11–51GC2 were retrieved during the NP05–11 cruise with R/V Lance in August 2005. The measurements are described and presented in continuous plots relative to depth. The obtained values show the water masses change of salinity and temperature throughout the water column.The CTD results from the cruise were unavailable for this thesis, however five CTD-profiles from the cruise from the Erik Eriksen Strait and nearby troughs were presented

in Kristensen et al. (2013). The CTD-profile from the core site, NP05–49, of this thesis key core NP05—11–49GC, display a current influence of Atlantic water as a subsurface layer between approximately 150 and 300m water depth. The Atlantic derived water is characterized by salinity of 34.9 psu and temperature of 2–2.5 °C (Kristensen et al., 2013). The top 150 m is occupied by cold Arctic surface waters originating in the Arctic Ocean flowing into the northwestern Barents Sea via the Franz Victoria-, St. Anna- and Hinlopen Troughs (Ślubowska et al., 2007; Gammelsrød et al., 2009). Core site 51, where core NP05–11–51GC2 in the Kvitøya Trough is retrieved from, display a cooler water mass distribution with lower salinity of 34.7 psu and temperatures between 1.1 and 0.8 °C.

The stations situated further east display warmer temperatures, which is in concordance with Gammelsrød et al. (2009), which suggested an easterly inflow of Atlantic water to the Erik Eriksen Strait via the Franz Victoria- and St. Anna troughs.

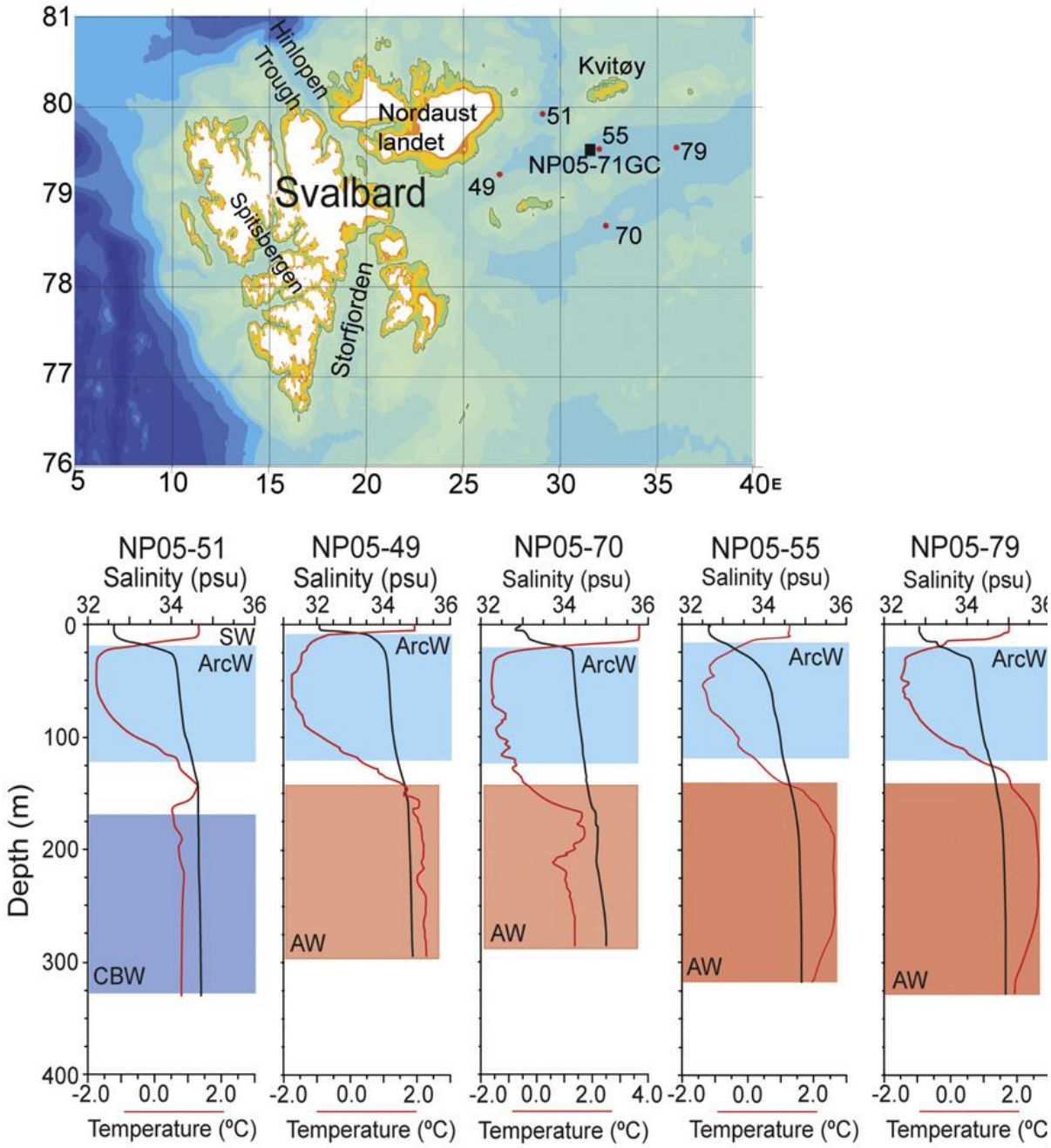


**Figure 5.5:** Map of the Svalbard archipelago with position of CTD-stations marked with red circles. Temperature and salinity profiles from each station retrieved in 2005 during the NP05–11 cruise are displayed below. Definition of water masses are according to Gammelsrød et al. (2009). Water masses are displayed in colours and marked with the abbreviations: SW= Surface water, ArcW= Arctic surface water, AW= Atlantic water, CBW= Cold bottom water. After Kristensen et al. (2013).

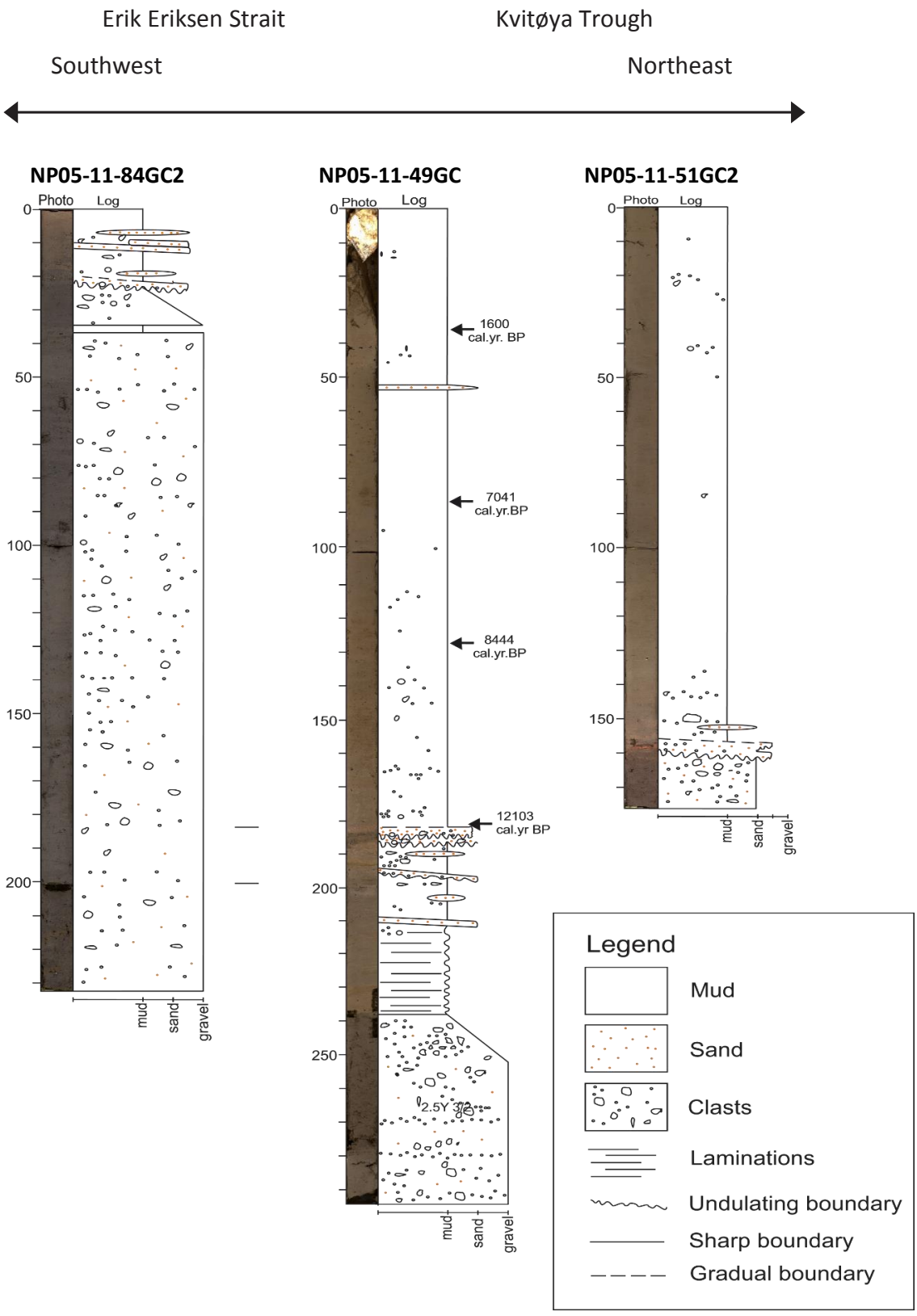


**Figure 5.6:** Lithological logs with colour photographs of the cores NP05–11–84GC2, NP05–11–49GC from Erik Eriksen Strait and of NP05–11–51GC2 from Kvitøya Trough. Arrows display dated levels in calibrated years before present. Legend in the right corner.

## 5.2.7. Core NP05-11-84GC2 – Western Erik Eriksen Strait

The core was retrieved from a water depth of 215 m in the western part of the Erik Eriksen Strait (Figure 2.1 and 5.1). The total length of the core is 231 cm (Table 3.1). The core is subdivided into two units, unit A1 and B1, based on lithofacies assosiations and the magnetic susceptibility graph (Figure 5.8 and 5.9). Sediment facies comprising this core are: Fm (Fines (silt, clay), massive), Sm (Sand, massive), D (Diamict, massive), (m2) (Matrix-supported, moderate), 2 (Friable, easy to excavate).

#### 5.2.7.1. Magnetic susceptibility

The magnetic susceptibility (Figure 5.9) displays most fluctuations and spikes within unit B1, but also unit A1 show several spikes with a general increase towards unit B1. The mean value is 61 ($x10^{-5}$ SI). A drop to 47 ($x10^{-5}$ SI) is observed at 47 cm. A positive spike is observed at 38 cm, correlating with the change from unit A1 to B1.

### 5.2.7.2. Unit B1 (231–38 cm)

#### 5.2.7.2.1. Lithology and stratigraphy

The basal unit B1 makes up most of the core and is 193 cm long with a very dark grey colour (2.5Y 3/1; Figure 5.8). The unit is characterized by numerous gravel-sized clasts suspended in a matrix of massive mud and sand. The sediments are more compact and less water saturated compared to the overlying unit A1. The observed clasts are subrounded to subanglurar and vary in abundance. Some crude planar structures are observed in the upper part of the x-ray photos (Figure 5.7). The unit is devoid of biogenic material and has a sharp upper boundary.

#### 5.2.7.2.2. Interpretation

The abundance of scattered clasts suspended in a massive sandy mud matrix, along with the degree of compaction and low water content, suggest that unit B is a diamictic deposit. The poor sorting of the grain size distribution, along with the subrounded clasts further indicates

glacier transportation and deposition (Hambrey et al., 1997). The moderate compaction of the sediment can indicate direct subglacial and ice-proximal deposition (Dowdeswell et al., 2008). Lacking biogenic material suggest harsh glaciomarine conditions (Hald & Korsun, 1997). The crude planar structures in the upper part of the unit suggest ice proximal deposition affected by subglacial meltwater, rather than direct deformation of till at the glacier bed (Hogan et al., 2010b). The core is retrieved from an acoustically transparent wedge-form (see 5.1.2 *Core site NP05–11–84GC2 – S-W Erik Eriksen Strait*). Based on this, the unit is interpreted to be a diamict deposit formed by direct subglacial and ice-proximal processes during a glacier advance or still-stand during deglaciation.

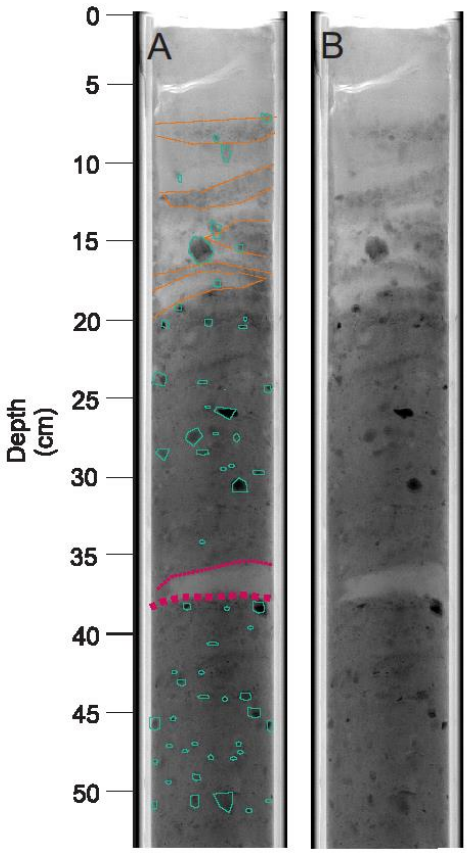


**Figure 5.7:** Two identical x- ray photographs (**A** and **B**) of split core of NP05–11–84GC2 displaying unit A1 (0–38 cm) and the top part of unit B1 (55–38 cm). **A:** Includes interpretation of the observed sediment features. Larger clasts are marked in green. Orange dotted lines mark sandy mud pockets and beds. Purple dotted line display a mud bed between 36 and 38 cm bordering unit B2. The lower thick purple dotted line show boundary between unit A1 and B1 at 38 cm.

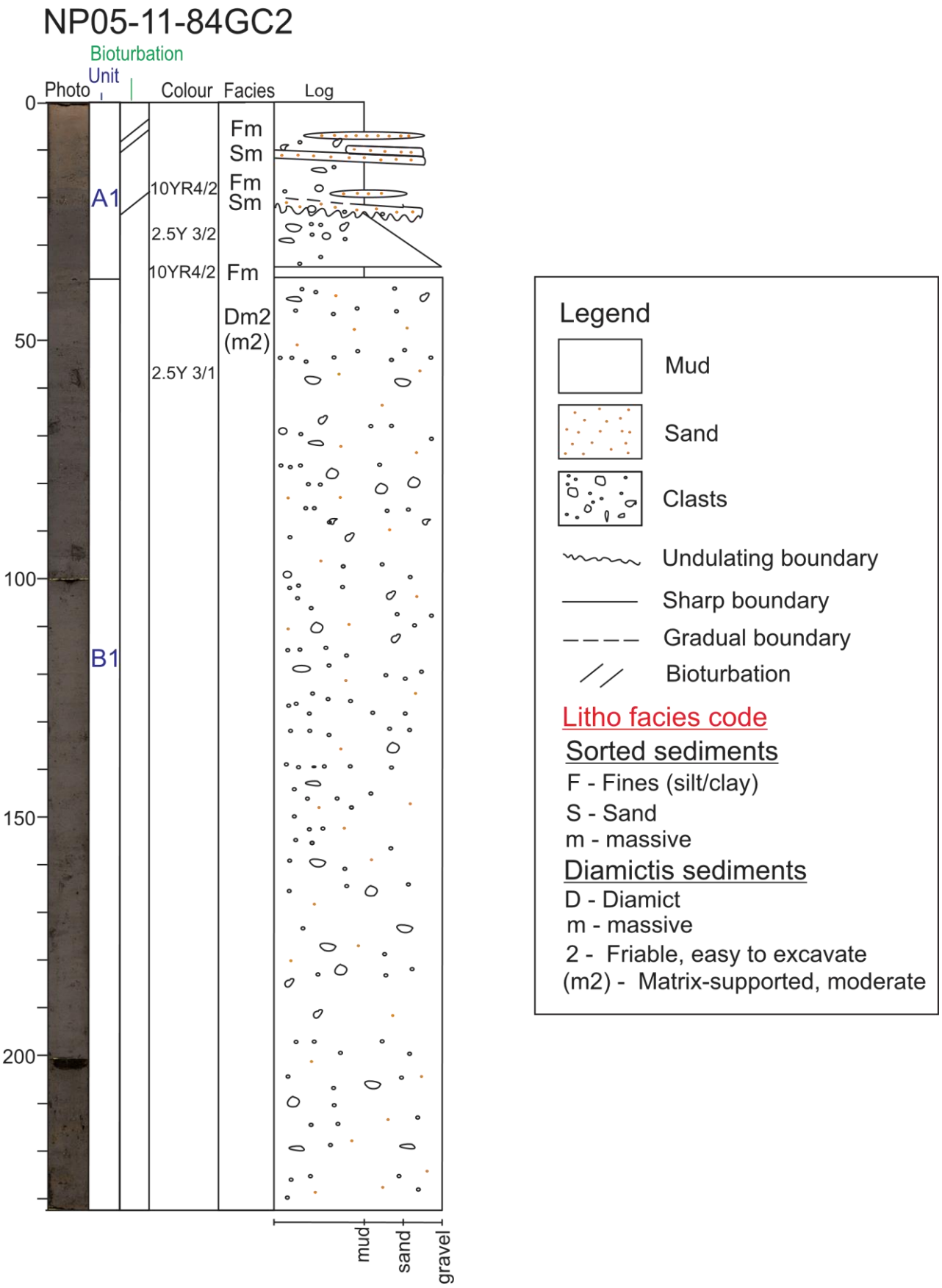


**Figure 5.8:** Lithological log of core NP05–11–84GC displaying colour photographs, units, bioturbation, Munsell colour codes, lithofacies codes and structures. Legend displayed to the right.

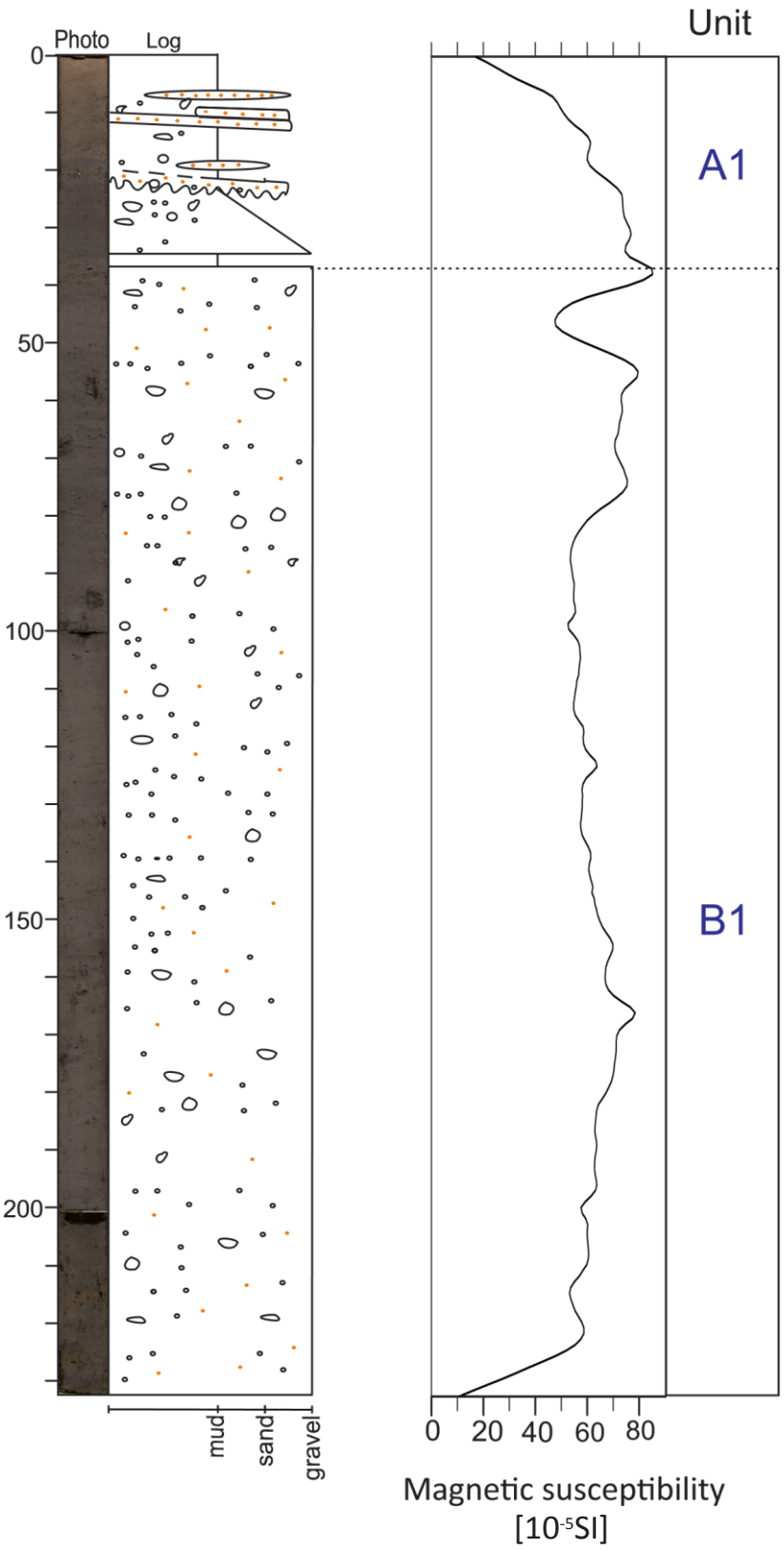


**Figure 5.9:** Measured magnetic susceptibility of core NP05–11–84GC2. Lithological log and colour photographs are included for reference.

### 5.2.7.3. Unit A1 (38–0 cm)

#### 5.2.7.3.1. Lithology and stratigraphy

Unit A1 is characterized by massive mud with several sandy mud pockets and beds (Figure 5.8). A 2 cm water saturated and soft greyish brown bed (10YR 4/2, similar to the top 17 cm of the unit, is found between 36 and 38 cm (Figure 5.7). Bioturbation is observed in the upper part. The underlying boundary to unit B1 is sharp. The lower part of the unit is characterized by a very dark grey (2.5Y 3/1) colour. A dipping bed with a sharp boundary consisting of muddy sand is observed between 22 and 21 cm. The upper 17 cm are softer and consists mostly of massive mud with dark greyish brown (10YR 4/2) colour. However, few very weak 1 mm laminas can be observed on the X-ray photos. A 2 cm subhorizontal muddy sand pocket and lamina with an undulating and sharp boundary to the underlying sediment are observed at 10 and 7 cm, respectively.

#### 5.2.7.3.2. Interpretation

The dominance of fines observed in unit A1 suggest a depositional environment with lower current activity compared to unit B1. The muddy sand pockets and beds, along with the scattered clasts are interpreted to be IRD deposited from icebergs or sea ice (Dowdeswell et al., 1994; Forwick & Vorren, 2007). The increase of the magnetic susceptibility in unit A1 suggest increased compaction of sediments down-core. The observed spikes are interpreted to be caused by the scattered clasts and muddy sand pockets or beds. The soft greyish brown lamina bordering unit B1, show the same characteristics as the upper 17 cm. It is interpreted to be a result of deposition as the glacier was lifted from the bed, allowing deposition from sediment rainout from the water column. The overlying dark grey and more compact sediment is similar to unit B1. The change of colour and appearance to more compact sediments again, with a higher sand content is interpreted to reflect a glacier proximal environment, where a glacier front was located close to the core site resulting in a higher deposition of coarser sediment (Dowdeswell et al., 1994; Lubinski et al., 1996). This suggest increased glacial activity and possibly a glacial advance of the nearby glacier front resulting in deposition of more compact sediments comparable to unit B1. The less compact and greyish brown upper sediment is interpreted to have been deposited as sediment rainout from the

water column in a glacier distal environment. The unit is suggested to be post-glacial accumulation of suspended sediments in a proglacial to distal glaciomarine environment (Lubinski et al., 1996). Acoustic data display that the core was retrieved from the top of a grounding zone wedge (Figure 5.2), making the sediments exposed to ocean current erosion. This can explain the shortness of the soft post-glacial unit and why it is not easily observed in the acoustic data.

### 5.2.8. Core NP05–11–49GC – Middle Erik Eriksen Strait

Results from core NP05–11–49GC make up the basis of this thesis. It was retrieved from a water depth of 320 m in the middle part of the Erik Eriksen Strait (Figure 2.1 and 5.1). The total length of the core is 293 cm (Table 3.1). The core is subdivided into four units, unit A2–D2, based on lithofacies association, grain size data and physical properties (Figure 5.11 and 5.12). Sediment facies comprising this core are: Fm (Fines (silt, clay), massive), Sm (Sand, massive), D (Diamict, massive), (m2) (Matrix-supported, moderate), 1 (Loose, not compacted).

The matrix of the core consists mainly of massive mud, with few short intervals of sandy mud. Few black (2.5Y 2.5/1) mottles are observed scattered throughout the core with a slight increase down core. The degree of compaction varies in intervals throughout the units, and an expected increase is observed down- core. Bioturbation is generally low. The observed decrease of water content and fraction porosity down-core, with a corresponding increase of wet bulk density and acoustic impedance is caused by an increase of compaction due to sediment loading.

#### 5.2.8.1. Unit D2 (293–238 cm)

Unit D2 is 55 cm long and characterized by a matrix of sandy mud with numerous very fine to very coarse gravels distributed throughout the unit (Figure 5.10 and 5.11). The grain size distribution display poorer sorting compared to overlying units. The mud fraction vary between 63 to 81%. Gravel clasts make up 20% of the sediment composition and are subrounded to subangular. The unit is very dark grey (10YR 3/1) and generally devoid of lineations. However, a slight alternation between dry and more water-saturated laminas are

observed between 289 – 284 cm and 248 – 240 cm. Gravels are sometimes confined to certain levels, as opposed to having a random distribution. Numerous very coarse gravels characterize the interval between 258 and 249 cm. The unit is more compact compared to the overlying units, however still friable and easy to excavate. A fining upward tendency and a decreasing degree of compaction is observed in the upper 15 cm the unit. The IRD count is constantly high throughout the unit. The unit has a sharp upper boundary.

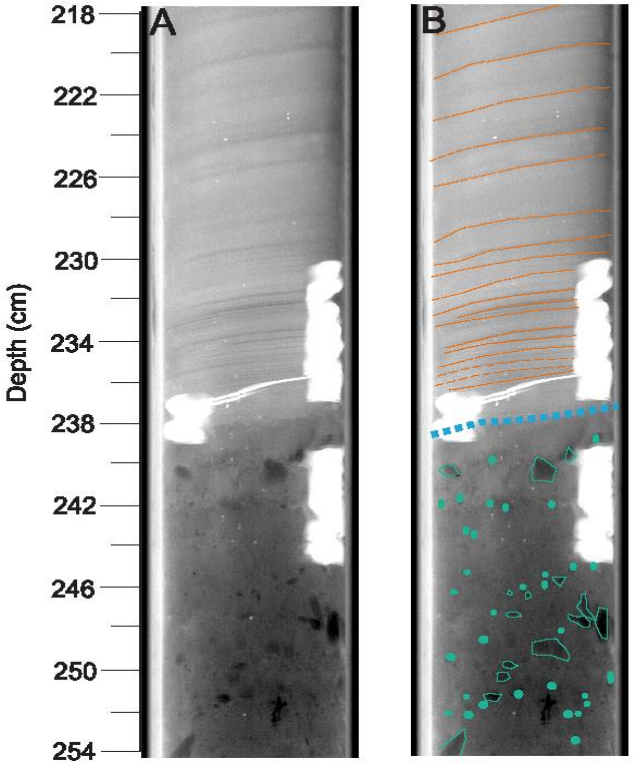


**Figure 5.10:** Two identical x-ray photographs (**A** and **B**) displaying the upper part of the diamictic unit D2 (254–238 cm) and the lower part of unit C2 (238–218 cm) of core NP05–11–49GC. **B:** X-ray photograph with interpretation of the observed sediment features: Larger clasts are marked in green. Blue dotted line display the boundary between the units and orange lines show laminations of unit C2.

#### 5.2.8.1.1. Physical properties

The mean values of the wet bulk density and acoustic impedance are slightly higher compared to unit C2. The fraction porosity is slightly lower. The three physical properties display a significant spike at 180 cm and numerous low-amplitude spikes. The magnetic susceptibility decreases in the lower part of the unit. Two positive spikes of 25 (*$10^5$ SI) at 287 and 42 (*$10^5$

SI) at 255 cm are observed. A negative spike of 25 (*$10^5$SI) is displayed at 180 cm. A negative drop of magnetic susceptibility observed at 238 cm corresponds well to the sharp boundary separating and the sedimentological different unit C2 and D2. Unit D2 has lower content of water compared to the overlying units. Small fluctuations around the mean value of 22 % is observed (Figure 5.12).

#### 5.2.8.1.2. Interpretation

The general grain-size distribution, with numerous gravel clasts suspended in a matrix of mud and sand, suggests that unit D2 is a diamict sediment. However, the softness of the sediments, the weak lamination and the slight sorting of clasts is indicative of ungrounded glacial deposition. Subglacial till is often over consolidated (Ó Cofaigh et al., 2007). The unit is therefore interpreted to be the result of rainout of IRD in a glacier-proximal setting during deglaciation (Dowdeswell et al., 1994; 2008; Forwick & Vorren, 2007). The unit is correlative with the observed acoustic layer, barely penetrated by the core, interpreted to be a diamictic facies (Hogan et al., 2010b¸ see *5.1.3.2. Interpretation*). The spikes displayed by the physical property graphs are interpreted to be a result of the unit's high clast content. The low water content suggest closer packing due to sediment loading and a higher variety of grain size. The fact that the unit is fining- upward in the upper 15 cm suggests a decrease in deposition of IRD, and conditions becoming more ice-distal (Dowdeswell et al., 2008).

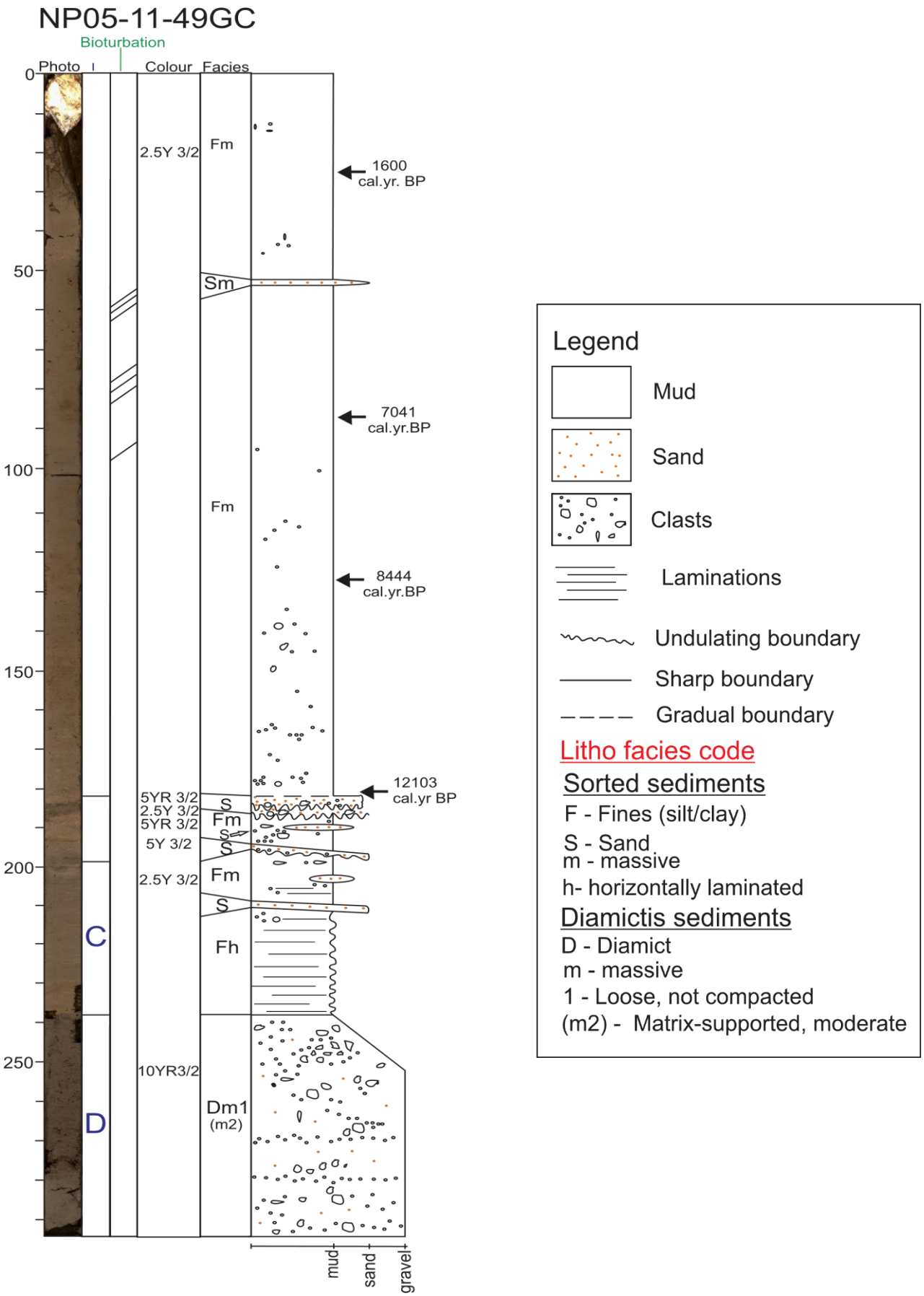


**Figure 5.11:** Lithological log of core NP05–11–49GC displaying colour photos, units, bioturbation, Munsell colour codes, lithofacies codes and structures. Legend displayed to the right.

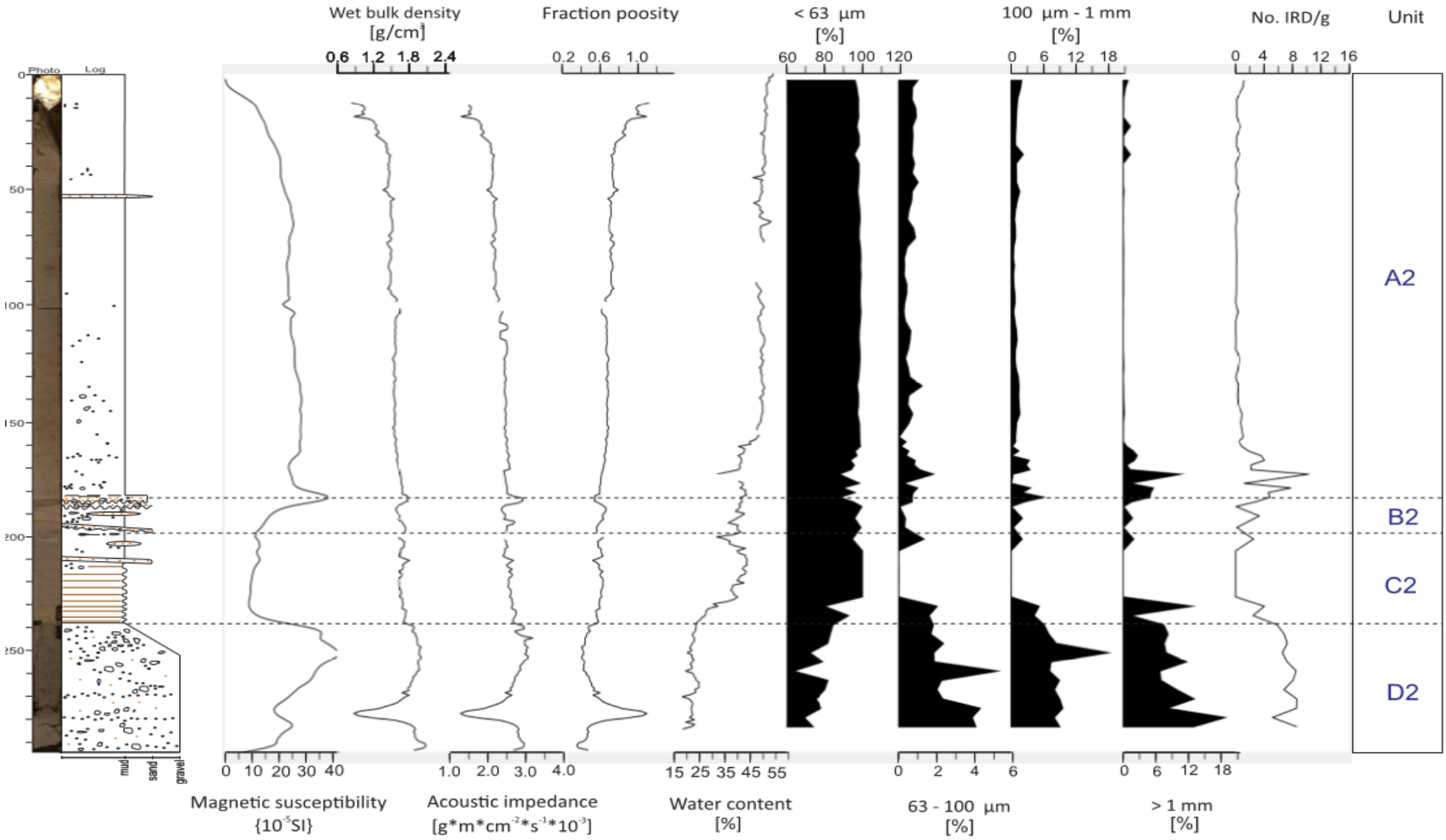


**Figure 5.12:** Measured physical properties, grain size distribution and IRD-count of core NP05–11–49GC. Units (A2 – D2) are divided by dotted lines. Lithological log and colour photographs are included for reference.

#### 5.2.8.2. Unit C2 (238–198 cm)

Unit C2 is characterized by subtle lineations observed between 238 and 198 cm (Figure 5.10 and 5.11). Mud lamina are seen alternating with thin subhorizontal lamina of 1-4 mm with slightly coarser sediment. The alternation is more frequent in the lower 9 cm of the unit. The interval has a dark greyish brown colour (10YR 3/1) and the sediment is relatively firm. The grain-size distribution graphs display a unit consisting of almost 100 % mud. The boundary to the underlying unit D2 is sharp and situated at 238 cm. A pocket and a bed of sandy mud, with a sharp upper and lower boundary are observed at 210 and 202 cm, respectively. The IRD count show that the unit is almost barren of dropstones. However, few clasts are found in the upper and lower part of the unit. The unit is devoid of biogenic material.

##### 5.2.8.2.1. Physical properties

The magnetic susceptibility in unit C2 drops down to 9(*$10^5$ SI) and is relatively stable throughout the unit (Figure 5.12). The wet bulk density, acoustic impedance and fraction porosity graphs also display a relatively stable interval. However, numerous peaks with slight change of amplitude are observed. The wet bulk density and acoustic impedance show a positive peak for the coarser sandy mud bed and pocket, with a corresponding negative peak observed on the fraction porosity graph. The mean amount of water content is approximately 10% lower compared to the overlying unit. Fluctuations between 32 and 44% are observed.

##### 5.2.8.2.2. Interpretation

The low magnetic susceptibility and the other relatively stable physical properties correlate well with the stable grain-size distribution with up to 100% mud. The numerous peaks with slight changes of amplitude reflected by physical property graphs, is in concordance to the observed lamination with frequent, but slight change of grain size. The scarce scattered gravels and sandy bed and pocket situated in the upper and lower part of the unit are interpreted as IRD and suggest increased formation of sea ice or iceberg rafting in the area (Dowdeswell et al., 1994; Forwick & Vorren, 2007). The laminated mud with low magnetic susceptibility, indicates rapid deposition from sediment-laden meltwater plumes in an ice-proximal glaciomarine setting (Hambrey & McKelvey, 2000). Laminas displaying slight changes of grain size can be the result of minor change in sediment source or slight changes in the

reigning ocean current regime during deposition (Reading, 1986). The rapid deposition from glacial melt water plumes is indicative of a quick shift from glacier-proximal to more ice-distal environments (Kristensen et al., 2013).

#### 5.2.8.3. Unit B2 (198–182 cm)

##### 5.2.8.3.1 Lithology and stratigraphy

Unit B2 is 17 cm long and strongly dominated by mud. However, several beds and pockets of muddy sand or sandy mud of varying colours also characterize the unit (Figure 5.11). The unit is barren of biogenic material and has a gradual upper boundary. A one cm thick undulating sandy mud bed is identified at 195 cm. An olive grey (5Y 4/2) colour is observed between 194 and 192 cm. At 190 cm, a pocket consisting of sandy mud is found. Two laminas with dark olive grey (5YR 3/2) colour are observed at 184 and 183 cm. The laminas are less compact and more water saturated compared to the over and underlying sediment. Two beds, with undulating boundaries, are found at 187 and 185 cm. The beds consist of a sandy mud matrix with several gravels. The abundance of IRD vary from 0 to 8 clasts per gram.

##### 5.2.8.3.2. Physical properties

The physical properties correlate well to the sedimentology and the created log (Figure 5.12). The observed muddy sand lenses and beds observed between 195 and 185 cm correspond to an increase of the magnetic susceptibility, wet bulk density and acoustic impedance values, with a corresponding decrease of the fraction porosity values down-core. Unit B2 has the most fluctuating water content compared to the other units.

##### 5.2.8.3.3. Interpretation

The beds and pockets of different colour, grain size and water content indicate varying depositional conditions. The sandy mud beds and pockets with sharp and undulating boundaries, along with the scattered gravel clasts, are interpreted to be IRD (Dowdeswell et al., 1994; Forwick & Vorren, 2007). It can possibly be deposition from long-reaching melt water

plumes (Hundert et al., 2003). The higher amount of IRD, compared to over- and underlying units, can indicate that the the unit was affected by increased glacial activity in the nearby area. The lack of biogenic material suggests harsh glaciomarine conditions (Hald & Korsun, 1997). The changing sediment colour is suggested to be caused by sediment input from multiple source areas (Forwick & Vorren, 2009). The positive peaks displayed by the wet bulk density and acoustic impedance graph, with a corresponding negative fraction porosity spike, correlate to the coarser beds and pockets and are interpreted to be caused by the change of grain size. The high amount of IRD and different laminas displaying different colours and degree of compaction suggest deposition in a glacier proximal environment characterized by multiple source sediment input and abundant, but a varying degree of ice rafting. The gradual change into a more stable depositional environment, characterizing the overlying unit A2, suggests  a gradual change into more ice-distal conditions.

### 5.2.8.4. Unit A2 (182–0 cm)

#### 5.2.8.4.1 Lithology and stratigraphy

Unit A2 is 182 cm long and consists largely of massive mud (Figure 5.11). Numerous clasts of very fine to very coarse gravel-size are seen scattered throughout the unit. The abundance of IRD is high with up to 11 clasts per gram in the lower 25 cm of the unit. The rest of the unit is almost barren of IRD. However, a slight increase is observed in the upper 50 cm with clasts consisting increasingly of quartz. The mud fraction strongly dominate the unit with an average of 99% of the total sediment volume. The grain size distribution varies slightly more in the lower 35 cm, with a mud fraction variation between 100– 90 %. Levels with a lower amount of mud display an increase of sand. The upper 183 cm has a dark greyish brown (2.5Y 4/2) colour. A sandy mud bed is observed between 52 and 50 cm.

#### 5.2.8.4.2. Physical properties

The wet bulk density, acoustic impedance and fraction porosity measurements correspond well to the sedimentology (Figure 5.12). The wet bulk density and acoustic impedance display a slight increase with subtle fluctuations around the mean value down-core (Table 5.1). The fraction porosity graph show a matching decline. The coarse muddy sand bed between 52 and

50 cm is reflected on the wet bulk density and acoustic impedance graphs as an increase, with a corresponding decline observed on the fraction porosity graph. The magnetic susceptibility of the unit has a mean value of 22 (*$10^5$ SI). A rapid decrease is observed in the upper 60 cm. A slight increase is observed throughout the rest of the unit.

The water content decreases slightly down core and has a mean value of 50% in the upper 150 cm. A drop is observed at 160 cm. The grain size distribution also reflect this drop with a mud fraction decrease from 99 to 87%. The water content fluctuates more in the lower 35 cm of the unit.

#### 5.2.8.4.3. Interpretation

The homogeneous mud interval in unit A2 is interpreted to be marine hemipelagic sediments (Lubinski et al., 1996). The high amount of fines indicates a relatively weak ocean current regime, allowing fines to be deposited (Reading, 1986). The scattered clasts found throughout the unit, along with the muddy sand bed at 50 cm, is interpreted to be IRD deposited from icebergs or sea ice (Dowdeswell et al., 1994; Forwick & Vorren, 2007). The higher amount of IRD in the upper and lower part of the unit can suggest increased iceberg rafting. The increase of quartz clasts is suggested to be the result of IRD originating from distant sources far from Svalbard (Jessen et al., 2010). The increase of sand and drop stones in the lower part of the unit is indicative of increased ice rafting. The slight increase of wet bulk density and acoustic impedance, along with a slight decrease of fraction porosity and water content is caused by an increased degree of compaction down-core. The sediments are, based on this, suggested to be post-glacial accretion of sediments from rainout from the water column in a glaciomarine and ice-distal environment. This is correlative with the top surface drape layer observed on the seismic profile displaying the location of core NP05–11–49GC (see *5.1.3.2. Interpretation;* figure 5.3).

## 5.2.9. Core of NP05–11–51GC2 – Eastern Erik Eriksen Strait

The core was retrieved from a water depth of 327 m in the eastern part of the Erik Eriksen Strait (Figure 2.1 and 5.1). The total length of the core is 176 cm (Table 3.1). The unit is subdivided into two units, unit A3 and B3, based on lithofacies association, grain size data and physical properties (Figure 5.13 and 5.14). Sediment facies that comprises this core are: Fm (Fines (silt and clay), massive), Sm (Sand, massive), D (Diamict, massive), (m2) (Matrix-supported, moderate), 1 (loose, not compacted).

### 5.2.9.1 Unit B3 (176–159 cm)

The basal unit B3 is a 19 cm long matrix-supported unit with numerous clasts scattered throughout the unit (Figure 5.13). The matrix consists of sandy mud with a very dark greyish brown (2.5YR 3/2) colour. Biogenic material is lacking. The observed clasts are subrounded to subangular and vary in size from very fine to very coarse gravel. The unit is more compact compared to unit A3, but still easily excavated.

#### 5.2.9.1.1. Physical properties

The physical property graphs correlate well to one another (Figure 5.14). The wet bulk density and acoustic impedance graphs display a jump in value for the lowest 20 centimetres of the core. A corresponding decrease is displayed by the fraction porosity graph. A large positive magnetic susceptibility spike of 68 ($x10^{-5}$ SI) is observed at 156 cm.

A significant drop of water content is observed corresponding to the boundary between the two units.

#### 5.2.9.1.2. Interpretation

The increase of wet bulk density, acoustic impedance and the decrease of fraction porosity and water content observed for unit B3 is interpreted to be a result of a change of lithology between the two units. Unit B3`s lack of biogenic material suggests cold and harsh

glaciomarine conditions (Hald & Korsun, 1997). The numerous subrounded to subangular clasts suspended in a sandy mud matrix suggest that unit B3 is a diamict sediment. Unit B3 is relatively soft and subglacial till is often over consolidated (Ó Cofaigh et al., 2007). The higher content of sand and scattered clasts, compared to unit A3, is therefore indicating iceberg rafted deposition from icebergs or sea ice (Dowdeswell et al., 1994; Forwick & Vorren, 2007). Unit B3 is suggested to reflect rainout of IRD during deglaciation in a glaciomarine environment close to a glacier front. The core penetrates into a seismic layer interpreted to reflect thin subglacial deformation till, or a diamictic layer representing a transitional facies and ice-proximal deposition from a retreating glacier front during deglaciation by Hogan et al. (2010; see 5.1.4.2. *Interpretation;* Figure 5.4). Unit B3 is correlative with this unit and further suggests IRD rainout during deglaciation, however the unit can also be a thin subglacial deformation till.

### 5.2.9.2. Unit A3 (159–0 cm)

#### 5.2.9.2.1. Lithology and stratigraphy

Unit A3 comprises of 159 cm of mostly massive mud (99 %) with a dark greyish brown (2.5Y 4/2) colour (Figure 5.13). Few scattered subangular to subrounded clasts are observed, with a higher abundance in the lower part of the unit. Scarce black coal pieces are scattered throughout the unit. A subhorizontal lamina of weak red (2.5YR 4/2) colour is observed bordering the basal unit. An undulating lamina with a muddy sand matrix and several gravels and pieces of coal is found above, at 157 cm. A pocket of sand is observed at 156 cm. Between 152–150 and 155–153 cm, two greyish brown subhorizontal beds are observed separated by a darker greyish brown lamina. The unit contains few shell fragments and is characterized by bioturbation (Figure 5.15). The unit has a gradual lower boundary.

#### 5.2.9.2.2. Physical properties

The physical property graphs display few fluctuations and correspond well to each other (Figure 5.14). The basal part of the core display higher amplitude spikes compared to the rest of the unit. A negative spike is observed at 14 cm on the wet bulk density and acoustic

impedance graphs, with a corresponding positive fraction porosity spike. The values are mostly situated around the mean values (Table 5.1). A slight increase down-core is displayed by the magnetic susceptibility, wet bulk density and acoustic impedance graphs, and a corresponding slight decrease displayed by the fraction porosity graphs. The magnetic susceptibility mean value of the core is 23 ($x10^{-5}$ SI). A negative and positive spike of 68 and 9 ($x10^{-5}$ SI) are displayed at 156 and 105 cm respectively.

The top of the core display the maximum amount of water (47%). A decrease is observed in the lower 28 cm of the unit. Slight fluctuations around 43% are observed in the upper 131 cm.

#### 5.2.9.2.3. Interpretation

The slight increase of the magnetic susceptibility, wet bulk density and acoustic impedance down-core, with a corresponding fraction porosity decline is suggested to be caused by increased compaction of sediments. The dominance of massive mud suggest accumulation of suspended sediments in a depositional environment with low ocean current activity (Reading, 1986; Lubinski et al., 1996). The few scattered clasts are interpreted to be IRD deposited from icebergs or sea ice (Dowdeswell et al., 1994; Forwick & Vorren, 2007). Increased occurrence of IRD in the lower part of the unit suggests increased iceberg rafting. Bioturbation indicates that the sediments are not reworked and is indicative of biological activity in the area (Forwick & Vorren, 2007). The beds and laminas of different grain size, water content and colour, observed above unit B3, is indicative of slight changes in the reigning ocean current regime during deposition, or deposition from long-reaching and non-eroding melt water plumes. It can also be the result of input from multiple source areas (Reading, 1986; Hundert et al., 2003; Forwick & Vorren, 2009). The boundary to the underlying unit B3, characterized by many dropstones, is gradual and suggests a gradual change into increasingly ice-distal conditions with less ice rafting and a steadier sediment depositional conditions. Hence, unit A3 is interpreted to be post-glacial accumulation of suspended sediments, mostly of Holocene origin, deposited in a glaciomarine ice-distal environment. It is correlative to the post-glacial surface drape observed on the seismic profile of the core site (See *5.1.4.2. Interpretation; Figure 5.4).*

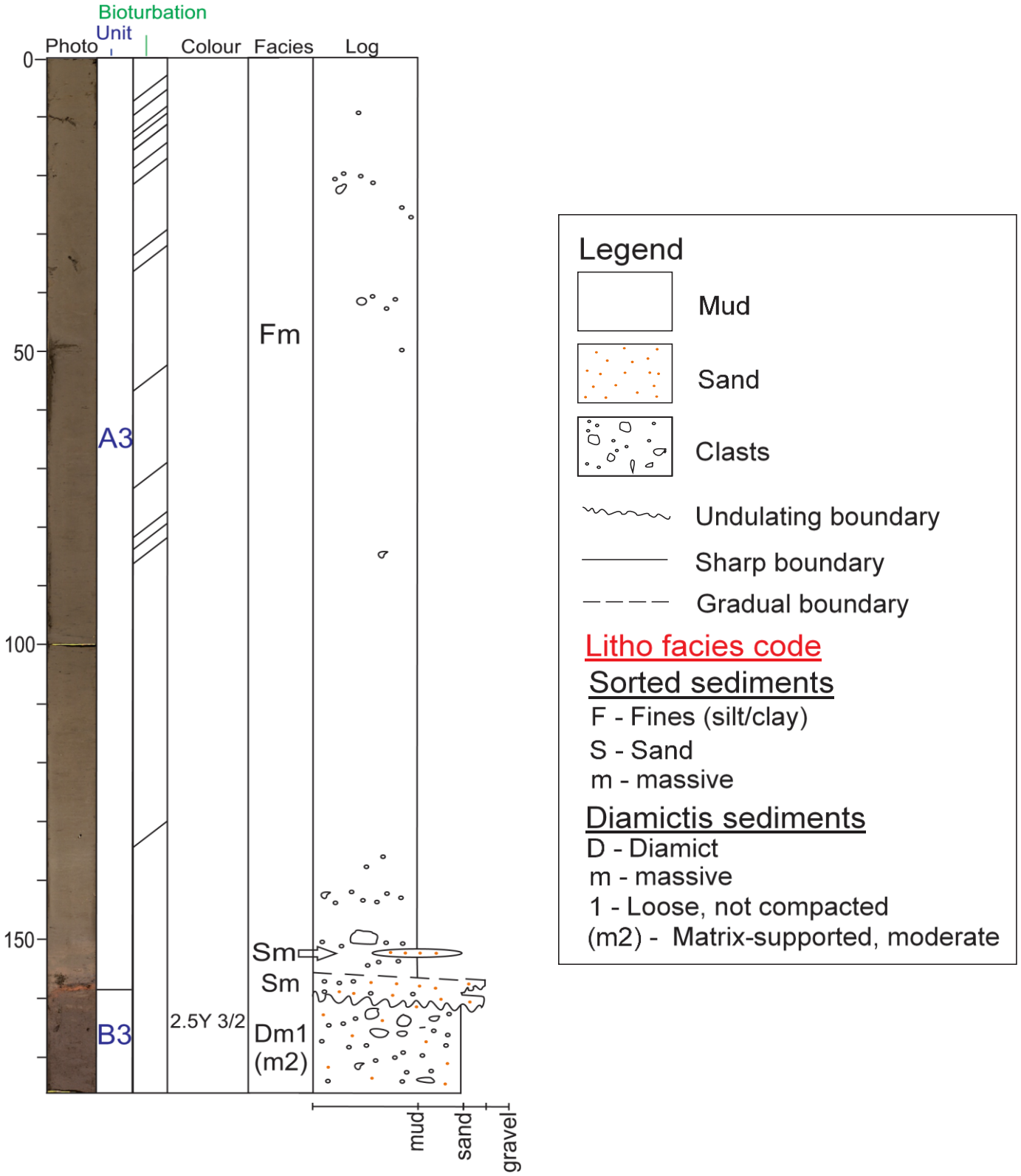


**Figure 5.13**: Lithological log of core NP05–11–51GC2 displaying colour photos, units, bioturbation, Munsell colour codes, lithofacies codes and structures .

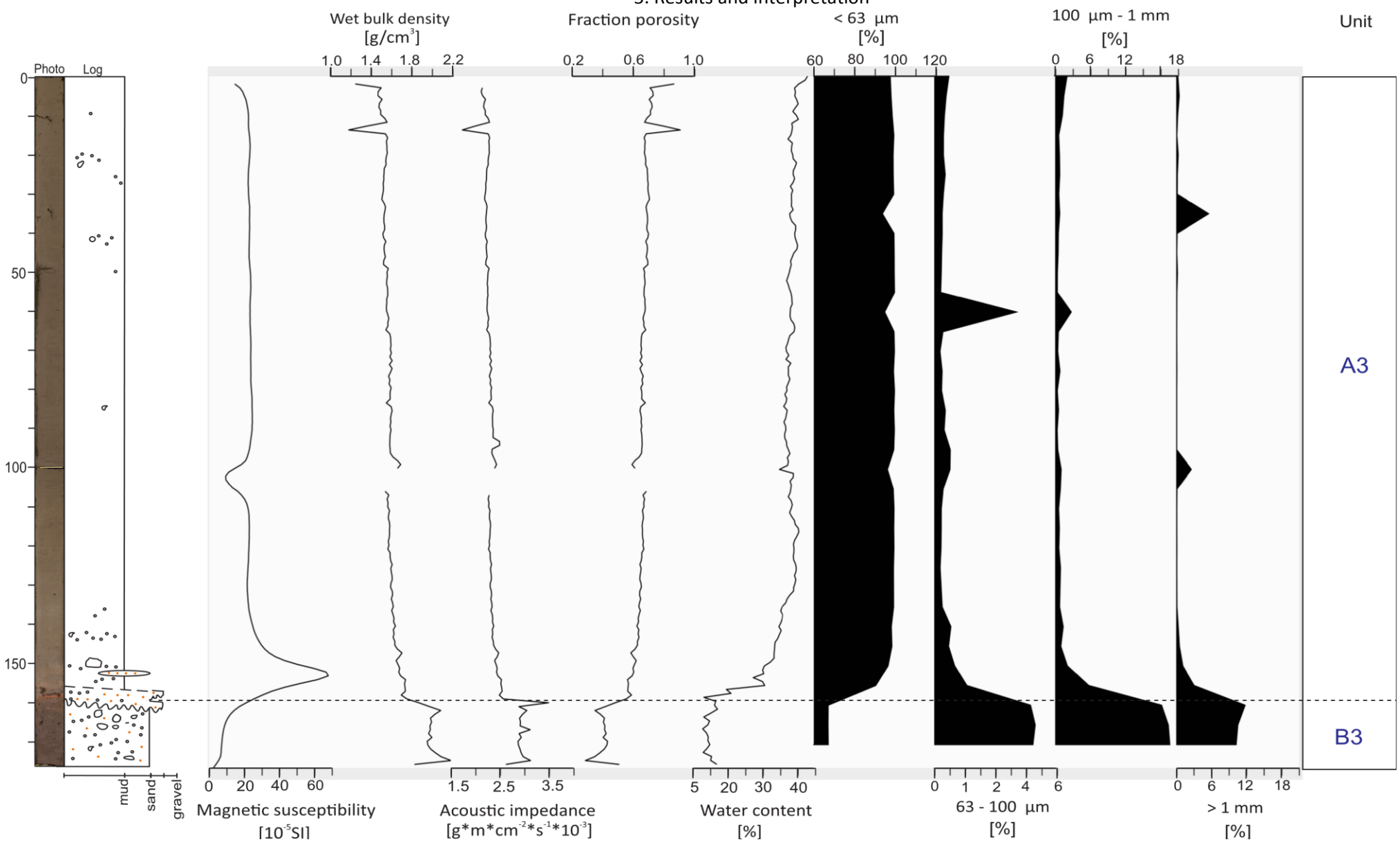


**Figure 5.14:** Measured physical properties and grain size distribution of core NP05–11–51GC2. Units (A3 – B3) are divided by dotted lines. Lithological log and colour photographs are included for reference.

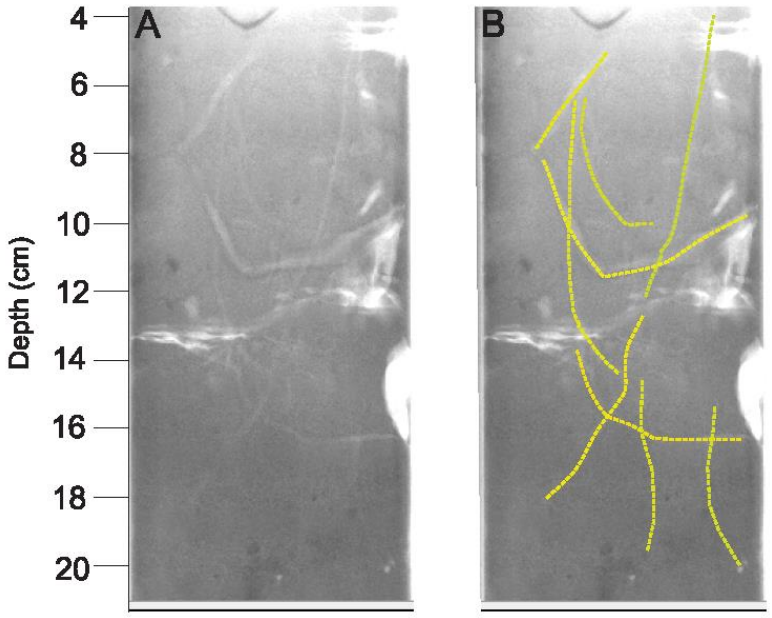


**Figure 5.15: A:** Two identical x-ray photographs (**A** and **B**) displaying unit A3 (4–22 cm) of core NP05–11–51GC2. **B:** Includes interpretation of bioturbation marked by yellow dotted lines.

## 5.3. Description of biozones

The distribution patterns of benthic foraminiferal species are analysed for the upper 185 cm of core NP05–11–49GC, where a minimum of 300 specimens in each sample were found. Continuous plots present the percentage of each of the 15 identified benthic calcareous species and the agglutinated foraminifera relative to the total amount of foraminifera in a sample (agglutinated plus calcareous specimens) down-core . Continuous plots displaying the total amount of benthic and planktic foraminifera per gram dry weight sediment relative to depth is also presented (Figure 5.16 and 5.17).

The core has been divided into 4 assemblage zones, referred to as assemblage zone 1–4, based on the change in distribution of the dominating species in different intervals. Description of the assemblage zones are presented in stratigraphic order, from the oldest and lowermost zone to the youngest and uppermost zone.

The dominating species of the assemblage zones are indicative of characteristics of the environment they lived in (See 4 *Benthic foraminifera*). A short interpretation are presented of every zone. Further discussion of the different assemblages, sedimentological

characteristics and reigning environmental factors are given in chapter *7 Discussion and Correlation*.

### 5.3.1. Assemblage zone 1: *Cassidulina neoteretis and Islandiella norcrossi* (185-160 cm)

The assemblage zone starts at 185 cm with a clear change from sediments almost barren of foraminifera to sediments where minimum 300 specimens are found (Figure 5.16 and 5.17). The lower part of the zone is characterized by a significant peak and the maximum amount of 216 benthic foraminifera per gram, before a drop and oscillating values are observed. The total number of species is slightly lower than overlying assemblage zones. The zone can roughly be divided into two steps based on prominent positive peaks displayed by the dominating species. The lowermost step, between 185 and 169 cm, show an increase and a dominance of *C. neoteretis* with a peak value of 55% and *C. lobatulus* at 23%. The abundance of *C. neoteretis* is generally high throughout the zone. This step contains a high amount of planktic foraminifera, which is in contrast with the overall low abundance in the rest of the core. Two peaks of up to 25 planktic foraminifera per gram are observed at 179 and 171 cm. The uppermost step, between 165 and 161 cm, display a dominance *of I. norcrossi* (63%) and *M. barleeanus* (25%). The assemblage zone display fluctuating percentages of *C. reniforme* with a maximum value of 33 % at 169 cm. The zones has the highest, however slight, occurrence of *A. gallowayi* of the core, which is almost absent in the overlying assemblage zones.

#### 5.3.1.1. Interpretation

The rapid change from sediments almost barren of foraminifera to foraminifera-rich sediments suggest a sudden change to less harsh conditions characterized by high biological activity. The fluctuating abundance of the dominating species implies an environment varying in current strength, salinity and temperature. The maximum amount of benthic foraminifera per gram points to highly productive conditions. However, this peak can be due to little dissolution of the calcareous forms due to less corrosive conditions (Hald & Steinsund, 1992).

The lower occurrence of *C.reniforme* suggest a change towards warmer bottom water (Polyak et al., 2002). The first step dominant species *C. neoteretis* is related to Atlantic water. Together with the decline in relative abundance of *C. reniforme,* it suggest a warming of the bottom-water (Ślubowska et al., 2005; Rasmussen et al., 2007). *Cibicides lobatulus* together with *A. gallowayi* suggests an environment influenced by stronger bottom currents (Steinsund et al., 1994; Wollenburg and Mackensen, 1998). *Cassidulina neoteretis* prefers deeper water (Rosoff & Corliss, 1992), and its dominance coincides with the highest abundance of planktic foraminifera for the core. This suggests a period with inflow of Atlantic water as a subsurface layer in a stratified water column with extensive, near-permanent sea-ice cover (Polyak & Solheim, 1994; Lubinski et al., 2001; Jennings et al., 2004). The high amount of planktic foraminifera, along with the benthic species that prefer deeper water, suggest an over-deepening and increased paleo sea level. The maximum abundance of cold bottom water thriving *C. reniforme*, along with a decrease of other dominant species at 169 cm, suggests a temporary cooling of the water masses and hence a possible reduction in the inflow of Atlantic water (Ślubowska et al., 2005; Rasmussen et al.,2007).

*Islandiella norcrossi* and *M. barleeanus* reach their maximum abundance in the upper step of the zone and are both suggested to reflect an inflow of chilled Atlantic-derived water (Hald & Steinsun, 1992). They further indicate increased salinities and increased fluxes of organic material to the seabed, possibly due to ice edge algal blooms (Hald & Steinsund, 1992; Steinsund et al., 1992). This indicates that the sea-ice was retreating and the sea-ice cover became seasonal. The rapid decrease of the dominating species towards the overlying assemblage zone 2, suggests a sudden change of bottom water conditions (Ślubowska et al., 2005).

### 5.3.2. Assemblage zone 2: *Cassidulina reniforme* (160 – 123 cm)

Assemblage zone 2 starts a 160 cm and is marked by a significant drop in the relative abundance of *C. neoteretis, C. lobatulus, M. barleeanus* and planktic foraminifera (Figure 5.16 and 5.17). The zone is strongly dominated by *C. reniforme* making up 80 % of the total fauna in the lower part of the zone. A gradual decrease down to 47% is observed up-core. *Buccella* spp. occur at 151 cm and is observed fluctuating between 2 and 8 % throughout the zone. *Elphidium excavatum* occurs in the lower part of the zone with an abundance of 6%. The graph displaying the number of benthic foraminifera per gram show a slight decrease, the number of species per sample show a slight increase up-core. A relative abundant species in assemblage zone 3, *E. subarcticum,* occurs at 140 cm with a maximum abundance of 6%. *Melonis barleeanus* increase towards the end of the zone with a maximum abundance of 27% at 127 cm. This correlates with the maximum abundance of *E. subarcticum.* A rapid decrease of the two species are observed towards the overlying assemblage zone.

#### 5.3.2.1. Interpretation

*Cassidulina reniforme's* strong dominance is indicative of cold bottom waters with seasonal sea-ice cover. It suggest a distal glaciomarine environment with salinity above 30psu under the influence of chilled Atlantic water (Hald & Vorren, 1987; Polyak & Solheim, 1994; Hald & Korsun, 1997). The introduction of *M. barleeanus* further points to the inflow of chilled Atlantic water, and is also indicative of higher sedimentation rates and fine sediments with high and steady rates of partly degraded organic carbon (Mackensen et al., 1985; Caralp, 1989; Steinsund et al., 1994). The slight increase of *E. excavatum* and *E. subarcticum* up-core suggest a lowering of the salinity (Steinsund et al., 1994; Hald & Steinsund, 1996; Hald & Korsun, 1997). The increase of *Buccella* spp. further suggest a polar environment with seasonal sea ice and ice edge algal blooms.

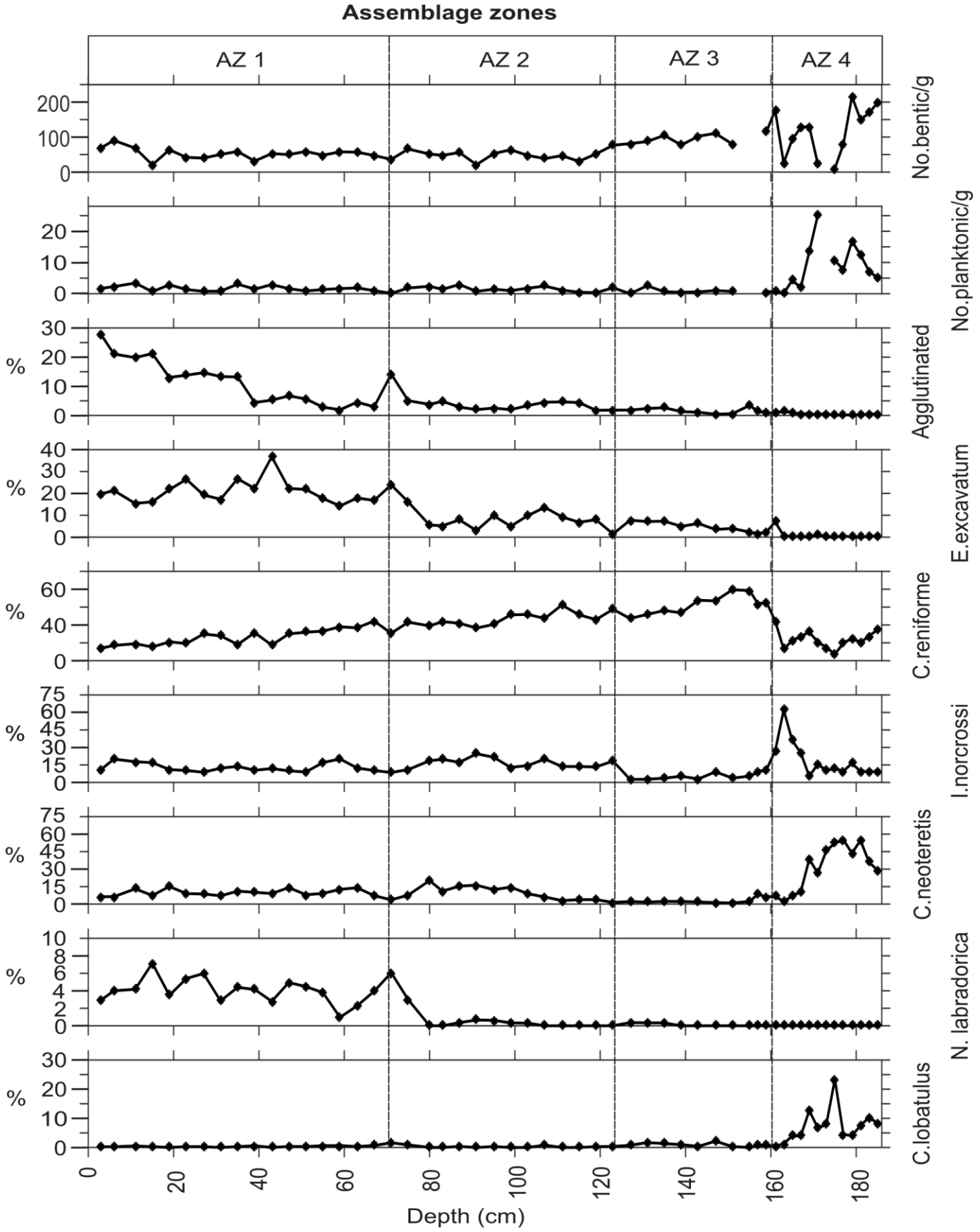


**Figure 5.16:** Number of planktic and benthic foraminifera per gram plotted against depth. Percentages of agglutinated and most common benthic calcareous foraminifera plotted against depth.

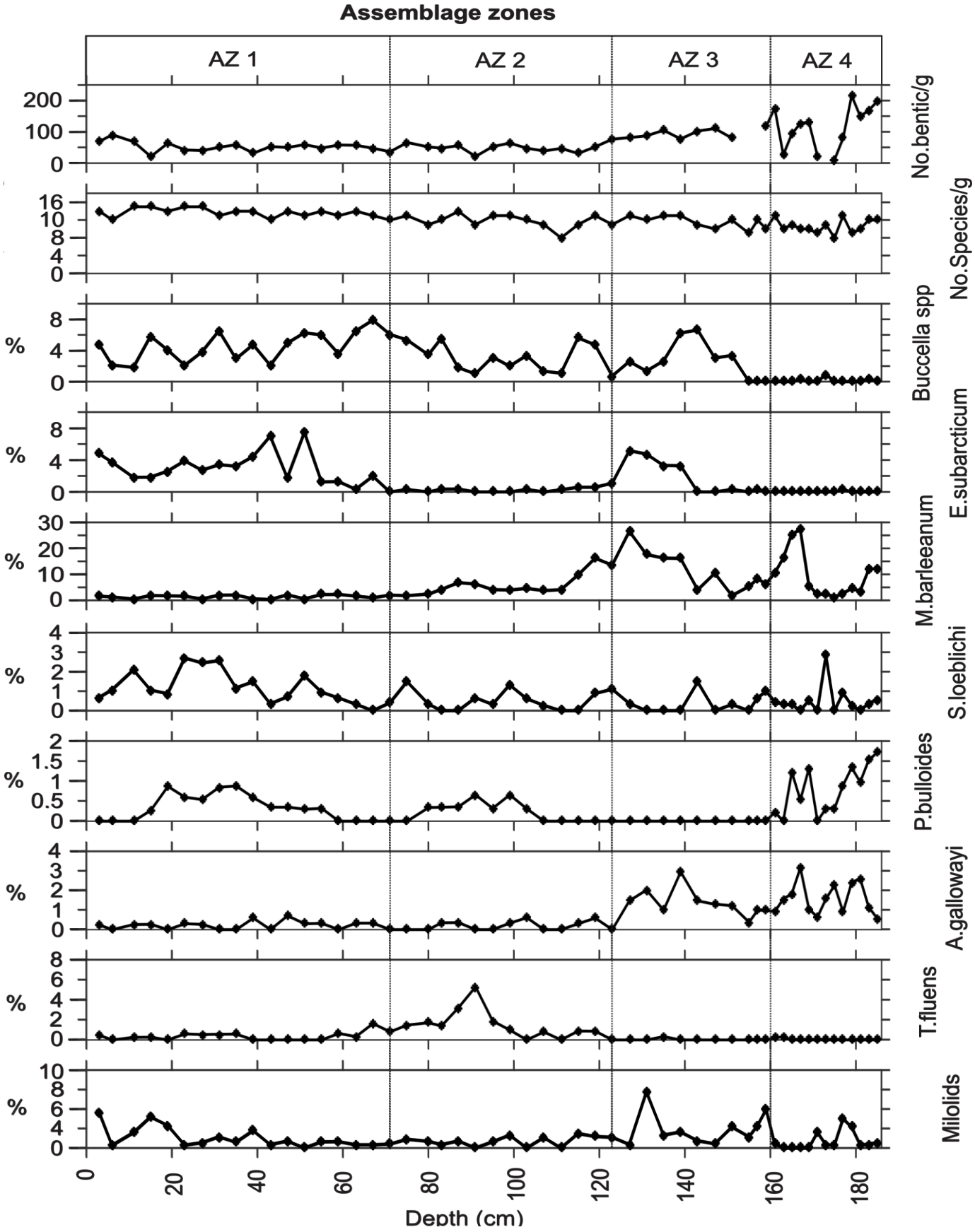


**Figure 5.17:** Number of benthic foraminifera per gram and number of species per gram plotted against depth. Percentages of most common benthic calcareous foraminifera plotted against depth.

### 5.3.3. Assemblage zone 3: *Cassidulina reniforme* and *Islandiella norcrossi* (123–70 cm)

The start of assemblage zone 3 at 123 cm is characterized by a drop in the relative abundance of several species (Figure 5.16 and 5.17). *Melonis barleeanus* drops from 27 to 4% and *E. subarcticum* from 5 to 1%. A slight negative oscillation is also observed on the graph displaying the abundance of *E. excavatum*. The decrease of these species are correlative with an increase of *I. norcrossi* from 3 to 18%, and a slight increase of *C. reniforme.* The number of benthic foraminifera per gram also display a drop at 123 cm from 77 to 30. *Cassidulina reniforme* dominates the fauna, however a decrease from 60 to 30% is observed throughout the zone. Positive oscillations of *C. reniforme* correlate to negative oscillations of *I. norcrossi.* The mean relative abundance of *E. excavatum* is 8% and the species increase slightly throughout the zone. *Cassidulina neoteretis* is observed increasing to 15% at 99 cm. The species fluctuates around 10% throughout the zone. A positive peak and a maximum abundance 5% of *T. fluens* is observed at 91 cm.

#### 5.3.3.1. Interpretation

The rapid of decrease of several species suggest a sudden change in environmental conditions. *I. norcrossi* increases while other species, along with the number of benthic foraminifera, decrease. *Islandiella norcrossi* is associated with ice edge alga blooms. The positive oscillation of *I. norcrossi,* with correlating negative oscillations of *C. reniforme*, indicate that a frontal system was located in close proximity of the core site (Steinsund et al., 1994). The maximum abundance of *T. fluens* and high percentages of *I. norcrossi* at 91cm points further to a nearby location of a front system, as *T. fluens* is associated with highly productive mixing zones between Atlantic and Arctic water (Steinsund et al., 1994). The positive oscillation of *C. reniforme* and negative oscillation of *E. excavatum* at 123cm suggest a slight salinity increase. However, the overall decrease of *C. reniforme* and increase of *E. excavatum* suggest a lowering of the salinity, a decrease in the inflow of Atlantic water and harsher environmental conditions (Kristensen et al., 2013). *Elphidium excavatum* is an opportunistic species associated with glaiomarine enviroments (Steinsund et al 1994; Hald & Steinsund, 1996; Hald & Korsun, 1997). The zone is therefore interpreted to reflect a change to a cooler climate. The dominance of *C. reniforme* suggest continued inflow of Atlantic water with cold bottom waters and seasonal

sea ice cover. The increase of *C. neoteretis* at 99cm suggest renewed and stronger Atlantic water inflow (Kristensen et al., 2013).

### 5.3.4. Assemblage zone 4: *Cassiduline reniforme* and *Elphidium excavatum* (70–0 cm)

Assemblage zone 4 is dominated by *E. excavatum, I. norcrossi* and *C. reniforme* with maximum values of 27%, 20% and 44%, respectively (Figure 5.16 and 5.17). *Elphidium excavatum* varies in abundance and displays an increase with a maximum relative abundance of 38%, before a declining trend within the upper 45cm is observed. *Cassidulina reniforme* decreases significantly throughout the zone, but still displays percentages above 20% in the upper part of the core. Other relatively abundant species are *C. neoteretis* (16%), *E. subarcticum* (8%), Buccella *spp* (8%) and *N. labradorica* (7%). *Nonionella labradorica* increases from 0 to 7% at 71 cm and is present throughout the upper part of the zone. This assemblage zone contains the largest amount of agglutinated species, with the highest peak in the uppermost sample (28%). Most of the agglutinated foraminifera are of *Reophax* species. The overall concentration of benthic and planktic foraminifera fluctuates. An increase in concentration of benthic foraminifera is observed within the top samples.

#### 5.3.4.1 Interpretation

The high relative abundance of *C. reniforme, E. excavatum* and *I. norcrossi* suggest ice-distal to ice-proximal glaciomarine conditions (see 4. *Benthic foraminifera*). The dominance of *E. excavatum* indicate colder bottom water along with a decrease of salinity. High precentages of *E. excavatum* further suggests harsher conditions, probably related to more extensive seasonal ice cover, waters with high turbidity, high sedimentation rates and increased glacial activity (Hald & Steinsund, 1996; Hald & Korsun, 1997; Jennings et al., 2004; Rasmussen & Thomsen, 2014). The occurrence of *C. neoteretis* suggest continued inflow of Atlantic water, however the decrease of *C. reniforme*, along with the increase of *E. excavatum,* suggest a reduction of the inflow (Polyak et al., 2002). The occurrence on *N. labradorica* together with *I. norcrossi* and Buccella *spp*. reflect high organic fluxes to the seabed. This suggests the area

was under the influence of a front system with seasonally sea ice cover and high productivity environments related to the ice margin (Polyak & Mikhailov, 1996; Zajaczkowski et al., 2010).

In the upper 15 cm of the zone, record a return to a modern day foraminferal distribution with a dominance of *E. excavatum* and *C. reniforme*, along with a high amount of number of foraminifera per gram. The high abundance of agglutinated forms suggest corrosive bottom waters caused by brines, or high productivity and thus increased organic material in the bottom sediments (Rasmussen & Thomsen, 2014).

## 5.4. Stable Isotopic analysis

Stable isotope analysis on oxygen and carbon isotopes of the benthic foraminifera sampled from key core NP05–11–49GC are presented as continuous plots against age for the upper 185 cm of core, where sufficient foraminiferal material was available for analysis (Figure 5.18). The infaunal *N. labradorica* and *M. barleeanus* record the pore water temperature and salinity changes. The epifaunal *C. lobatulus* record bottom water temperature and salinity changes. Discussion and interpretation of the stable isotope record, along with comparison to other proxies, are done in 7. *Discussion and Correlations*.

### 5.4.1. Description $\delta^{18}O$ values

The $\delta^{18}O$ values (ice volume corrected; Figure 5.18) measured on the epifaunal *C. lobatulus* are oscillating and low (2.2–3.5‰) between 12 650 and 11 300 cal. yr BP. The infaunal *N. labradorica* values oscillate between 3.7–4.2‰ are relatively stable in the upper 5800 cal. yr BP. The values in the overlap interval between *M. barleeanus* and *C. lobatulus* between 11 600 and 11 300 cal. yr BP display correlative oscillations. The infaunal *M. barleeanus* show increasing values from 3.7 to 4.6‰ until 8300 cal. yr BP. A decrease until 7600 is observed, before the values stabilize and fluctuate slightly between 3.8 and 4.1‰ until 4100 cal. yr BP.

### 5.4.2. Description $\delta^{13}C$ values

The measured $\delta^{13}C$ values (Figure 5.18) on the epifaunal *C. lobatulus* are relatively high (0.6 – 1.2) between 12 650 and 11 300 cal. yr BP. The measurement of $\delta^{13}C$ are done to obtain

information of the water mass ventilation through time. As *N. labradorica* and *M. barleeanus* are infaunal and therefore record information of pore water, their $\delta^{13}C$ values are not further discussed.

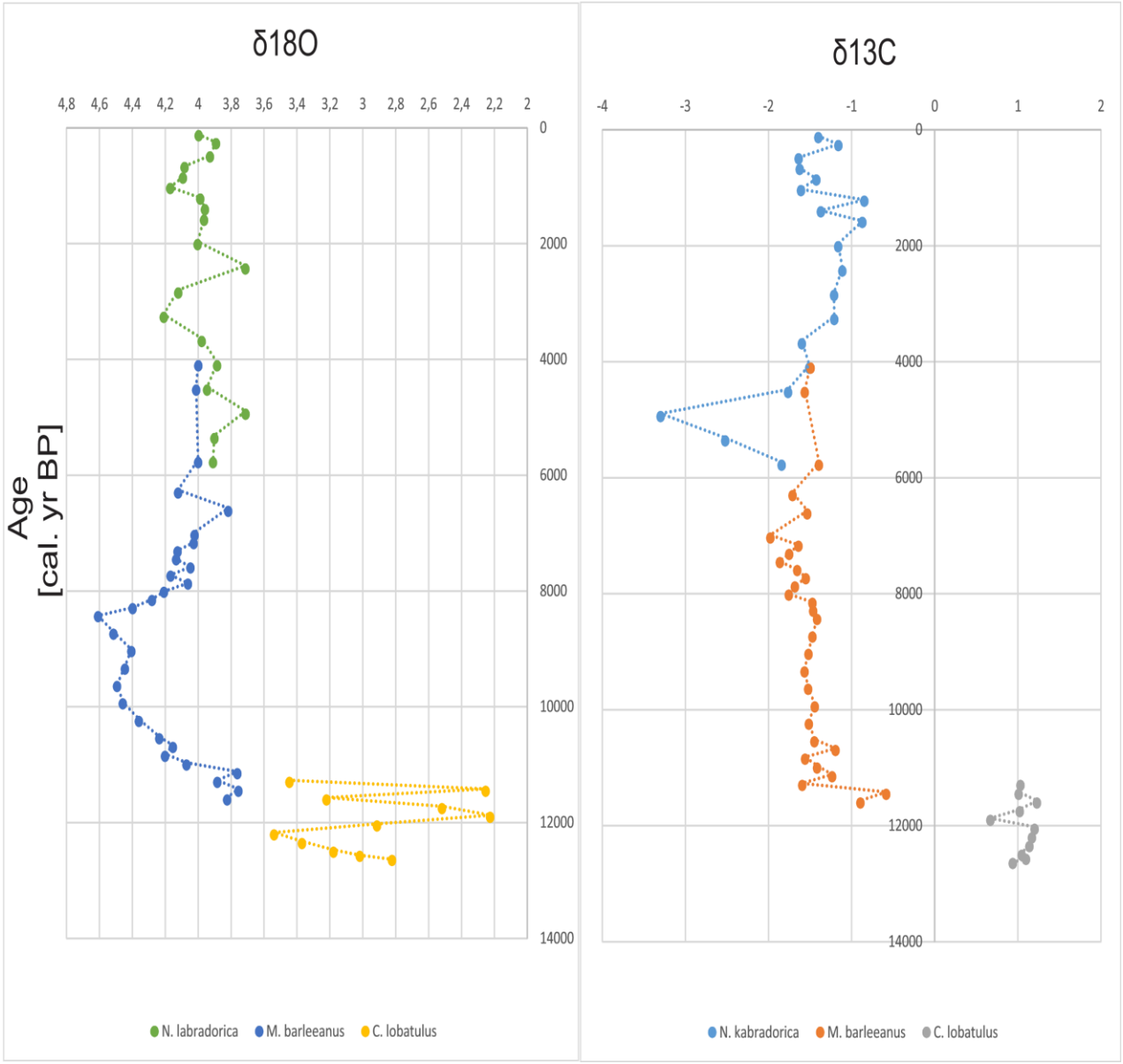


**Figure 5.18:** Left graph display the stable oxygen isotope record measured on *Cibicides lobatulus, Melonis barleeanus* and *Nonionella labradorica* of the top 185 cm of core NP05–11–49GC plotted against age. *Cibicides lobatulus* is displayed in yellow, *Melonis barleeanus* in dark blue and *Nonionella labradorica* in green. Right graph display stable carbon isotope record measured on *Cibicides lobatulus, Melonis barleeanus* and *Nonionella labradorica* of the top 185 cm of core NP05–11–49GC plotted against age. *Cibicides lobatulus* is displayed in grey, *Melonis barleeanus* if orange and *Nonionella labradorica* in light blue.

# 6. Chronology

## 6.1 Correlation of radiocarbon dates

High precision dating is important to get the timing of observed events in a data set. In addition, high precision dating is needed to get an accurate correlation between different data sets.

Four accelerator mass spectrometry (AMS) radiocarbon dates, obtained from the core NP05–11–49GC, make up the basis for the chronology of this core (Table 6.1). The CALIB 7.0.4 program (Stuiver & Reimer, 1993) and the calibration curve Marine 13 (Reimer et al., 2013) is used to calibrate from radiocarbon dates to calibrated years before present.

**Table 6.1:** Results of radiocarbon dating of core NP05–11–49GC.

| Lab code | Depth (cm) | Radiocarbon age | Cal. Yr BP 1σ range | Cal. Yr BP 1σ mean | Dated material |
|---|---|---|---|---|---|
| UBA-30512 | 35 | 2091±33 | 1544–1656 | 1600±56 | Foraminifera |
| UB-17202 | 87 | 6578±40 | 6969–7112 | 7041±72 | *Nucula* spp. |
| UB-17203 | 127 | 8045±44 | 8389–8499 | 8444±55 | *Nucul*a spp. |
| UBA-30513 | 181 | 11,000±56 | 12032– 12174 | 12.103±71 | Foraminifera |

### 6.1.2 Choice of reservoir age and ΔR for Holocene

Choosing a reservoir age for an area and a time period before dating a sample is difficult and debated (see *3.4.9.3 Marine reservoir effect and calibration*). Mangerud et al. (2006) concludes that the reservoir age and the regional offsets (ΔR) are latitude and time dependant. The sea surface reservoir age is 360 ± 20 years along the west coast of Norway (Bondevik et al., 2006; Mangerud et al., 2006).

The Atlantic Ocean ΔR values varies, and an increase northward along the Norwegian coast is observed (Mangerud & Gulliksen, 1975; Eiriksson et al., 2004; Bondevik et al., 2006; Mangerud

et al., 2006. Mangerud in Mangerud et al. (2006) recommend using the same reservoir age and ΔR for the North Atlantic and the Barents Sea. Gulliksen and Bondevik in Mangerud et al. (2006) concludes that the ΔR values along the Norwegian coast are latitude dependant and increase northwards. Though the results of the study are based upon few dates, the results show a clear trend of increased reservoir age for the Svalbard area. Gulliksen and Bondevik hence suggest a ΔR of 105 ± 24 for the Svalbard area for samples spanning the Holocene.

A ΔR of 105 ± 24, along with a reservoir age of 360± 20, is therefore chosen for the calibration of the samples UB–17202, UB–17203 and UB–30512 of Holocene age.

### 6.1.3 Choice of reservoir age and ΔR for Younger Dryas

A study from the west coast of Norway by Bondevik et al. (2006) revealed an increase of the sea surface reservoir age during the early Younger Dryas to 600 years from 400. After 900 stable years, the reservoir age dropped by 300 years within a century across the Younger Dryas–Holocene transition. Another study by Bard et al. (1994) also detect increased reservoir ages in the North Atlantic during the Younger Dryas of 700 to 800 years. This is caused by a decreased rate of North Atlantic Deep Water formation, making it half as efficient as today. The reduced advection of surface waters to the North Atlantic, together with the presence of sea ice for at least half of the year north of 50° and changes in the positioning of the polar front, causes the increase of the reservoir age (Bard et al., 1994). Sea ice prohibits gas exchange at the ocean-atmosphere interface, leading to a slower mixing of $^{14}C$ into the ocean (Bowman, 1990). Thus, the reservoir age is closely related to changes in ocean circulation in the North Atlantic. Colder periods have higher reservoir ages, while the warmer periods with greater ocean ventilation and circulation, show a lowering of the reservoir age (Bondevik et al., 2006).

The Younger Dryas on Svalbard was characterized by polar surface conditions with extensive sea ice cover and diminished Atlantic-derived water inflow (Ślubowska et al., 2005). Due to the fact that reduced advection of surface waters and an extensive sea ice cover increased the North Atlantic reservoir age, it is likely to assume an increase of the Younger Dryas reservoir age for the Svalbard area. However, similar studies are lacking from the Svalbard–Barents Sea area, which makes the reservoir age here unknown (Rasmussen & Thomsen, 2014). Based on

the studies by Bondevik et al (2006), a reservoir age of 400 ± 20 and a ΔR of 105 ± 24 is chosen for the sample UB-30512 of early Younger Dryas age. This is further discussed in chapter 7.4 Younger Dryas–Holocene Transition)

## 6.2 Age model

The CALIB 7.0.4 program (Stuvier & Reimer, 1993) and the calibration curve Marine 13 (Reimer et al., 2013) is used to calibrate the radiocarbon dates to calibrated years before present. The program uses a global average reservoir age of 408 years, however the reservoir age of 360 ± 20 years and a ΔR of 105 ± 24 is used for the dates of Holocene age. The difference is corrected for by setting the ΔR to 57 years before calibration. For sample UB-30512 of Younger Dryas age, the reservoir age of 400 ± 20 years and a ΔR of 105 ± 24 is used. The difference is corrected for by setting ΔR to 297 years before calibration.

All of the four dates has values well within the highest probability 1σ range. Based on the calibrated probability graph, the age with the highest probability is chosen. An age model is created based upon the four calibrated ages and by assuming a linear accumulation rate between the dated levels (Figure 6.1).

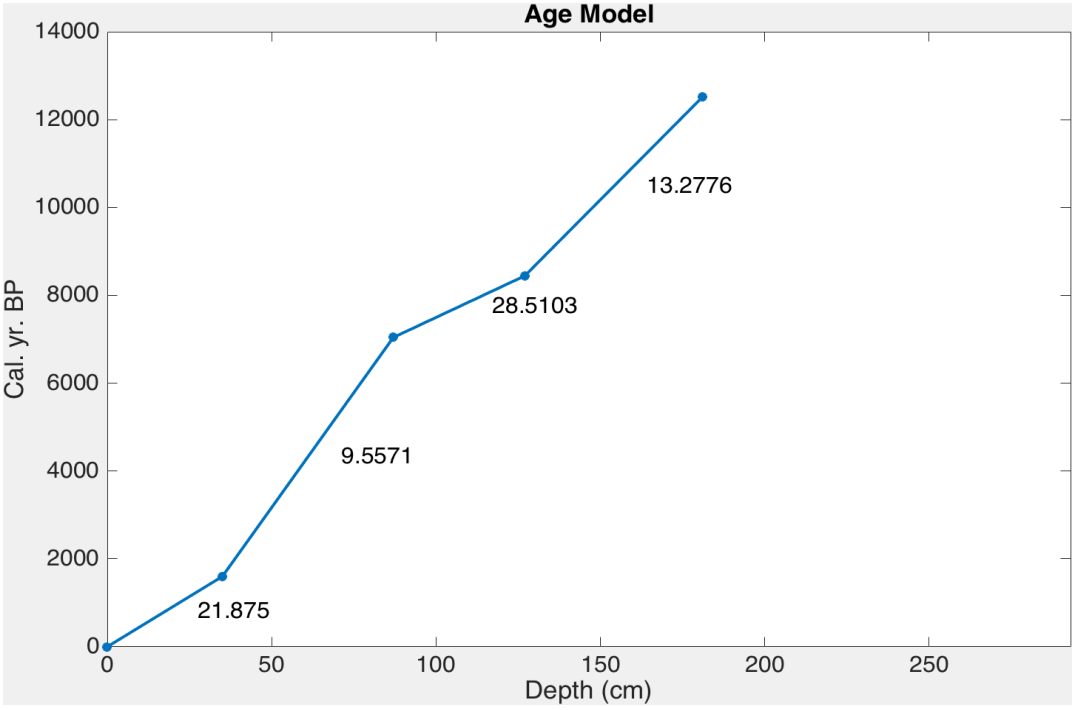


**Figure 6.1:** Age model for core NP05–11–49GC with dated levels in calibrated years before present plotted against depth. The numbers next to the graph show the average sedimentation rate (cm/kyr) between the dated levels.

### 6.2.1 Sedimentation rate

The sedimentation rate, accumulated centimetres of sediment per 1000 years, is calculated for each dated interval (Table 6.2). The average sedimentation rate for the core is 18.68 cm/kyr. The sedimentation rate is lowest in the 1600–7041 Cal. Yr BP interval. The highest rate of sedimentation is observed in the first 1600 years of the core (21.88 am/kyr) and between 7041–8444 Cal. Yr BP (28.51 cm/kyr).

**Table 6.2:** Sedimentation rate for the dated intervals of core NP05–11–49GC.

| Age interval (Cal. Yr. BP) | Depth interval (cm) | Sedimentation rate (cm/kyr) |
|---|---|---|
| 0-1600 | 0-35 | 21.88 |
| 1600-7041 | 35-87 | 9.56 |
| 7041-8444 | 87-127 | 28.51 |
| 8444-12103 | 127-181 | 14.76 |

# 7. Discussion and correlation

A discussion and correlation of the obtained sedimentological and foraminiferal data, with the created age model is presented in the first part of this chapter. The results are divided and discussed within different time intervals from the deglaciation to the present. This is done to reconstruct the Late Weichselian deglaciation and Holocene paleoenvironment and paleoceanography of the study area. The last part aims to put the results in a wider context with observations and implications of the paleoceanography of the Nordic Sea, Barents Sea and the Svalbard margin.

Core NP05–11–49GC make up the basis for this thesis. Interpretation of the lithostratigraphy and the chronology of the core is mainly based on analysis done on this core. The two other cores, NP50–11–51GC2 and NP05–11–84GC2, are included for lithostratigraphic analysis. This is done to get an enhanced understanding of the depositional environment in the Erik Eriksen Strait and Kvitøya Trough.

## 7.1. Deglaciation (16 000–14 100 cal. Yr BP)

Streamlined mega-scale glacial lineations (MSGL), crag and tails and incised channels in hard bedrock were described by Hogan et al. (2010 a and b) from the Kvitøya Trough and Erik Eriksen Strait as being produced at the base of the SBIS as it occupied the troughs and reached out to the northern Barents Sea shelf edge (*See 1.2.2 Previous studies*).

The diamictic units (B1, D2 and B3) from the three investigated cores are all matrix-supported, but vary in degree of compaction and clast abundance (Figure 5.8, 5.11, 5.13). Similar poorly unconsolidated diamicts of different thickness from the Erik Eriksen Strait and Kvitøya Trough are described by Hogan et al. (2010a and b). The three diamicts cores are barren of biogenic material, which suggest deposition in cold climatic and harsh glaciomarine conditions with lowered productivity and possibly high dissolution (Steinsund & Hald, 1994; Hald & Korsun, 1997). Several processes can lead to the formation of a diamict in a glaciomarine environment

(Hogan et al., 2010b). Such processes are direct subglacial deformation and deposition under grounded ice, subaquatic debris flow deposition and rainout of IRD deposited in a sandy mud or muddy sand matrix (Dowdeswell et al., 1994; Hambrey & McKelyey, 2000; Ó Cofaigh et al., 2005; Hogan et al., 2010b).

Hogan et al (2010b) questioned if the looseness and high porosity of the diamicts contradicts direct subglacial deposition from grounded ice. The unconsolidated matrix-supported diamicts observed in the middle part of the Erik Eriksen Strait and at the southern head of the Kvitøya Trough, unit D2 and B3, are therefore interpreted to be the result of rainout of IRD in a glacier-proximal setting during deglaciation. This is further supported by the seismic data displaying a large-scale somewhat homogenous and smooth seabed and an underlying relatively smooth, but distinct sub-bottom reflector correlating with the observed diamicts of the two cores (Figure 5.3 and 5.4).

Diamict B1 was retrieved from an acoustically transparent lobate-form in at the southwestern head of the Erik Eriksen Strait (Figure 5.2). This diamict is slightly more consolidated compared to the diamicts from the middle part of Erik Eriksen Strait and southern Kvitøya Trough. It comprises most of core NP05–11–84GC2. Similar wedge-forms are found in the southwestern head of the strait. The forms were described by Hogan et al. (2010b) as a grounding zone wedge formed during a glacier front still-stand as the SBIS melted and retreated eastward through the trough (Figure 7.1). Comparable subglacial deposits, termed grounding-zone wedges, are found on other glaciated continental margins (Evans et al., 2005; Ó Cofaigh et al., 2005). Based on the wedging geometry, acoustic transparency, and poorly sorted sediment composition it is possible to assume that unit B1 is such a grounding zone wedge. Deglaciation of Arctic shelves occurs either rapidly by floating and break-up of ice, episodically by still-stands or by slow retreat of grounded ice (Dowdeswell et al., 2008). Grounding zone wedges are often formed during a longer still stand or re-advance of a glacier front (Dowdeswell et al., 2008), and hence indicate an episodic retreat of the ice sheet at the southern head of the Erik Eriksen Strait. The hummocky seabed and sub-bottom reflectors situated further east of the wedge-form further suggest grounded glacial activity and are possibly recessional moraines (See *5.1.2 Core site NP05–11–84GC2 – S-W Erik Eriksen Strait*), as grounding-zone wedges are

often associated with moraine ridges (Bachelor & Dowdeswell et al., 2015). However, more seismic and bathymetric analysis are needed to determine the origin if the hummocky seabed. A 2000 to 3000 m thick ice dome is suggested to have been located over Kong Karls Land or southern Hinlopen Strait during the late glacial (Forman et al., 1995; Dowdeswell et al., 2010; *see 1.2.1.1 Late Weichselian and figure 1.2*). Such thick ice can further imply grounded warm-based glacial activity forming grounding-zone wedges during the retreat through Erik Eriksen Strait.

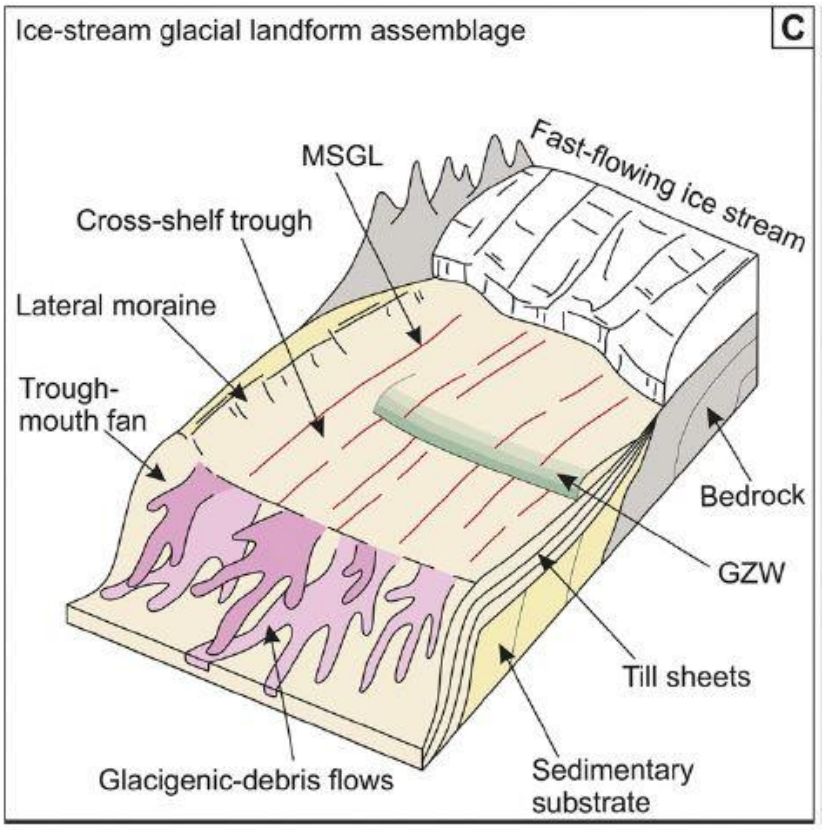


**Figure 7.1:** Schematic diagram displaying the position of a grounding zone wedge deposited as the margin of an ice sheet with a floating ice shelf retreats through a trough (From Batchelor & Dowdeswell, 2015).

Grounding-zone wedges, recessional moraines, debris lobes and other ice-proximal landforms produced in a melt water-dominated environment during still-stands are absent in the Kvitøya Trough. Hogan et al. (2010a) suggested that the absence of grounding events and an icebergturbated sea floor suggests a swift retreat through the trough by floating and break up

of ice, rather than by the release of melt water. Kleiber et al. (2000) also observed this in the Franz Victoria Trough, where a lack of recessional moraines was interpreted to reflect decoupling of the northern glacier bed during deglaciation, leading to a rapid retreat mainly by the release of icebergs. This suggests that deglaciation was first rapid in the Kvitøya Trough, closer to the shelf edge, before the retreat became more episodically with grounding events in lower water depths further in on the continental shelf in the Erik Eriksen Strait. This is further supported by the occurrence of laminated sequences in unit C2 from the middle part of the Erik Eriksen Strait (see *7.2 Bølling–Allerød*). Stiff diamicts were not sampled in the three investigated cores, or by Hogan et al. (2010b) from the Erik Eriksen Strait. An explanation for this can be that a stiffer diamict, formed by warm based active ice, resides underneath the looser diamict formed by IRD-rain out.

Little is known of how the SBIS could have altered the oceanography and the inflow of Atlantic Water to the region. A physical blocking of the water flow is possible, or the ice sheet may have indirectly altered the ocean currents by isostatic suppression in the region, creating seafloor bathymetric changes (Lubinski et al., 2001). Kleiber et al. (2000) suggests that the marine-based nature of the SBIS, made it especially sensitive to sea level changes causing ice sheet decoupling of the glacier bed and a rapid retreat.

As no dates are obtained from the lowest part of the key core NP05–11–49GC, due to the lack of dateable material, estimations of the age of the base of the core remains unconstrained. Based on the lowermost date of 12 103 cal. yr BP at 185 cm, an assumption that the lowermost part was deposited during the deglaciation is reasonable. Since sedimentation rates were on average high for the Svalbard-Barents Sea area during the deglaciation (Dowdeswell & Elverhøi, 2002), the highest obtained sedimentation rate of the core of 28.51 cm/kyr is chosen for the lower part of the core (See *6.2 Age Model*). The maximum age of the core is, based on the created age model, thus estimated to be approximately 16 000 cal. yr BP. However, this age is highly uncertain as it is possible that the lowermost diamictic unit potentially can be slump deposits.

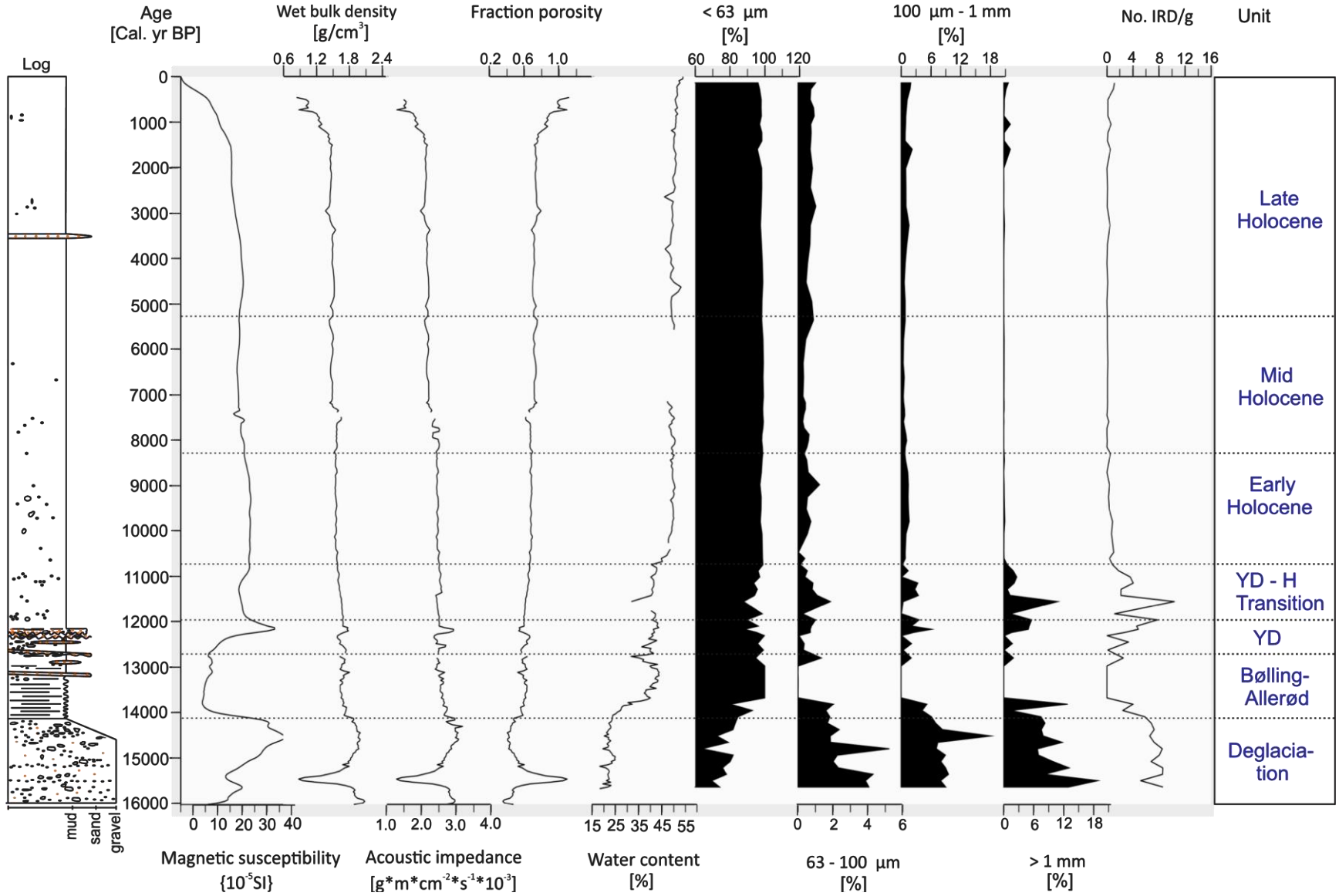


**Figure 7.2:** Log of core NP05–11–49GC with measured physical properties, grain size distribution and IRD-count. Dotted lines mark time zone borders. The abbreviations YD-H Transition stands for Younger Dryas Transition and YD stands for Younger Dryas.

## 7.2. Bølling-Allerød (14 100–12 700 cal. yr BP)

The Bølling–Allerød time-period is recorded as warm interstadials in the Greenland ice cores (Rasmussen et al., 2007). The period was characterized by a relatively strong inflow of Atlantic Water, however still as a subsurface layer (Ślubowska-Woldengen et al., 2008). This relatively warm period resulted in a rapid retreat of the Svalbard-Barents Sea Ice sheet into the fjords with turbid meltwater plumes causing a high sedimentation rate, and the deposition of laminated fine clays (Jessen et al., 2010).

Unit C2 of Bølling–Allerød age above the diamict in core NP05–11–49GC from the central part of Erik Eriksen Strait is characterized by laminated mud with laminas displaying slight changes of grain size and low magnetic susceptibility (Figure 5.11 and 7.2). This is a typical sediment facies deposited from sediment-laden meltwater plumes in a glaciomarine setting (Hambrey & McKelvey, 2000). Rasmussen et al. (2007) observed laminated sediments of Bølling–Allerød age, deposited under extremely high sedimentation rates, in Storfjorden Trough southeast of the Erik Eriksen Strait. Diamicts overlain by laminated sediments, deposited from turbid meltwater plumes of Bølling–Allerød age with a low IRD content, is furthermore found northeast of the study area in the Franz Victoria Trough by Kleiber et al. (2000) and by Duplessey et al. (2001). Kristensen et al. (2013) found a similar laminated sediment facies with low magnetic susceptibility and IRD overlaying diamictic deposits from the unnamed trough east of Erik Eriksen Strait. The laminated muds with thin sandy interbeds of unit C2 is therefore a typical sediment facies deposited in the northwestern Barents Sea corner as the SBIS retreated.

The deglaciation and retreat became, as mentioned in the 7.1 *Deglaciation* subchapter, episodically with still-stands in lower water depths further in on the continental shelf. This is evident by the formation of the grounding zone wedge from the southwestern head of the Erik Eriksen Strait. The laminated sequence found in unit C2 east of the wedge from the middle and deeper part of the Erik Eriksen Strait may therefore represent the deposition of turbid meltwater plumes from a nearby tidewater glacier margin located at the southern head of the

trough. Similar laminated facies, between deglacial diamicts and post-glacial muds, were also observed from the deeper part of Erik Eriksen Strait by Hogan e al. (2010b). The rapid deposition from glacial melt water plumes is indicative of a quick shift from glacier-proximal to a more ice-distal environment (Kristensen et al., 2013).

Unit B1 of core NP05–11–84GC2, retrieved from the grounding-zone wedge at the southern head of the Erik Eriksen Strait (Figure 5.2), lacks this laminated sequence. This can be due to the bathymetric high the wedge-form display in the trough, exposing the sediments to ocean current erosion and prohibiting sediments to settle. This is evident by the short post-glacial mud overlying the diamict. Alternatively, it can suggest rapid retreat with little melt water discharge of the glacier front as it left the southern head of the trough. The lack of a similar laminated sequence in core NP05–11–51GC2 from the Kvitøya Trough is interpreted to reflect rapid glacial retreat governed by extensive iceberg rafting rather than by the release of meltwater. A lack of such an interval was also observed by Hogan et al. (2010a) from the Kvitøya Trough.

Unit C2 from the central part of Erik Eriksen Strait is barren of foraminifera, which suggests an environment influenced by cold climatic and harsh glaciomarine conditions *(see 5.2.4.2. Unit C2*)**.** Based on the foraminiferal distribution in a study by Rasmussen et al. (2007) from the Storfjorden slope and shelf in the southwestern Barents Sea, cold surface conditions with a relatively strong influence of Atlantic water at the bottom were suggested to prevail during the Bølling–Allerød interstadials. Similar conditions with cold surface waters and a subsurface inflow of Atlantic water is recorded in the unnamed trough east of Erik Eriksen Strait by Kristensen et al. (2013), north of the Hinlopen Strait by Koç et al. (2002) and by Hald et al. (1999) from the St. Anna trough. The strong inflow of Atlantic water brought along a flux of warmth to the area (Koç et al., 2002). This led to a retreat of the SBIS into Spitsbergen fjords (Jessen et al., 2010). Set in conjunction with the high sedimentation rates from turbid meltwater plumes, it is likely that the inflow of Atlantic water similarly caused a rapid melting of the SBIS on the eastern side of Spitsbergen during the Bølling–Allerød interstadials. This is

also seen by the deglaciation of Murchinsonfjorden on Nordaustlandet at the end of the Bølling–Allerød interstadials by 12 650 Cal yr. BP (Kubischta et al., 2011).

The colder surface waters and the release of cold fresh meltwater could have led to enhanced sea ice formation and reduced iceberg rafting. This is in concordance with low occurrence of IRD in unit C2, and the other mentioned laminated sequences from the Barents Sea area of Bølling–Allerød age. Alternatively, the higher sedimentation rate could possibly mask the IRD-signal. From 12 900 cal. yr BP more IRD is deposited and found in unit C2 (Figure 7.2) in the central Erik Eriksen Strait, suggesting increased deposition of dropstones from either ice bergs of sea ice. A study from the northern Svalbard shelf by Ślubowska et al. (2005) display similar increased glacial influence towards the end of the Bølling–Allerød interstadials with a deteoriation of water bottom conditions due to further reduced inflow of Atlantic water.

The laminated muds overlaying diamicts represent the minimum age of the glacial retreat in the strait (Dowdeswell et al., 2008). However, due to the lack of biogenic material from this unit, its age is still unconstrained. The upper and lower boundary of unit C2 of Bølling–Allerød age is based on visual description of the sediment, grain size distribution displaying a stronger dominance of mud compared to the underlying diamict and an interval reflecting stable low magnetic susceptibility values (Figure 7.2). Based on the lowermost date of 12 103 cal. yr BP at 185 cm, an assumption that the lower part was deposited during the deglaciation is reasonable. Since sedimentation rates were on average high for the Svalbard-Barents Sea area during the deglaciation (Dowdeswell & Elverhøi, 2002), and the laminated sediments are interpreted to reflect high sedimentation rates and rapid deposition, the highest obtained sedimentation rate of the core of 28.51 cm/kyr is chosen for the lower part containing unit C2 (See 6.2 Age Model). The lower boundary of the laminated unit C2, bordering the diamictic unit D2, is based on the created age model and assumed linear interpolation estimated to be approximately 14 100 cal. yr BP. This early Bølling age is in concordance with the age of laminated sequences in the studies referred to earlier from the northwestern Barents Sea corner. However, more dates enabling better calculations of the sedimentation rates of the lower part of the core is needed to achieve a more accurate timing of the glacial retreat.

## 7.3. Younger Dryas (12 700–11 950 cal. yr BP)

The Younger Dryas, a period associated with cooling and glacial advances at the end of the Late Weichselian glaciation, has been difficult to identify on Svalbard (Mangerud & Landvik, 2007; Ślubowska- Woldengen et al., 2008; Forwick & Vorren, 2009).

Most of the Younger Dryas sediments of unit B2 from the key core of the Erik Eriksen Strait (Figure 5.11 and 7.2), is barren of foraminifera, which reflects a harsh cold environment with low biological activity (see 5.2.4.3. *Unit B2*). Kristensen et al. (2013) found similarly a sparse foraminiferal fauna and a low IRD-signal characterizing the Younger Dryas stadial in the unnamed trough east on Erik Eriksen Strait, which was interpreted to reflect very cold climatic conditions under almost permanent sea-ice cover. Rasmussen et al. (2007) recorded a stronger Polar surface waters inflow with colder and less saline conditions compared to the preceding Bølling– Allerød interstadials in Storfjorden. Low abundance of IRD suspended in a fine grained matrix is recorded several places along the Svalbard margin (e.g Ślubowska-Woldengen et al., 2008). The extensive sea ice cover could have hindered deposition of IRD, as multi-annual and/or shorefast sea-ice can suppress the drift of icebergs (Forwick & Vorren, 2009). This is in concordance with laminas being absent of IRD from the Younger Dryas unit. However, laminas displaying increased IRD deposition are also observed, and the IRD record for the Younger Dryas in unit B2 is overall more varying compared to the preceding Bølling–Allerød interval. This suggests that the Younger Dryas was also was charactherized by seasonal open waters. The increase of IRD can be due to increased iceberg rafting (Forwick & Vorren 2009). Ślubowsk et al. (2005) and Koç  et al. (2002) also recorded seasonal open water during the Younger Dryas from the shelf north of the Hinlopen Strait. A glacier readvance from Nordenskioldkysten, eastern Svalbard, during the Younger Dryas was suggested by Landvik et al. (1987) based on retarded isostatic rebound. This glacial loading suggests increased glacial activity in the area, which is possibly reflected by the increased IRD flux observed in unit B2. However, the IRD can also be sea ice-derived (Forwick & Vorren, 2009).

The sediments from unit B2 have been interpreted to reflect a glaciomarine and ice distal environment. The higher sand and gravel content, along with several beds and pockets of

different colours, suggests a multiple sediment source input. A change of sediment colours from Isfjorden at the end of the deglaciation were interpreted by Forwick & Vorren (2009) to reflect input from individual glaciers surrounding the fjord. Release of icebergs from individual tidewater glaciers, eroding the different lithology of the nearby islands (see *2.3 Bedrock geology)*, could cause the deposition of the sediments of different lithology and colour observed in unit B2. This suggests that the deposition was characterized by melt-out from icebergs or sea ice. The strong IRD-signal could be due to decreased accretion of sediment-rainout from the water column caused by a widespread sea ice cover. This is in concordance with the extensive sea ice cover, prevailing in the area during the Younger Dryas, recorded by Kristensen et al. (2013). However, more dates are needed to obtain the actual sedimentation rate of the unit. A multiple source input is also displayed by beds with different colours, observed in the lowest part of postglacial unit of core NP05–11–51GC2 from the Kvitøya Trough. Further geochemical analyses are needed to identify the origin of the deposited sediments.

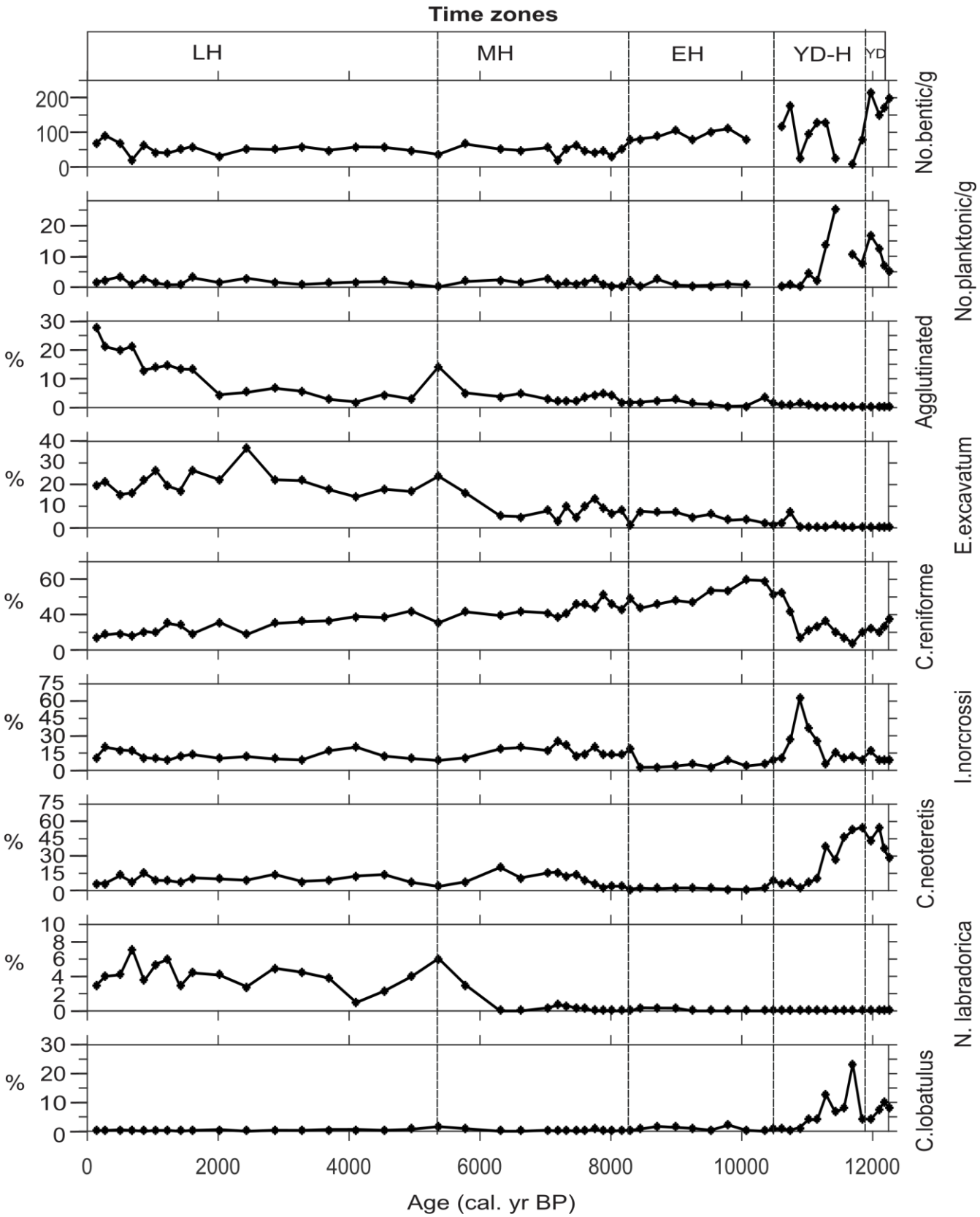


**Figure 7.3:** Number of planktic and benthic foraminifera per gram plotted against age. Percentages of agglutinated and the most common benthic calcareous foraminifera plotted against age. Abbrivations stand for: YD-Younger Dryas, YD–H-Younger Dryas–Holocene Transition, EH- Early Holocene, MH-Middle Holocene, LH- Late Holocene.

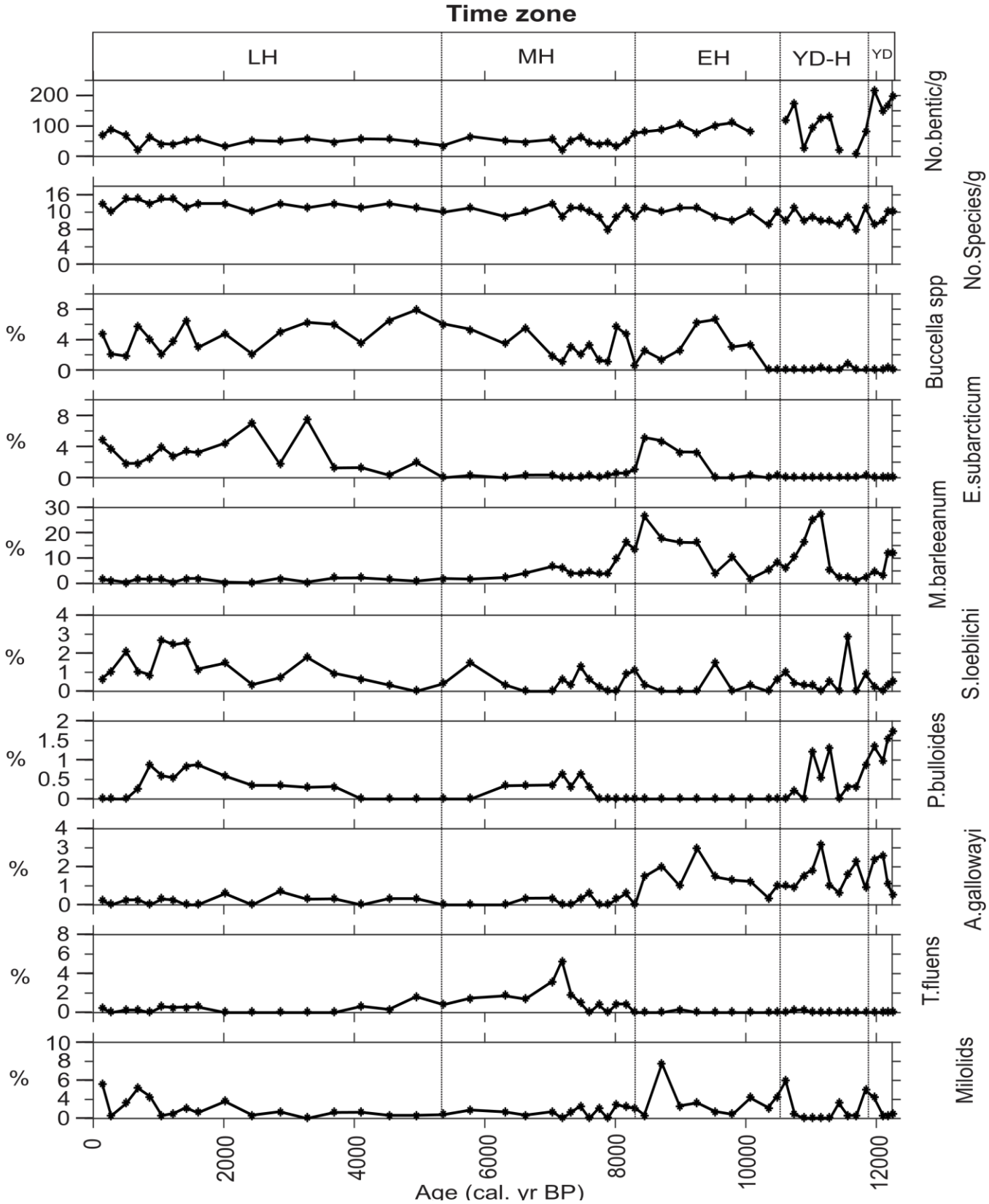


**Figure 7.4:** Number of benthic foraminifera per gram and number of species per gram plotted against age. Percentages of the most common benthic calcareous foraminifera plotted against age. Abbrivations stand for: YD-Younger Dryas, YD–H-Younger Dryas–Holocene Transition, EH- Early Holocene, MH-Middle Holocene, LH- Late Holocene.

## 7.4 Younger Dryas – Holocene Transition (11 950 – 10 680 cal. Yr BP)

The abrupt change from sediments almost barren of foraminifera to a foraminifera-rich fauna dominated by planktic forms and *C. neoteretis* from 11 950 cal. yr BP at the end of the Younger Dryas period, suggests an early and strong inflow of Atlantic water in Erik Eriksen Strait, and an amelioration of the environmental conditions causing increased biological activity. The high amount of planktic foraminifera together with a high abundance of *C. neoteretis* (Figure 7.3), characterizing the transition, suggests an over-deepening of the area resulting in a deeper paleo sea level. When the Svalbard-Barents Sea Ice Sheet retreated and melted during the deglaciation, water flowed over the still isostatically suppressed seafloor, which caused a widespread transgression and deeper water depths (Foreman et al., 1987). This is in conjunction with a high isostatical rebound registered for Kong Karls Land south of the Erik Eriksen Strait, easternmost Spitsbergen and Hinlopen Strait (Ingolfsson et al., 1995; Salvigsen et al., 1995; Dowdeswell et al., 2010).

Both the planktic and benthic record of core key core NP05–11–49GC points to an inflow of chilled Atlantic water in a stratified water column occurring in two steps (See 5.3.1. Assemblage zone 1: *Cassidulina neoteretis and Islandiella norcrossi***;** Figure 7.3 and 7.4). A two-step warming and transition from the Younger Dryas to Holocene is similarly displayed by several records in the Svalbard-Barents Sea area and Nordic Seas (e.g. Björk et al., 1996; Ślubowska-Woldengen et al., 2008). The first step occurred between 11 950 – 11 290 cal. yr BP, and is displayed by a significant increase in relative abundance of *C. neoteretis* and *C. lobatulus*, along with planktic species and the maximum absolute abundance of benthic foraminifera. The rapid increase indicates a swift termination of the Younger Dryas stadial and a change to warmer bottom water conditions with retreating polar waters. *Cassidulina neoteretis* follows chilled Atlantic Water and is often found in a stratified water column possibly overlain by sea ice (Hald et al., 1999). The significant peak of benthic foraminifera indicate a significant increase of the biological activity, and/or reflect increased preservation due to sea ice cover. The increase is early, starting at the end of the Younger Dryas around 12 200 cal. yr BP. Rasmussen et al. (2007) recorded a similar increase marked by a maximum

abundance of subpolar planktonic species interpreted to reflect a strong inflow of Atlantic Water at the end of the Younger Dryas in Storfjorden. A swift termination of the Younger Dryas, by increased inflow of Atlantic Water, and the return of the Polar Front were observed on the shelf north of Hinlopen Strait by Ślubowska et al. (2005). The warming was rather reflected by the inflow of chilled Atlantic water, than the rise of temperature (Ślubowska et al., 2005, Kubischta et al., 2011).

The Younger Dryas–Holocene Transition is characterized by generally high, but fluctuating abundance of IRD in unit B2 (Figure 5.11 and 7.2). The maximum amount of IRD is deposited at the same time as when *C. neoteretis* dominates the fauna. A possible explanation for this can be that the inflow of Atlantic water lead to glacial retreat and increased iceberg rafting. However, the IRD can also have been deposited by sea ice (Dowdeswell et al., 1994; Forwick & Vorren, 2007). A distinct IRD-peak at 11 500 cal. yr BP, before the amount of IRD declines, can represent rapid retreat of nearby glaciers causing a strong IRD-signal. Thereafter only a few icebergs melted over the site. This correlates to the increase of dropstones at 11 700 cal. yr BP observed by Kristensen et al. (2013) from the unnamed trough east of Erik Eriksen Strait.

The $\delta^{18}O$ values (ice volume corrected) measured on the epifaunal *C. lobatulus* are oscillating and low (2.2–3.5‰) during the transition (see *5.4.1. Description $\delta^{18}O$ values*; Figure 7.5). Lower values can be due to an increase of temperature, which is in concordance with the higher abundance of planktic foraminifera and *C. neoteretis*. However, the low values are unlikely to solely reflect a rise in temperature (Lubinski et al., 2001). Freshwater input due to melting of ice sheets during deglaciation lower the salinity of the water masses, and thus the $\delta^{18}O$ values. A modest increase of temperature can be the cause of the lowered $\delta^{18}O$, however the decrease is more likely a result of increased fresh water input (Hald et al., 1999; Lubinski et al., 2001). This is supported by the observed high $\delta^{13}C$ (Figure 5.18), which is indicative of prominent water mass ventilation. The observed higher and varying amount of IRD during the transition correlate with lower $\delta^{18}O$ values, which further suggests glacial melting, causing release of icebergs and fresh meltwater into the hydrological system. Low and decreasing $\delta^{18}O$

values were also recorded by Kristensen et al. (2013) from the unnamed trough at the end of the Younger Dryas between 11 700 and 11 000 cal. yr BP.

A short cooling lasting approximately 150 years interrupts the warming, albeit based on only two measurements. The cooling is reflected by a drop of IRD, an increase in percent of *C. reniforme* and a rapid decrease of Atlantic-water indicating species (see 4. *Benthic foraminifera*). Similar short cooling events are recorded from the Barents Sea and is termed the Pre-Boreal Oscillation (see *1.2.1.4 Holocene).* The oscillation is related to melt water discharge of retreating ice sheets (Hald et al., 1998). A freshening of the waters in Erik Eriksen Strait is reflected by the slight increase in percent of *C. reniforme* at the expense of the species *C. neoteretis* and *C. lobatulus,* which thrives in slightly higher salinities. A drop of IRD and an increase of *S. loeblichii* from Kongsfjorden were interpreted to reflect increased sea ice cover during the Pre-Boreal cooling. The Pre-Boreal Oscillation is also observed on the shelf north of the Hinlopen Strait by the deterioration of the climate by the return of the Polar Front by Koç et al. (2002) and Ślubowska et al. (2005). Exact pinpointing of the length of the interval from Erik Eriksen Strait requires a record with a higher resolution.

The second step occurs between 11 020 and 10 750 cal. yr. BP. Maximum relative abundances of *I. norcrossi* and *M. barleeanus* suggests renewed inflow of chilled Atlantic water. Similar assemblages dominated by *N. labradorica* and *I. norcrossi* are recorded on the northern Svalbard shelf by Ślubowska et al. (2005), which situates the Polar Front near the Hinlopen Strait during the second warming. The species are interpreted to reflect higher salinities and probably warmer bottom waters. *I. norcrossi* typically take advantage of ice-edge algal blooms (Steinsund et al., 1994). This imply that the core site was situated in close proximity of a front system, probably a bit further north, leading to increased ventilation in a well-mixed water column, which is in concordance with the higher $\delta^{13}C$ values indicating a high ventilation of water masses.

The sediments of the lower part of unit A2 are strongly dominated by mud, which indicates a relatively weak ocean current regime, allowing fines to be deposited (Reading, 1986). However, the high relative abundance of *C. lobatulus* together with a slight occurrence of *A. gallowayi* points to stronger bottom currents between 11 900 and 11 300 cal. yr BP, which is in concordance with the increase of the deposition of sand. The sediment colour characterizing the period is constant greyish brown, which is similar to the post-glacial units of the two other cores NP05-84GC and NP05-51GC. This is a transformation from the more frequent changes of colour and compaction observed during the Younger Dryas stadial. The few changes indicates a more stable depositional environment with little variation of sediment source input and relatively stable ocean current activity. This is similar to observations from Erik Eriksen Strait and Kvitøya Trough by Hogan et al. (2010 a and b), which interpreted the post-glacial sediments to be accretion of suspended sediments in a glaciomarine environment with dropstones suggesting occasional ice-rafted debris deposition. The observed increase of Atlantic water inflow brought along a flux of warmth to the area that could initiate the deglaciation of Edge and Barentsøya east of the Erik Eriksen Strait at the end of the Younger Dryas period (Landvik et al. 1995; Koç et al. 2002). Hogan et al. (2010b) suggested that grounded ice had retreated from south of Nordaustlandet by 11 700 cal. yr BP. Elverhøi & Solheim (1987) suggests a glacial retreat to an onshore position with only minor outlet glaciers present by 10 600 cal. yr BP. The glaciomarine ice-distal environment characterizing the Erik Eriksen Strait and Kvitøya Trough after the Younger Dryas stadial is therefore in concordance with the retreat of glaciers onto the nearby islands. The observed IRD-peak at 11 500 cal. yr BP can represent the end of the deglaciation with a final retreat of the nearby glaciers.

*Cassidulina neoteretis* is usually associated with Holocene records from the Svalbard-Barents Sea area (Ślubowska et al., 2005; Kristensen et al., 2013). The early appearence of this species and the general higher biological productivity concomitant with the inflow of Atlantic water during the transition raises the question whether these assemblages are of early Holocene age; a period associated with increased temperatures and improved climatic conditions leading to increased biological activity (Kutzbach & Guetter, 1986; Svendsen & Mangerud, 1997; Ślubowska-Woldengen et al., 2008). The boundaries between each time-period are based upon the age model and the correlation between foraminiferal, physical and

sedimentological data. The boundary between the Younger Dryas Period and the Younger Dryas–Holocene Transition is placed at 11 950 cal. yr BP due to the maximum abundance of planktic and benthic species. This can indicate that the obtained date at 181 cm, giving a Younger Dryas age of 12 103 cal. yr BP, possibly is slightly old. This is also in concordance with a later increase of *C. neoteretis* c. 10 600 cal. yr BP in the Franz Victoria Trough (Lubinski et al., 2001). The obtained date is from the top part of unit B2, just above an interval containing sandy beds and pockets, which could indicate the sediments is slightly reworked causing dating uncertainties. The early inflow of C. neoteretis and planktic foraminifera can be explained by that a glacial-isostatic induced deepening, as postulated by Lubinski et al. (2001) from the Franz Victoria Trough to be an important factor in paleooceanographic reconstructions. A lowered seafloor could have facilitated a stronger inflow of Atlantic water as a subsurface layer at the end of the Younger Dryas when the epicontinental Barents Sea was still suppressed due to the glacial loading of the SBIS.

Colder periods have higher reservoir ages, while the warmer periods, with greater ocean ventilation and circulation, show a lowering of the reservoir age (Bondevik et al., 2006; See *6.1.3 Choice of reservoir age and ΔR for Younger Dryas*). Since the Younger Dryas on Svalbard was characterized by polar surface conditions with extensive sea ice cover and diminished Atlantic-derived water inflow (Ślubowska et al., 2005), it is likely to assume an increase of the Younger Dryas reservoir age for the Svalbard area. A higher reservoir age of 400 years, as recommended by Bondevik et al. (2006) for the Norwegian coast during the Younger Dryas, was therefore chosen for the date at 181 cm (See *6.Chronology).* However, similar studies are lacking from the Svalbard–Barents Sea area, which makes the reservoir age here unknown (Rasmussen & Thomsen, 2014). The northwestern Svalbard corner is today cooler and more subjected to sea ice formation than the western side. If a similar difference prevailed during the Younger Dryas, it is possible that an even higher reservoir age should have been chosen for the Younger Dryas date, resulting in a slightly younger date.

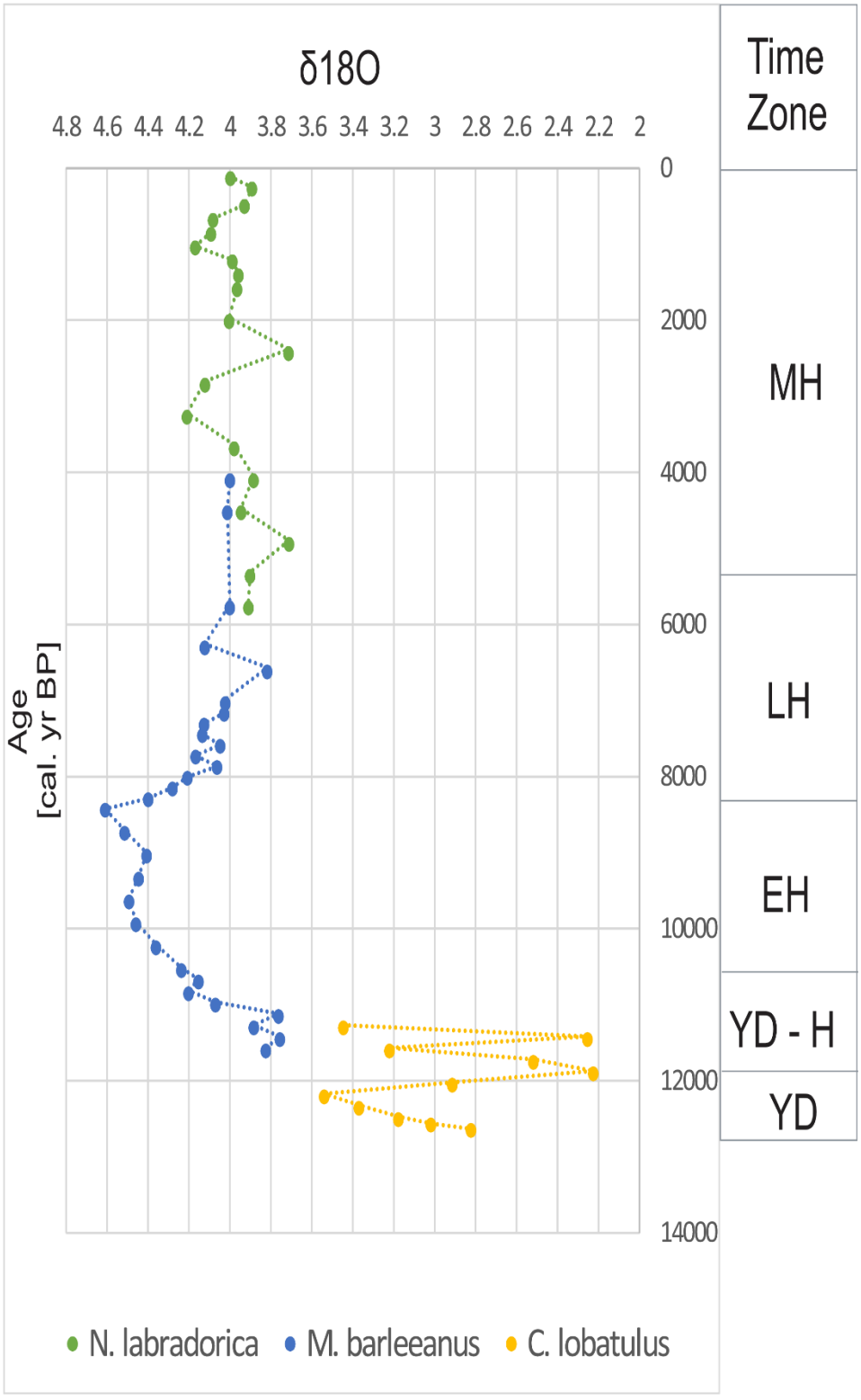


**Figure 7.5:** Stable oxygene isotope record (measured on *Nonionella labradorica, Melonis barleeanus* and Cibicides lobatulu) of core NP05–11–49GC from Erik Eriksen Strait plotted against age. The time zone abbreviations stand for: YD- Younger Dryas, YD–H- Younger Dryas–Holocene Transition, EH- Early Holocene, MH- Middle Holocene and LH- Late Holocene.

## 7.5. Early Holocene (10 680 –8300 cal. yr BP)

The early Holocene was a period characterized by increased summer insolation and a significantly warmer climate than today. The period is widely registered in the Nordic and Barents Sea, and the warming is referred to as the Early Holocene Climatic Optimum (Kutzbach & Guetter, 1986; Svendsen & Mangerud, 1997). The rapid decrease of *I. norcrossi* in the Erik Eriksen Strait prior to the onset of the early Holocene, suggest a northward retreat of the Polar front (Figure 7.3). This is in concordance with studies by Ślubowska et al. (2005) and Koç et al. (2002) from the northern Svalbard margin, which places the Polar Front at the northern Svalbard shelf during the Early Holocene due to increased abundance of *N. labradorica*. *Islandiella norcrossi* and planktic foraminifera thrives in deeper water (Steinsund et al., 1994). Their reduction at the onset of the early Holocene suggests a lowering of the paleo sea level. Kubischta et al. (2011) suggests a paleo-water reduction from c. 140 to 110 m in the Hinlopen Strait during this time, and Salvigsen & Mangerud (1991) recorded the highest marine level of 55–60 m around 10 000 cal. yr BP in Agardhbukta, eastern Spitsbergen. This is probably caused by a crustal uplift of the sea floor, rather than an increase of the global sea level. This is, as mentioned previously, in concordance with the high isostatic rebound of the area, which is closely connected to the deglaciation process with reduced glacial loading (Nagy, 1984; Ingolfsson et al., 1995; Salvigsen et al., 1995; Dowdeswell et al., 2010).

The dominance of fine sediments recorded for the period, which is displayed in unit A2 of the key core NP05–11–49GC (Figure 5.11 and 7.2) and the post-glacial units of the two other cores, suggests an environment little influenced by strong ocean currents (See *5.2.4.4. Unit A2*). The IRD content drops prior to the early Holocene, and subsequently almost disappears. The low amount of IRD and sand suggests a transition from an ice-proximal setting to increasingly ice-distal conditions. This is in concordance with the Holocene mud unit, containing scattered dropstones interpreted to reflect similar ice-distal conditions in a glaciomarine environment, described by Hogan et al. (2010a and b) from the Erik Eriksen Strait and Kvitøya Trough. The high abundance of mud and low IRD-content suggests reduced iceberg rafting probably due to a minimum extent of the nearby islands glaciers during the Holocene Climatic Optimum. This is in accordance with Elverhøi & Solheim (1987) suggesting a glacial retreat to an onshore

position with only minor outlet glaciers by 10 600 cal. yr BP, and Landvik et al. (1995) suggesting receding glaciers on Edgeøya and the establishment of modern flora of the area just prior to the Early Holocene.

The foraminiferal record (Figure 7.3 and 7.4) from the Erik Eriksen Strait display a clear shift with a significant increase of *C. reniforme,* dominating up to 80% of the total fauna, and a relatively high absolute number of calcareous benthic foraminifera. *Cassidulina reniforme* is typically found in areas affected by Atlantic water and is associated with the warmer part of the Holocene, where it indicates an ice-distal glaciomarine environment as described for the Northern Norwegian shelf by Hald & Vorren (1987). Relatively high absolute number of calcareous benthic foraminifera together with little IRD implies higher primary production and points to open water conditions with reduced sea ice cover and a strong inflow of Atlantic water. This is correlative with studies by Kristensen et al. (2013), which correspondingly detected an Early Holocene characterized by high productivity with a *C. reniforme*-dominated fauna and scarce amounts of IRD in the unnamed trough east of Erik Eriksen Strait. A *C. reniforme*-dominated fauna is also correlative with the faunas studied by Lubinski et al. (2001) from the St. Anna and Franz Victoria Troughs and by Ślubowska et al. (2005) from north of the Hinlopen Strait.

Introduction of the opportunistic species *E. excavatum* together with the decrease in relative abundance of *C. reniforme,* observed throughout the zone, suggest conditions became less saline and cooler. *Elphidium excavatum* is often related to the Late Holocene record on western Svalbard margins (eg. Ślubowska et al., 2007). The early introduction of this species after the deglaciation is also observed by Hald et al. (1999) in the St. Anna trough, and indicate a cooler Early Holocene Climatic Optimum in eastern Svalbard, compared to western and southern Svalbard records. However, high amount of planktic species observed in the unnamed trough east of Erik Eriksen Strait suggests a warming of the surface waters and a strong inflow of Atlantic water during the Early Holocene (Kristensen et al., 2013). Which is also observed on the western and southern Svalbard margins (e.g. Ślubowska et al., 2005;

Ślubowska-Woldengen et al., 2007; Rasmussen et al., 2007; Jessen et al., 2010; Rasmussen and Thomsen, 2015).

The increase of $\delta^{18}O$ values (Figure 7.5) can be due to lowered temperatures or increased salinity. However, high values together with the dominance of *C. reniforme* imply that the rise of $\delta^{18}O$ values are caused by inflow of saline, chilled Atlantic water. This is in concordance with the $\delta^{18}O$-record from the Franz Victoria Trough, which displayed a cool start of the Early Holocene followed by a warming from the subsurface to the bottom due to increased inflow of Atlantic water (Duplessy et al., 2001). High $\delta^{18}O$ values are also recorded from the St. Anna Trough during the Early Holocene by Hald et al. (1999).

## 7.6. Middle Holocene (8300 – 5300 cal. yr BP)

The mid-Holocene sediments are, as the Early Holocene sediments, dominated by the deposition of mud displayed in unit A2 of the key core NP05–11–49GC, suggesting accretion of sediment rain-out from the water column with little influence by strong ocean currents (Figure 5.11 and 7.2; See *5.2.4.4. Unit A2)*. This is correlative with the mud dominated post-glacial units of the two other cores, and postglacial units found by Hogan et al. (2010a,b) from the Erik Eriksen Strait and Kvitøya Trough.

A drop of the absolute abundance of benthic foraminifera and especially a reduction of *M. barleeanus* and *E. subarcticum*, is observed at the start of Mid-Holocene at 8300 cal. yr BP. The drop is also correlative with the $\delta^{18}O$ record from the Erik Eriksen Strait, displaying a decrease (Figure 7.5). This decrease of $\delta^{18}O$ -valuesis is either caused by a temperature increase or a reduction of salinity (Lubinski et al., 2001). The observed increase of *E. excavatum* at the expense of *C. reniforme* suggests a reduction of salinity. The foraminiferal record together with the $\delta^{18}O$ record therefore display a sudden and lasting decrease of salinity. The event is correlative with a climatic cooling event registered in Greenland ice cores and is referred to as the 8.2 event (Rasmussen et al., 2006). The 8.2 event is suggested to be a result of fresh meltwater release from the final collapse of the Laurentide Ice sheet, leading

to a cooling (Broecker et al., 1992; Andrews et al., 1992). It is correlative with a minor increase of IRD. The slightly older age observed in the investigated key core may be due to age-model uncertainties or too low sampling intensity and hence a too low resolution to exactly pinpoint the event. A cooling event, although the timing differs slightly, is similarly displayed in several foraminiferal records from the Svalbard and Barents Sea area. A similar reduction of $\delta^{18}O$ were observed by Kristensen et al. (2013) from the unnamed trough east of Erik Eriksen Strait during the Early Holocene between 8600 and 7600 cal. yr BP. An abrupt change is displayed by the foraminiferal fauna in the St. Anna Trough by Hald et al. (1999). The Franz Victoria Trough foraminiferal record display a cooling between 8250 – 7850 cal. yr BP (Duplessy et al., 2001). Hald & Korsun (2008) found two cooling events in Van Mijenfjorden on western Spitsbergen dated to have happened between 8200 – 8450 cal. yr BP.

The cooling and decrease of salinity is in concordance with the increase of the relative abundance of *E. excavatum* at the expense of *C. reniforme* in the key core from Erik Eriksen Strait, as *E. excavatum* prefers slightly lower salinities than *C. reniforme* and it dominates in a pure arctic environment with the presence of sea-ice and high turbidity and high sedimentation rates (Steinsund et al., 1994; Hald & Steinsund, 1996; Hald & Korsun, 1997). A decrease of *C. reniforme* and an increase of *E. excavatum* along with a reduction of the absolute abundance of benthic foraminifera is in concordance with the Early Holocene fauna, displaying an increase of *E. excavatum*, from the unnamed trough (Kristensen et al., 2013). This distribibution pattern resembles most other Holocene records from the Svalbard and Barents Sea area (e.g Lubinski et al., 1996; Hald et al.,1999; Duplessy et al.,2001; Rasmussen et al., 2007; Kubishcta et al., 2011), and is in concordance with a gradual cooling following the Holocene Temperature optimum into and through the middle and Late Holocene observed in the aforementioned studies. The cooling and reduced salinity is probably due to a decrease in the inflow of Atlantic water with an increase of Arctic surface water and more extensive seasonal sea ice cover.

An increase of *C. neoteretis* along with high percentages of *C. reniforme* and the stabilization of the $\delta^{18}O$ values from 7600 cal. yr BP, observed in Erik Eriksen Strait indicate renewed and

stronger influence of Atlantic water. Ameliorated conditions by an increase of *C. neoteretis* and higher concentrations of benthic and planktic foraminifera were also recorded in the unnamed trough east of Erik Eriksen Strait between 7600 and 6500 cal. yr BP by Kristensen et al. (2013).

## 7.7. Late Holocene (5300 cal. yr BP – present)

The transition from mid-Holocene to the Late Holocene is marked by an increase in the relative abundance on *E.* excavatum (Figure 7.3). The species abundance is seen increasing during the Late Holocene, and its dominance suggest harsher conditions with high turbidity and increased sedimentation rates (See 4.2.2 *Elphidium excavatum* forma *clavatum)*. This is further supported by the decrease of *C. reniforme*, indicating decreased salinites due to reduced inflow of Atlantic water and a dominance of Arctic waters. However, the presence of *I. norcrossi* together with *C. reniforme* indicates a continued inflow of Atlantic water as a subsurface layer (Ślubowska et al., 2007). The observed increase of *E. Excavatum,* along with a slight increase of IRD and sedimentation rate is correlative to the Late Holocene *E. excavatum*-dominated fauna recorded by Kristiensen et al. (2013) from the unnamed trough east of Erik Eriksen Strait. *Elphidium excavatum* is seen increasing in numerous Late Holocene records from the Barents Sea, around Svalbard and the Greenland shelf (Hald et al., 2004; Ślubowska et al., 2005; Ślubowska-Woldengen et al., 2007; 2008; Skribekk et al., 2010; Rasmussen & Thomsen et al., 2014). This is interpreted to reflect a regional general cooling and a paleoenvironmental shift due to a return to more polar conditions (Kristensen et al., 2013).

The relatively high abundance of *Buccella* spp. and *N. labradorica* observed in the Erik Eriksen Strait from this time is also indicative of a glacimarine environment affected by Atlantic water (Figure 7.3 and 7.4; Hald & Korsun et al, 1997). These two species are often found in Late Holocene faunas dominated by *E. excavatum* and *C. reniforme* (Jennings et al., 2004), such as the observed Late Holocene-fauna from Erik Eriksen Strait. Both species, together with *I. norcrossi*, thrives in areas with high seasonal productivity related to ice marginal zones (Polyak & Mikhailov 1996; Kristensen et al., 2013). The increase of these species at the start of the Late Holocene suggests increased sea ice cover and a southward migration of the Polar Front,

which is also recorded in the unnamed trough east of Erik Eriksen Strait by Kristensen et al. (2013). Higher primary production provides sufficient food for the benthic environment and can explain the rise of total abundance of benthic foraminifera during the latest part of the Holocene. This increase can also be due to little dissolution as the sediments are young. Duplessy et al. (2001) found a similar Late Holocene assemblage displaying a reduction of *C. reniforme* at the expence of *E. excavatum, Buccella* spp. and *N. labradorica*, interpreted to reflect temperature decrease affecting the whole water column and a southward shift of the summer sea-ice margin.

The period is characterized by similar benthic oxygen isotope values as the Mid Holocene, with fluctuations around a mean value of 4.0 ‰ (Figure7.5). The values are overall lower than the early Holocene and supports the foraminiferal assemblages reflecting cooler climatic conditions and decreased salinities. Lower values are similarly found in Late Holocene records from the Franz Victoria Trough by Lubinski et al. 2001). The reduction of Atlantic water inflow displayed by the benthic fauna and by low $\delta O^{18}$ values, suggest a less stratified water column.

The Late Holocene sediments from the three investigated cores (Figure 5.8, 5.11, 5.13) have a similar colour and consists mainly of mud with occasional scattered sand pockets and dropstones. The similarity implies that the cores from Erik Eriksen Strait and Kvitøya Trough were subjected to a similar depositional environment during the Late Holocene. Similar mud units, with scattered IRD, resembles the postglacial interval associated with sea-ice sedimentation, high productivity conditions and current re-distributed sediments found in Erik Eriksen Strait and Kvitøya Trough by Hogan et al. (2010 a and b), and other records from the north-western Barents Sea (Elverhøi & Solheim,1983; Polyak & Solheim, 1994). The unit is suggested to be accumulation of suspended sediments in a distal glaciomarine environment and is a typical sediment facies for Barents Sea shelf depressions (Lubinski et al., 1996). The slight increase of IRD at the end of the Late Holocene is in concordance with a small increase of IRD in the unnamed trough recorded by Kristensen et al. 2013 (Figure 7.2). Increased IRD during the Late Holocene is documented many places along the Svalbard margin and in the Barents Sea. The increase has been interpreted to reflect increased glacial activity due to a

return to more polar conditions (eg. Ślubowska et al., 2008 and references therein). Several surge glaciers occupy Nordaustlandet north of Erik Eriksen Strait, and one of them, Bråsvellebreen, has undergone at least two surges. The latest one in 1938 (Solheim, 1991). The increase of IRD can therefore be related to surge events of Nordaustlandet glaciers.

The increase of agglutinated forms in the Erik Eriksen Strait during the Late Holocene suggests corrosive conditions at the seabed or acidic pore water. The corrosive conditions are caused by brine formationor by high productivity leading to high content of organic material in the sediments (see 4.3.6 *Agglutinated species;* Hald & Steinsund, 1992). The increase is in concordance with studies from Storfjorden by Rasmussen & Thomsen (2014), where a high abundance of agglutinated forms were related to cold phases during the Late Holocene characterized by increased sea ice formation, polynyal activity and brine formation. An increase in productivity during the Late Holocene in the Erik Eriksen Strait is further supported by the relatively high abundance of the high primary production related species *Buccella* spp. and *N. labradorica*. Brine formation during the Late Holocene, caused by cooling and mixing of northward flowing Atlantic Water with colder surface waters, is displayed in other modern foraminiferal records in the Franz Victoria Trough and St. Anna Troughs (Lubinski et al., 2001). Brines can form acidic bottom water conditions, which causes calcareous forms to dissolve, resulting in an agglutinated foraminiferal dominance in fossil faunas (Alve & Murray, 1995). The increase and high percentages of agglutinated foraminifera found in Erik Eriksen Strait is therefore likely to reflect a general cooling causing increased brine formation and sea ice formation, which again results in corrosive bottom conditions and dissolution of calcareous forms. Records displaying a dominance of agglutinated species is uncommon west and north of Svalbard (Ślubowska et al., 2005; Ślubowska-Woldengen et al., 2007; Skirbekk et al., 2010). This can be due to less formation of brines on the western and northern shelves of Svalbard.

## 7. 8. Paleoceanographic implications

The heat transport to the Svalbard region is very sensitive to changes in both air masses and ocean currents and circulation (Isaksson et al., 2005). Changes in these parameters have been the driving factors behind climatic variations, and hence the buildup and decay of glaciers and the distribution of water masses surrounding the archipelago (Ślubowska et al., 2005; Ślubowska-Woldengen et al., 2008; Schlichtholz & Goszczko, 2006). The Svalbard area is highly sensitive to variations of the inflow of Atlantic water (Ślubowska-Woldengen et al., 2007). The rate of inflow of the Atlantic water is controlled by several factors. Since the studied core site is affected by a mixture of the Fram Strait and cold Barents Sea branches of Atlantic water, a change in either of these branches can affect the inflow of the Atlantic water through time (Lubinski et al., 2001). Variations of these branches can be due to changes in several factors on both a global and regional scale. One of which is the thermohaline circulation and deep-water formation in the North Atlantic. Broecker (1991) states that the thermohaline circulation is mainly driven by the water masses' differences in density caused by temperature and salinity differences. A reduction of North Atlantic deep-water (NADW) formation is due to a meltwater input causing the salinity and hence the density of Atlantic waters to decrease. This turns 'off' and slows down the Atlantic conveyor system, and is associated with periods characterized by ice growth (Figure 7.6). The NADW formation is re-initiated as salt builds up due to that less salt is exported out of the system, and the conveyer system is turned 'on'. In addition, a reduction of meltwater input increases the salt content of the Atlantic (Broecker et al., 1990).

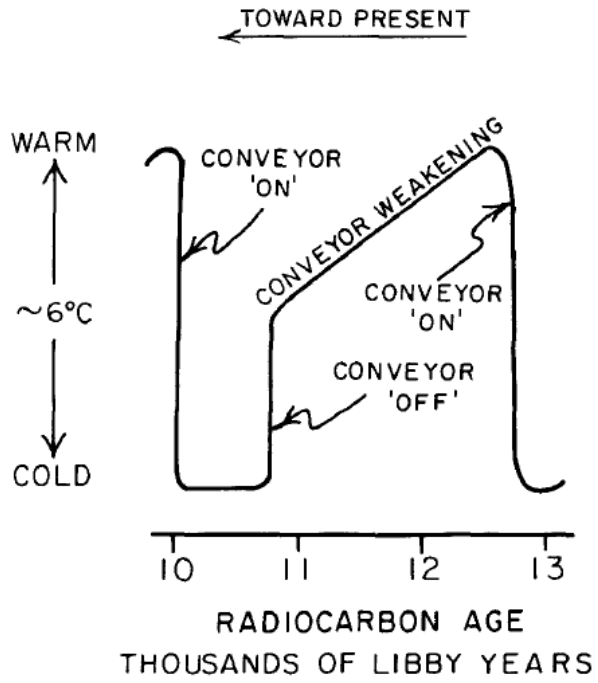


**Figure 7.6:** Diagrammatic representation of the northern Atlantic basin temperature record from approximately 13 000 to 10 000 $^{14}$C yr BP. A rapid warming are observed at 12 700 and 10 000 $^{14}$C yr BP (From Broecker et al., 1990).

The inflow of Atlantic water is also affected by atmospheric circulation patterns, such as the North Atlantic Oscilliation. Feedback mechanisms with temperatures and sea ice can alter the inflow (Loeng, 1991; Lubinski et al., 2001; Ślubowska-Woldengen et al., 2007). The paleoceanographic conditions of the western and Svalbard region is closely linked to the sea surface temperatures of the Nordic Seas since the deglaciation (Ślubowska- Woldengen et al., 2007), and the changes of sea surface conditions follows the summer insolation curve (Koç et al., 1993). The warming in the Holocene in the Greenland, Iceland and Norwegian Seas (GIN) is correlative to the maximum solar insolation during the Holocene Climate Optimum occurring at 9000 cal. yr BP, which was 8% higher than today at 80°N (Ślubowska-Woldengen et al., 2007; Figure 7.7). Sea surface temperatures (SST) in the western Barents Sea were possibly 4°C higher that today (Sarnthein et al., 2003b). The drop of insolation through the Holocene causes a cooling trend in step with the insolation. This is seen by a southward migration of the sea-ice margin, polar waters and the Arctic and Polar fronts in the GIN Seas (Koç et al., 1993). The surface water warming in the Nordic Seas is correlative with increased inflow of Atlantic water to the bottom waters west and north of Svalbard (Ślubowska et al., 2005). The record from Erik Eriksen Strait and several records along the Svalbard and Barents

Sea margins display synchronous oceanographic changes with an early Holocene warming followed by a cooling, correlative with the insolation (e.g: Hald et al., 1999; Duplessey et al., 2001; Ślubowska-Woldengen et al., 2007; 2008; Kristensen et al., 2013; Rasmussen & Thomsen, 2014). The fact that the Atlantic water inflow follows the insolation curve, show that among the many factors affecting the Atlantic water inflow to the region, they may be indirectly affected by the solar insolation curve.

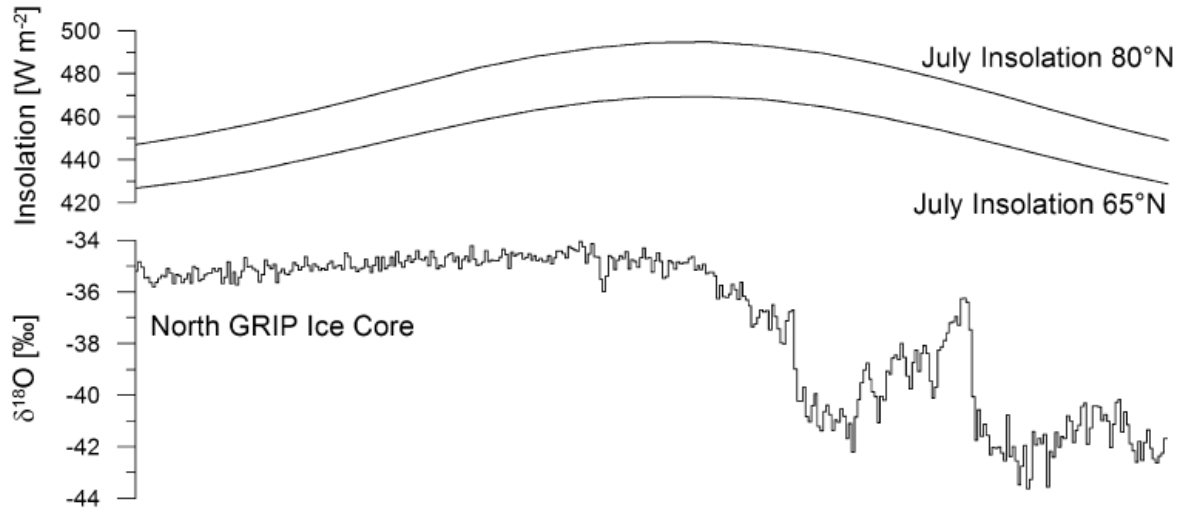


**Figure 7.7:** July insolation [Wm $^{-}$2] at 65 and 80 °N plotted against cal. yr BP and the $\delta^{18}O$ record from North GRIP Ice Core plotted against cal. yr BP (From Ślubowska et al., 2005).

Koç et al. (1993) suggested that a time transgressive development of surface conditions is the cause of an asynchronous timing of the Holocene Climatic Optimum in the GIN Seas. The relatively cool start of the Early Holocene observed in the Erik Eriksen Strait and records further east from the Franz Victoria and St. Anna Troughs by Hald et al. (1999) and Duplessy et al. (2001), could also be due to a time transgressive development of surface conditions.

The fact that the fauna display a cooler start of the Holocene compared to the western and southern side of Svalbard can be due to numerous factors. Today Atlantic water flows around the western and northern Svalbard margin as a subsurface layer, before it enters the Barents Sea via the troughs located on the northern margin toward the Arctic Ocean (Ślubowska et al., 2005; Gammelsrød et al., 2009; see *2.4 Oceanography*). On its way north, the water masses loose heat causing a reduced Atlantic water inflow into the Barents Sea. This, together with a higher influence of Arctic surface waters, causes the eastern Svalbard climate to stand in stark

contrast to the western side. The modern water mass distribution and inflow of Atlantic water can provide a context for interpreting the paleohydrographic system. It is possible that a similar stark contrast also existed throughout the Holocene, when the oceanographic system operated in a similar manner to the present (Lubinski et al., 2001). Explanation for the cooler Atlantic water signal registered in the Erik Eriksen Strait, compared to western Spitsbergen, can be that a temperature gradient, similar to today, existed between east and west. Ślubowska et al. (2005) found that the general Atlantic water inflow at the northern Svalbard margin at the start of the Holocene did not result in a strong temperature increase through the Holocene. This suggests that the loss of heat the Atlantic water experiences on its way north, causes a slightly reduced Holocene Climatic Optimum signal north and east of the Svalbard archipelago compared to the western side of Svalbard. This is in concordance with a study by Forwick & Vorren (2009) from Isfjorden located on the west coast of Spitsbergen. Glaciers along the west coast were absent during the early Holocene (Svendsen & Mangerud, 1997), which led Forwick & Vorren (2009) to assume that the deposited IRD during the Early Holocene in Isfjorden originated from glaciers on the eastern side of Spitsbergen. Thus implying a strong east-west temperature gradient causing an iceberg melt-out occurring when the icebergs reached the warmer western side of Spitsbergen.

The foraminiferal record from the Erik Eriksen Strait show that the high isostatic rebound also affected the inflow of Atlantic water to the region. High abundance of planktic foraminifera and *C. neoteretis,* during the transition from the Younger Dryas to the Holocene, suggests an increase of the paleo sea level caused by the isostatically-suppressed seafloor in the Erik Eriksen Strait. This was also hypothesized by Lubinski et al. (2001) from the Franz Victoria and St. Anna Troughs, which stated that a deepening and increase of paleo sea level, caused by a glacio-isotatically depressed seafloor of 150 m, happened at the start of the deglaciation. This resulted in increased inflow of Atlantic water to the region as the SBIS retreated from the shelf edge. During the Bølling interstadial, records from the Svalbard margin show an increased inflow of Atlantic water, flowing along the western and northern coast of Spitsbergen, before it entered the Barents Sea from the north (Ślubowska-Woldengen et al., 2008). Another example of how the isostatically rebound can affect the water mass distribution of the northwestern Barents Sea region is the Kvitøya Trough. The CTD- station NP05–51 from the

Kvitøya Trough show no present presence of Atlantic water in the water column (Figure 5.5). During the Bølling interstadial, the isostatically depressed sea floor, could have induced inflow also in this trough, which was already deglaciated by the Bølling interstadial (Hogan et al., 2010b) and making the Kvitøya Trough a short-cut for the Atlantic Water into the Erik Eriksen Strait (Kristensen et al., 2013). This can explain the high paleo sea level and strong and chilled Atlantic water inflow during the Younger Dryas–Holocene Transition in the Erik Eriksen Strait.

## 7.9. Short-term cooling events

Several abrupt cooling events interrupted the warming of the northern hemisphere during the last deglaciation (Meissner et al., 2006). The three largest ones, the Younger Dryas, the Pre-Boreal Oscillation and the 8.2-ka cold event, are observed in the foraminiferal record in Erik Eriksen Strait. Climatic cold events are registered several records from the Nordic Seas and in the Svalbard Barents Sea region (e.g : Koç et al., 1993; Rasmussen et al., 1996; Ślubowska-Woldengen et al., 2008; Jessen et al., 2010; Jessen & Rasmussen, 2015). The cause of these climatic cold events are debated. The climate during the last glacial was fluctuating on millennial time scales. Dansgaard/Oeshger (DO) events, described from Greenland ice cores (Dansgaard et al., 1993; Figure 7.7), are registered in marine geological data as a result of changes in the northward flow of surface Atlantic water and deep water formation in the GIN Seas (Rasmussen et al., 1996; Koç et al., 1993; Jessen & Rasmussen, 2015). Colder events like the Younger Dryas showed continued convection in the Nordic Seas, but with increased spread of Polar waters southward (Rasmussen et al., 2002). An increase of meltwater release from melting icebergs during glacial conditions caused a slowdown of the thermohaline circulation and the advection of warm Atlantic water to higher latitudes every 1000 to 2000 years, resulting in a cooling (Bond et al., 1993; Jessen & Rasmussen, 2015). As the Laurentide Ice Sheet retreated, the proglacial Lake Agassiz flooded causing an outburst of freshwater, which due to routing events caused a weakening of the thermohaline circulation in the northern hemisphere, and hence the flux of Atlantic water to the Svalbard and Barents Sea region (Broecker et al., 1990; Meissner et al., 2006). This led to a widespread sea ice formation (Ślubowska-Woldengen et al., 2008). The deposited Younger Dryas sediments from the key core retrieved from Erik Eriksen Strait is almost barren of foraminifera, which has been interpreted to reflect harsh glaciomarine conditions with increased formation of sea ice (see

*7.4 Younger Dryas – Holocene Transition)*. The Pre-Boreal Oscilliation is detected in the Erik Eriksen Strait record as a decrease of the most common benthic species. At 8300 cal. yr BP a drop of salinity, registered by the $\delta^{18}O$ record, and a slight drop of the total abundance of benthic foraminifera show a cooling (see 7*.5 Early Holocene and 7.6. Middle Holocene)*. This show that the outburst of fresh water from the Laurentide ice sheet also affected the water column as far north as the Svalbard margin. However, it is unlikely that the freshwater release had a direct impact on the benthic fauna in the northwestern Barents Sea corner and the Erik Eriksen Strait, but was due to a slowdown of the thermohaline circulation and the reduced advection of warm Atlantic water to higher latitudes with increased spread of Polar waters southward.

# 8. Conclusions and Summary

The study of benthic foraminifera, stable isotopes and sedimentology of key core NP05–11–49GC, along with the sedimentology of core NP05–11–84GC2 and NP05–11–51GC2 display the depositional environment of the Kvitøya Trough and the depositional environment, paleooceanography and paleoenvironment of Erik Eriksen Strait, northwestern Barents Sea from approximately 14 100 cal. yr BP to present.

- The deglaciation of the Kvitøya Trough and the deeper central part of Erik Eriksen Strait occured approxiamtely 14 100 cal. yr BP and was characterized by rainout of IRD from icebergs released by a rapidly retreating Svalbard-Barents Sea Ice Sheet in a glacier-proximal setting. The formation of a grounding zone wedge at the southwestern head of Erik Eriksen Strait show the positioning of a glacier front still-stand and that the retreat became episodic in shallower waters as the Svalbard Barents- Sea Ice Sheet melted and retreated eastward through the trough. The lack of biogenic material in the sediments show that the deglaciation was characterized by a cold climate and harsh glaciomarine conditions.
- The retreat of the Svalbard-Barents Sea Ice Sheet, during the Bølling–Allerød interstadials, was characterised by the release of turbid meltwater plumes between 14 100 and 12 700 cal. yr BP, resulting in deposition of laminated clays in the deeper central part of Erik Eriksen Strait.
- Harsh glaciomarine conditions in an ice-distal environment with increased sea ice cover characterized the Younger Dryas cooling (12 700 –11 950 cal. yr BP). Occasional ice rafting shows that the Erik Eriksen Strait also experienced periods with seasonally open waters during the cooling. A varying depositional environment, reflected by beds varying in colour, sand and IRD content, showed a multiple sediment source input from individual glaciers surrounding the Erik Eriksen Strait and Kvitøya Trough.
- At the end of the Younger Dryas stadial at 12 200 cal. yr BP, a rapid transition from sediments almost barren of foraminifera to sediments dominated by *Cassidulina neoteretis* reflect a strong inflow of chilled Atlantic water.
- The Younger Dryas-Holocene transition was the start of a two-step warming. The first step, between 11 960 and 11 290 cal. yr BP, reflect a swift termination of the Younger Dryas and a continued strong inflow of Atlantic water, causing an amelioration of the environmental conditions and very high biological activity recorded by benthic and planktic foraminiferal maximum abundance. Freshwater input due to melting of ice sheets during deglaciation lowered the salinity of the water masses reflected by low

$\delta^{18}O$ values. The glacio-isostatically suppressed sea floor caused an over-deepening of the area and a deeper paleo sea level.

- The warming was interrupted by a 150 year long cooling event termed the Pre-Boreal Oscillation.
- The second step, between 11 020 and 10 750 cal yr. BP, was characterized by increased ventilation in a well-mixed water column, reflected by increased $\delta^{13}C$ values. The maximum relative abundances of *Islandiella norcrossi* and *Melonis barleeanus* revealed renewed inflow of chilled Atlantic water and that Erik Eriksen Strait was situated in close proximity of the Polar Front.
- The depositional environment during the Holocene was strongly dominated by accretion of sediment rainout from the water column and occasional deposition of IRD from icebergs or sea ice in a relatively weak ocean current regime in an ice-distal environment.
- The onset of the Early Holocene is reflected by a northward retreat of the Polar Front and a high paleo sea level due to reduced glacial loading. A *Cassidulina reniforme*-dominated fauna with a low occurrence of *Elphidium excavatum* showed a cooler Early Holocene Climatic Optimum in Erik Eriksen Strait in eastern Svalbard, compared to western and southern Svalbard records, and that the east-west climatic gradient observed today, also existed in the Early Holocene.
- At 8300 cal. yr BP, the foraminiferal record, together with decreased $\delta^{18}O$ values, indicated a sudden cooling and a lasting decrease of salinity. An increase of *C. neoteretis* along with high percentages of *C. reniforme* and the stabilization of the $\delta^{18}O$ values from 7600 cal. yr BP, showed renewed and stronger influence of Atlantic water.
- Thereafter, a deterioration of the environment with decreased salinities due to reduced inflow of Atlantic water and a stronger dominance of Arctic waters, reflected by increased abundance of *Elphidium Excavatum* and a reduction of *Cassidulina reniforme*, characterized the Late Holocene.
- The study show that the high isostatically rebound of the area have affected the inflow of Atlantic water to the northwestern Barents Sea corner and must be considered when reconstructing the areas paleooceanography.
- The data from Erik Eriksen Strait generally display regional changes that are correlative with studies from the Svalbard-Barents Sea area. It suggests that an east-west climatic gradient, similar to today, existed between eastern and western Svalbard in the Early Holocene.

# References

**Aagaard, K., 1975.** Oceanography of the Arctic seas. *Reviews of Geophysics and Space Physics*, Vol. **13**, No. 3, pp. 614–615.

**Alve, E. & Murray, J. W., 1995**. Experiments to determine the origin and palaeoenvironmental significance of agglutinated foraminiferal assemblages. *In* Kaminski, M. A., Geroch, S. & Gasinski, M. A. (eds.): *Proceedings of the Fourth International Workshop on Agglutinated Foraminifera (Krakow, Poland) September 12—19, 1993, 1—11. Grzybowski Foundation Special Publication,* No. 3.

**Andersen, E. S., Dokken, T. M., Elverhøi, A., Solheim, A. & Fossen, I., 1996.** Late Quaternary sedimentation and glacial history of the western Svalbard continental margin. *Marine Geology*, Vol. **133**, pp. 123–156.

**Antonsen, P., Elverhøi, A., Dypvik, H. & Solheim, A., 1991.** Shallow Bedrock Geology of the Olga Basin Area, Northwestern Barents Sea. *The American Association of Petroleum Geologists Bulletin,* Vol. **75**, No. 7, pp. 1178–1194.

**Bard, E., Arnold, M., Mangerud, J., Paterne, M., Labeyrie, L., Duprat, J., Mélières, M-A., Sønstegaard, E. & Duplessy, J-C., 1994**. The North Atlantic atmosphere-sea surface $^{14}C$ gradient during the Younger Dryas climatic event. *Earth and Planetary Science Letters*, Vol. **126**, pp. 275–287.

**Batchelor C.L. & Dowdeswell J.A., 2015.** Ice-sheet grounding-zone wedges (GZWs) on high-latitude continental margins. *Marine Geology*, Vol. **363**, pp. 65–92

**Björck, S., Rundgren, M., Ingolfsson, O. & Funder, S., 1997.** The Preboreal oscillation around the Nordic Seas: Terrestrial and lacustrine responses. *Journal of Quaternary Science*, Vol. **12**, pp. 455–465.

**Bond, G., Broecker, W., Johnsen, S., McManus, J., Labeyrie, L., Jouzel, J. & Bonani, G., 1993.** Correlations between Climate Records from North Atlantic Sediments and Greenland Ice. *Nature*, Vol. **365**, pp. 143—147.

**Bondevik, S., Mangerud, J., Birks, H. H., Gulliksen, S. & Reimer, P., 2006.** Changes in North Atlantic radiocarbon reservoir ages during the Allerød and Younger Dryas. *Science*, New *Series,* Vol. **312**, No. 5779, pp. 1514–1517.

**Blott, S. J. & Pye, K., 2001.** GRADISTAT: A grain size distribution and statistics package for the analysis of unconsolidated sediments. *Earth Surface Processes and Landforms,* Vol. **26**, No. 11, pp. 1237—1248.

**Bowman, S., 1990.** Interpreting the past: radiocarbon dating. *British Museum Publications, London.*

**Broecker, W.S., T.-H. Peng, J. Jouzel, & G. Russell, 1990.** The magnitude of global fresh-water transports of importance to ocean circulation. *Climate Dynamics*, Vol. **4**, No. 2, pp 73-79.

**Broecker, W. S., 1991.** The Great conveyor. *Oceanography*, Vol. **4**, No. 2, pp. 79–89.

**Caralp, M. H., 1989.** Abundance of *Bulimina exilis* and *Melonis barleeanum:* Relationship to the quality of marine organic matter. *Geo-Marine Letters*, Vol. **9**, pp. 37—42.

**Coplen, T., 1996.** New guidelines for reporting stable hydrogen, carbon, and oxygen-ratio data. *Geochimica et Cosmochimica Acta,*Vol. **60**, pp. 3359—3360.

**Ó Cofaigh, C., Dowdeswell, J. A., Allen, C. S., Hiemstra, J. F., Pudsey, C. J., Evans, J. & Evans, D. J. A., 2005.** Flow dynamics and till genesis associated with a marine-based Antarctic palaeo-ice stream. *Quaternary Science Reviews,* Vol. **24**, pp. 709—740.

**Corliss, B. H., 1991.** Morphology and microhabitat preferences of benthic foraminifera from the Northwest Atlantic Ocean. *Marine Micropaleontology*, Vol. **17**, No. 3—4, pp. 195—236.

**Comiso, J. & Parkinson, C. L., 2004**. Satellite-Observed Changes in the Arctic. *American Institute of Physics- Physics today,* pp. 38–44.

**Dansgaard, W., Johnsen, S. J., Clausen, H. B., Dahl-Jensen, D., Gundestrup, N. S., Hammer, C. U., Hvidberg, C. S., Steffensen, J. P., Sveinbjörnsdottir, A. E., Jouzel, J., & Bond, G., 1993.** Evidence for general instability of past climate from a 250-kyr ice-core record. *Nature,* Vol. **364**, pp. 218-220.

**Day, J. J., Bamber, J. L., Valdes, P. J. & Kohler, J., 2012**. The impact of seasonally ice free Arctic Ocean on the temperature, precipitation and surface mass balance of Svalbard. *The Cryosphere*, Vol. **6**, No. 1, pp. 35–50.

**Dowdeswell, J. A. & Dowdeswell, E. K., 1989.** Debris in icebergs and rates of glaci- marine sedimentation: observations from Spitsbergen and a simple model. *Journal of Geology*, Vol. **97**, No. 2, pp. 221–231.

**Dowdeswell, J. A., Whittington, R. J. & Marienfeld, P. 1994.** The origin of massive diamicton facies by iceberg rafting and scouring, Scoresby Sund, east Greenland. *Sedimentology*, Vol. **41**, pp. 21–35.

**Dowdeswell, J. & Bamber, J. L., 1995**. On the glaciology of Edgeøya and Barentsøya, Svalbard. *Polar Research*, Vol. **14**, No. 2, pp. 105–122.

**Dowdeswell J. A., Ottesen, D., Evans, J., Ó Cofaigh, C. & Anderson, J. B., 2008.** Submarine glacial landforms and rates of ice-stream collapse. *Geology,* Vol. **36**, No. 10, pp. 819—822.

**Dowdeswell, J. A., Hogan, K. A., Evans, J., Noormets, R., Ó Cofaigh, C. & Ottesen, D., 2010**. Past ice-sheet flow east of Svalbard inferred from streamlines subglacial landforms. *Geological Society of America*, Vol. **38**, No. 2, pp. 163–166.

**Drange, H., Dokken, T., Furevik, T., Gerdes, R. & Berger, W., 2005.** The Nordic Seas: An Overview. Integrated Perspective, *Geophysical Monograph Series*, Vol. **158**, pp. 1–10.

**Duplessy, J. C., Ivanova, E., Murdmaa, I., Paterne, M. & Labeyrie, L., 2001.** Holocene paleoceanography of the northern Barents Sea and variations of the northward heat transport by the Atlantic Ocean. *Boreas,* Vol. **30**, pp. 2–16.

**Duplessy, J. C., Cortijo, E., Ivanova, E., Khusid, T., Labeyrie, L., Levitan, M., Murdmaa, I. & Paterne, M., (2005).** Paleoceanography of the Barents Sea during the Holocene. *Paleoceanography*, Vol. **20**, PA4004.

**Eiriksson, J., Larsen, G., Knudsen, K. L., Heinemeier, J. & Simonarson, L. A., 2004**. Marine resevoir age variability and water mass distribution in the Iceland Sea. *Quaternary Science Reviews*, Vol. **23**, pp. 2247–2268.

**Elverhøi, A. & Solheim, A., 1983.** Marin-geologiske og -geofysiske undersøkelser i Barentshavet 1983 – Toktrapport. *Norsk polarinstitutt*, Vol. **14**, pp. 1—103.

**Elverhøi, A., Andersen, E. S., Dokken, T., Hebbeln, D., Spielhagen, R., Svendsen, J. I., Sørflaten, M., Rørnes, A., Hald, M. & Forsberg, C. F., 1995.** The growth and decay of the Late Weichselian ice sheet in western Svalbard and adjacent areas based on provenance studies of marine sediments. *Quaternary Research,* Vol. **44***,* pp. 303–316.

**Evans, J., Pudsey, C. J., Ó Cofaigh, C. & Domack, E., 2005.** Late Quaternary glacial history, flow dynamics and sedimentation along the eastern margin of the Antarctic Peninsula Ice Sheet. *Quaternary Science Reviews*, Vol. **24**, pp. 741—774.

**Fairbanks, R. G., 1989**. A 17,000-year glacio-eustatic sea level record: influence of glacial melting rates on the Younger Dryas event and deep-ocean circulation. *Nature*, Vol. **342**, pp. 637 – 642.

**Feyling-Hanssen, R. W., 1972.** The foraminifer Elphidium excavatum (Terquem) and its variant forms. *Micropaleontology*, Vol. **18**, pp. 337–354.

**Forman, S. L., Mann, D. H. & Miller, G. H., 1987.** Late Weichselian and Holocene relative sea-level history of Brøggerhalvøya, Spitsbergen. *Quaternary Research*, Vol. **27**, pp. 41–50.

**Forman, S. L., Lubinski, D., Miller, G. H., Matishov, G., Korsun, S. & Myslivets, V., 1995**. Postglacial emergence and distribution of late Weichselian ice-sheet loads in the northern Barents and Kara seas, Russia. *Geology*, Vol. **23,** No. 2, pp. 113–116.

**Forman, S. L., Lubinski, D. J., Ingòlfsson, Ò., Zeeberg, J. J., Snyder, J. A., Siegert, M. J. & Matishov, G. G., 2004.** A review of postglacial emergence on Svalbard, Franz Josef Land and Novaya Zemlya, northern Eurasia. *Quaternary Science Reviews*, Vol. **23**, pp. 1391–1434.

**Forwick, M. & Vorren, T.O., 2007.** Holocene mass-transport activity and climate in outer Isfjorden, Spitsbergen: marine and subsurface evidence. *The Holocene,* Vol. **17**, pp. 707.

**Forwick, M. & Vorren, T. O., 2009.** Late Weichselian and Holocene sedimentary environments and ice rafting in Isfjorden, Spitsbergen. *Palaeogeography, Palaeoclimatology, Palaeoecology*, Vol. **280**, pp. 258–274.

**Forwick, M. & Vorren, T. O., 2011.** Stratigraphy and deglaciation of the Isfjorden area, Spitsbergen. *Norwegian Journal of Geology*, Vol. **90**, pp 163-179.

**Førland, E. J., Benestad, R. E., Flatøy, F., Hanssen-Bauer, I., Haugen, J. E., Isaksen, K., Sorteberg, A. & Ådlandsvik, B., 2009.** Climate development in North Norway and the Svalbard region during 1900–2100. Norsk Polarinstitutt Rapportserie nr. 128.

**Gammelsrød, T., Leikvin, Ø., Lien, V., Budgell, P. W., Loeng, H. & Maslowski, W., 2009**. Mass and heat transports in the NE Barents Sea: Observations and models. *Journal of Marine Systems*, Vol. **75,** pp. 56–69.

**GEOTEK. (2014a).** Retrieved 20.11.2015, from "Manual; Multi Sensor Core Logger": http://www.geotek.co.uk/sites/default/files/MSCLmanual.pdf.

**Grauel, A-L., Schmid, T. W., Hu, B., Bergami, C., Capotondi, L., Zhou, L. & Bernasconi, S. M. 2013.** Calibration and application of the 'clumped isotope' thermometer to foraminifera for high-resolution climate reconstructions. *Geochimica et Cosmochimica Acta,* Vol. **108**, pp. 125—140.

**Gustafsson, M. & Nordberg, K., 2001**. Living (stained) benthic foraminiferal response to primary production and hydrgraphy in the deepest part of the Gullmar fjord, Swedish west coast, with comparisons of Höglund's 1927 material*. Journal of Foraminiferal Research*. Vol. **31**, No. 1, pp 2–11.

**Hald, M. & Korsun, S., 1997.** Distribution of modern benthic foraminifera from fjords of Svalbard, European Arctic. *Journal of Foraminiferal Research,* Vol. **27**, No. 2, pp. 101–122.

**Hald, M. & Korsun, S., 2008.** The 8200 cal. yr BP event reflected in the Arctic fjord, Van Mijenfjorden, Svalbard. *The Holocene*, Vol. **18**, No. 6, pp. 981–990.

**Hald, M. & Steinsund, P. I., 1992**. Distribution of surface sediment benthic foraminifera in the southwestern Barents Sea. *Journal of Foraminiferal Research,* Vol*.* **22**, No. 4, pp. 347–362.

**Hald, M. & Steinsund, P. I., 1996**. Benthic foraminifera and carbonat dissolution in the surface sediments of the Barents and Kara seas. *Berichte zur Polaraforschung*, Vol. **212**, pp. 285–307.

**Hald, M. & Vorren, T. O., 1984.** Modern and Holocene foraminifera and sediments on the continental shelf off Troms, northern Norway. *Boreas*, Vol. **13**, pp. 133–154.

**Hald, M. & Vorren, T. O., 1987**. Foraminiferal stratigraphy and environment of Late Weichselian deposits on the continental shelf off Troms, Northern Norway. *Marine Micropaleontology,* Vol. **12**, pp. 129–160.

**Hald, M., Kolstad, V., Polyak, L., Forman, S.L., Herlihy, F. A., Ivanov, G. & Nescheretov, A., 1999.** Late-glacial and Holocene paleoceanograohy and sedimentary environments in the St. Anna Trough, Eurasian Arctic Ocean margin. *Palaeogeography, Paleoclimate, Paleoecolog*y, Vol. **149**, pp. 229–249.

**Hald, M., Ebbesen H., Forwick, M., Godtliebsen, F., Khomenko, L., Korsun, S., Olsen, L. R. & Vorren, T. O., 2004.** Holocene paleoceanography andglacial history of the West Spitsbergen area, Euro-Arctic margin. *Quaternary Science Reviews*, Vol. **23**, pp. 2075–2088.

**Hansen, A. & Knudsen, K. L., 1995**. Recent foraminiferal distribution in Freemansundet and early Holocene stratigraphy on Edgeoya, Svalbard, PONAM Project in eastern Svalbard. Norsk Polarinstitutt, Norway, pp. 215–238.

**Hambrey, M. J., Bennett, M. R., Huddart, D. & Glasser. N., 1997.** Genesis of "hummocky moraine" by thrusting in glacier ice: evidence from Svalbard and Britain. Journal of the Geological Society, Vol. **154**, No. 4, pp. 623—632.

**Hambrey, M. J. & McKelvey, B., 2000.** Neogene fjordal sedimentation on the western margin of the Lambert Graben, East Antarctica. *Sedimentology*, Vol. **47**, pp. 577—607.

**Hisdal, V., 1998.** Svalbard: Nature and history. Norsk Polarinstitutt Polarhåndbok No. 12.

**Hogan, K. A., Dowdeswell, J. A., Noormets, R., Evans, J., Ó Codaigh, C. & Jakobsson, M., 2010a.** Submarine landforms and ice-sheet flow in the Kvitøya Trough, northwestern Barents Sea. *Quarternary Science Reviews*, Vol. **29**, No. 25, pp. 3545–3562.

**Hogan, K. A., Dowdeswell, J. A., Noormets, R., Evans, J. & Ó Cofaigh, C., 2010b**, Evidence for full-glacial flow and retreat of the Late Weichselian Ice Sheet from the waters around Kong Karls Land, eastern Svalbard. *Quarternary Science Reviews*, Vol. **29,** No. 25, pp. 3563–3582.

**Humlum, O., Instanes, A. & Sollid, J. L., 2003.** Permafrost in Svalbard: a review of research history, climatic background and engineering challenges. *Polar Research*, Vol. **22**, pp. 191–215.

**Hundert, T., Mackie, J., Hill, P. S., Weir, S. L. & Piper, D. J. W., 2003.** Paleoceanography and distal plume sedimentation associated with Heinrich events; eastern Canadian margin. *Abstracts with Programs - Geological Society of America,* Vol. **35**, No. 3, pp. 9.

**Ingólfsson, Ó., Rögnvaldsson, F., Bergsten, H., Hedenäs, L., Lemdahl, G., Lirio, J. M. & Sejrup, H. P., 1995.** Late Quarternary glacial and environmental history of Kongsøya, Svalbard. *Polar Research,* Vol. **14**, No. 2, pp. 123–139.

**Isaksson, E., Kohler, J., Pohjola, V., Moore, J., Igarashi, M., Karlöf, L., Martma, T., Meijer, H., Motoyama, H., Vaikmäe & van de Wal, R. S. W., 2005.** Two ice-core δ18O records from Svalbard illustrating climate and sea-ice variability over the last 400 years. *The Holocene*, Vol. **15**, pp. 501–509.

**Ivanova, E. V., Ovsepyan, E. A., Risebrobakken, B. & Vetrov, A. A. 2008**. Downcore distribution of living calcareous foraminifera and stable isotopes in the western Barents Sea. *Journal of Foraminiferal Research,* Vol. **38,** No. 4, pp. 337–356.

**Jennings, A. E., Weiner, N. J., Helgadottir, G. & Andrews, J. T., 2004.** Modern foraminiferal faunas of the southwestern to northern Iceland Shelf; oceanographic and environmental controls. *Journal of Foraminiferal Research*, Vol. **34**, pp. 180–207.

**Jessen, S. P., Rasmussen, T. L., Nielsen, T. & Solheim, A., 2010.** A new Late Weichselian and Holocene marine chronology for the western Svalbard slope 30,000-0 cal years BP. *Quarternary Science Reviews* **29**, pp. 1301–1312.

**Jessen, S.P. & Rasmussen, T. L. 2015.** Sortable silt cycles in Svalbard slope sediments 74–0 ka. *Journal of Quaternary Science*, Vol. **30**, No. 8, pp. 743–753.

**Kleiber, H. P., Knies, J. & Niessen, F., 2000.** The Late Weichselian glaciation of the Franz Victoria Trough. Northern Barents Sea: ice sheet extent and timing. *Marine Geology*, Vol. **168,** pp. 25–44.

**Kristensen, D. K., Sejrup, H. P. & Haflidason, H., 2001.** The last 18 kyr fluctuations in Norwegian Sea surface conditions and implications for the magnitude of climatic change; evidence from the North Sea. *Paleoceanography*, Vol. 1**6**, pp. 455–467.

**Kristensen, D. K., Rasmussen, T. & Koç, N., 2013.** Palaeoceanographic changes in the northern Barents Sea during the last 16 000 years – new constraints on the last deglaciation of the Svalbard –Barents Sea Ice Sheet. *Boreas*, Vol. **42**, No. 3, pp. 798—813.

**Koç, N., Kristensen, D. K., Hasle, K., Forsberg, C. F. & Solheim, A., 2002.** Late glacial palaeoceanography of Hinlopen Strait, northern Svalbard. *Polar Research*, Vol. **21**, pp. 307–314.

**Koç, N., Jansen, E. & Haflidason, H., 1993.** Paleoceanographic reconstructions of surface ocean conditions in the Greenland, Iceland and Norwegian Seas through the last 14 ka based on diatoms. *Quaternary Science Reviews,* Vol. **12**, pp. 115–140.

**Korsun, S. & Hald, M., 2000.** Seasonal dynamics if benthic foraminifera in a glacially fed fjord of Svalbard, European arctic. *Journal of Foraminiferal Research*, Vol. **30**, No. 4, pp. 251–271.

**Kubischta, F., Knudsen, K. L., Ojala, A. E. K. & Salonen, V.-P., 2011.** Holocene benthic foraminiferal record from a high-arctic fjord, Nordaustlandet, Svalbard. *Geografiska Annaler: Series A, Physical Geography,* Vol. **93**, pp. 227–242.

**Kutzbach, J. E. & Guetter, P. J., 1986.** The influence of Changing Orbital Parameters and Surface Boundary Coditions on Climate Simulations for the Past 18 000 Years. *Journal of the Atmospheric Science*, Vol**. 43,** No. 18, pp. 1726–1959.

**Landvik, J. Y., Bondevik, S., Elverhøi, A., Fjeldskaar, W., Mangerud, J., Salvigsen, O., Siegert, M. J., Svendsen, J. I. & Vorren, T. O., 1998.** The last glacial maximum of Svalbard and the Barents Sea area: Ice sheet extent and configuration*. Quaternary Science Reviews*, Vol. **17**, pp. 43–75.

**Landvik, J. Y., Brook, E., Gualtieri, L., Raisbeck, G., Salvigsen, O. & Yiou, F., 2003.** Northwest Svalbard during the last glaciation: Ice-free areas existed. *Geology*, Vol. **31**, No. 10, pp. 905–908.

**Landvik, J. Y., Ingólfsson, Ó., Mienert, J., Lehman, S. J., Solheim, A., Elverhøi, A. & Ottesen, D., 2005.** Rethinking Late Weichselian ice-sheet dynamics in coastal NW Svalbard. *Boreas*, Vol. **34**, pp. 7–24.

**Lehman, S. J. & Forman, S. L., 1992.** Late Weichselian glacier retreat in Kongsfjorden, west Spitsbergen, Svalbard. *Quaternary Research*, Vol. **37**, pp. 139–154.

**Linke, P. & Lutze, G. F., 1993**. Microhabitat preferences of benthic foraminifera – a static concept or a dynamic adaption to optimize food acquisition. *Marine Micropaleonotoly,* Vol. **20**, pp. 215–234.

**Loeng, H., 1991**. Features of the physical oceanographic conditions of the Barents Sea. *Polar Research,* Vol. **10**, No. 1, pp. 5–18.

**Lowe, J. & Walker, M., 1997**. Reconstruction quaternary environments. *Addison Wesley Longman*, pp. 215–217.

**Lubinski, D. J., Korsun, S., Polyak, L., Forman, S. L., Lehman, S. J., Herlihy, F. A. & Miller, G. H., 1996.** The last deglaciation of the Franz Victoria Trough, northern Barents Sea. *Boreas,* Vol. **25**, No. 2, pp. 89—100.

**Lubinski, D. J., Polyak, L. & Forman, S. L., 2001.** Freshwater and Atlantic water inflows to the deep northern Barents and Kara seas since ca 13 $^{14}$Cka: foraminifera and stable isotopes. *Quaternary Science Reviews,* Vol. **20**, pp. 1851–1879.

**Mackensen, A., Sejrup, H. P. & Jansen, E., 1985.** The distribution of living benthic foraminifera on the continental slope and rise off southwest Norway. *Marine Micropalentology*, Vol. **9**, pp. 275—306.

**Mangerud, J. & Gulliksen, S., 1975.** Apparent Radiocarbon Ages of Recent Marine Shells from Norway, Spitsbergen, and Arctic Canada. *Quaternary Research,* Vol. **5**, pp. 263–273.

**Mangerud, J. & Landvik, J. Y., 2007.** Younger Dryas glaciers in western Spitsbergen: smaller than during the Little Ice Age. *Boreas*, Vol. **36**, pp. 278–285.

**Mangerud, J., Bolstad, M., Elgersma, A., Helliksen, D., Landvik, J. Y., Lønne, I., Lycke, A. K., Salvigsem O., Sandahl, T. & Svendesn, J. I., 1992.** The Last Glacial Maximum on Spitsbergen, Svalbard. *Quaternary Research,* Vol. **38,** pp. 1–31.

**Mangerud, J., Dokken, T., Hebbeln, D., Heggen, B., Ingólfsson, Ó., Landvik, J. Y., Mejdahl, V., Svendsen J. I. & Vorren, T. O., 1998.** Fluctuations of the Svalbard- Barents Sea Ice Sheet during the last 150 000 years. *Quaternary Science Reviews,* Vol*.* **17***,* pp. 11–42.

**Mangerud, J., Bondevik, S., Gulliksen, S., Hufthammer, A. K. & Høisæter, T., 2006.** Marine $^{14}$C reservoir ages of 19th century whales and molluscs from the North Atlantic. *Quaternary Scinece* Reviews, Vol. **25,** pp. 3228–3245.

**Meissner, K. J. & Clark, P. U., 2006.** Impact of floods versus routing events on the thermohaline circulation. *Geophysical research letters*, Vol. **33**, No. 15.

**Munsell, R., 1973**. Soil colour charts. Macbeth division of Kollmorgen corporation, New York, 19.

**Murray, J. W., 2001**. The niche of benthic foraminifera, critical thresholds and proxies. *Marine Micropaleontology*, Vol. **41,** pp. 1–7.

**Nagy, J., 1984.** Quaternary glaciomarine deposits and foraminifera from Edgeoeya, Svalbard. *Boreas,* Vol. **13**, pp. 319–332.

**Ó Cofaigh, C., Evans, J., Dowdeswell, J. A. & Larter, R. D., 2007.** Till characteristics, genesis and transport beneath Antarctic paleo-ice streams. *Journal of Geophysical Research*, Vol. **112**, F03006.

**Osterman, L., 1984**. Benthic foraminiferal zonation of a glacial/ interglacial transition from Frobisher Bay, Baffin Island, Northwest Territories, *Canada, Bulletin des Centres de Recherches Exploration Production Elf Aquitaine*, Vol. **6**, pp. 471–476.

**Ottesen, D., Dowdeswell, J. A., & Rise, L., 2005.** Submarine landforms and the reconstruction of fast-flowing ice streams within a large Quaternary ice sheet: The 2500-km-long Norwegian-Svalbard margin (57°-80°N). *Geological Society of America Bulletin*, Vol. **117**, pp. 1033–1050.

**Ottesen, D. & Dowdeswell, J.A., 2009.** An inter-ice-stream glaciated margin: Submarine landforms and a geomorphic model based on marine-geophysical data from Svalbard. *Geological Society of America Bulletin*, Vol. **121**, pp. 1647–1665.

**Ottesen, D., Dowdeswell, J. A., Landvik, J. Y. & Mienert, J., 2007.** Dynamics of the Late Weichselian ice sheet on Svalbard inferred from high-resolution sea-floor morphology. *Boreas*, Vol. **36**, pp. 286–306.

**Piechura, J. & Walczowski, W., 1995**. The Arctic Front: structure and dynamics. *Oceanologia,* Vol. **371,** pp. 47–73.

**Pirrung, M., Fütterer, D., Grobe, H., Matthiessen, J. & Niessen, F., 2002**. Magnetic susceptibility and ice-rafted debris in surface sediemnts of the Nordic Seas: implications for Isotope Stage 3 oscilliations. *Springer-Verlag. Geo-Mar Lett,* Vol. **22**, pp. 1–11.

**Polyak, L. & Solheim, A., 1994**. Late- and postglacial environments in the northern Barents Sea west of Franz Josef Land. *Polar Research*, Vol. **13**, No 2, pp. 197–207.

**Polyak, L. & Mikhailov, V., 1996**. Post-glacial environments of the southeastern Barents Sea: foraminiferal evidence. Late Quaternary Palaeoceanography of the North Atlantic Margins, *Geological Society Special Publications*, Vol. 111, pp. 323–337.

**Polyak, L., Korsun, S., Febo, L.A., Stanovoy, V., Khushid, T., Hald, M., Paulsen, B. E. & Lubinski, D. J., 2002**. Benthic foraminiferal assemblages from the southern Kara Sea, a river-influenced arctic marine environment. *Journal of Foraminiferal Research*, Vol. **32**, No. 3, pp. 252–273.

**Rasmussen, T. L., & Thomsen, E., 2014.** Brine formation in relation to climate changes and ice retreat during the last 25 000 years in Storfjorden, Svalbard, 76 -78°N. *Paleoceanography,* Vol. **29,** pp. 911–929.

**Rasmussen, T. L., Thomsen, E., Labeyrie, L. & van Weering, T. C. E., 1996.** Circulation changes in the Faeroe-Shetland Channel correlating with cold events during the last glacial period (58 –10 ka). *Geology*, Vol. **24**, No. 10, pp. 937–940.

**Rasmussen, T. L., Bäckström, D., Heinemeier, J., Kristensen, D. K, Knutz, P. C., Kuijpers, A., Lasseng, S., Thomsen, E., Troelstra, S.R. & van Weering, T.C.E., 2002b.** The Faroe–Shetland Gateway: Late Quaternary water mass exchange between the Nordic seas and the northeastern Atlantic. *Marine Geology*, Vol. **188**, No. 1–2, pp. 165–192.

**Rasmussen, T. L., Thomsen, E., Ślubowska, M. A., Jessen, S., Solheim, A. & Koç, N., 2007.** Paleoceanographic evolution of the SW Svalbard margin (76°N) since 20,000 14C yr BP. *Quaternary Research*, Vol. **67**, pp. 100–114.

**Rasmussen, T. L., Forwick, M. & Mackensen, A., 2012.** Reconstruction of inflow of Atlantic Water to Isfjorden, Svalbard during the Holocene: Correlation to climate and seasonality. *Marine Micropaleontology*, Vol. **94–95**, pp. 80–90.

**Reading, H. G., 1986.** Sedimentary environments and facies. *Blackwell Scientific Publications*, Oxford, pp. 615.

**Reimer, P. J., Bard, E., Bayliss, A., Beck, J. W., Blackwell, P. G., Ramsey, C. B., Buck, C. E., Cheng, H. & Edwards, R. L., 2013.** Intcal13 and Marine13 radiocarbon age calibration curves 0–50,000 years Cal BP. *Radiocarbon*, Vol**. 55**, No. 4, pp. 1869–1887.

**Rosoff, D. B. & Corliss, B. H., 1992**. An analysis of Recent deep-sea benthic foraminiferal morphotypes from the Norwegian and Greenland seas. *Palaeogeography, Palaeoclimatology, Palaeoecology,* Vol. **91**, pp. 13–20.

**Salvigsen, O., 1987**, Radiocarbon dated raised beaches in Kong Karls Land, Svalbard, and their consequences for the glacial history of the Barents Sea area. *Geografiske Annaler*, Vol. **63**, No. 3–4, pp. 283–291.

**Salvigsen, O., Adrielsson, L., Hjort, C., Kelly, M., Landvik, J. Y. & Ronnert, L., 1995**. Dynamics of the last glaciation in eastern Svalbard as inferred from glacier-movement indicators. *Polar Research*, Vol. **14**, No. 2, pp. 141–152.

**Saloranta, T. M. & Haugan, P. M., 2004.** Northward cooling and freshening of the warm core of the West Spitsbergen Current. *Polar Research*, Vol. **23**, No. 1, pp. 79–88.

**Sarnthein, M., Van Kreveld, S., Erlenkeuser, H., Grootes, P. M., Kucera, M., Pflaumann, U. & Schulz, M., 2003b.** Centennial-to-millennial-scale periodicities of Holocene climate and sediment injections off the western Barents shelf, 75°N. *Boreas*, Vol. **32**, pp. 447–461.

**Schlichtholz, P. & Goszczko, I., 2006.** Interannual variability of the Atlantic water layer in the West Spitsbergen Current at 76,5 °N in summer 1991-2003. *Deep-Sea Research I*, Vol. **53**, pp. 608–626.

**Shackleton, N. J., 1974**. Attainment of isotopic equilibrium between ocean water and the benthonic foraminifera genus Uvigerina: isotopic changes in the ocean during the last glacial. *Colloques Internationaux du C.N.R.S*, Vol. **219**, 203–209.

**Skirbekk, K., Kristensen, D. K., Rasmussen, T. L., Koç, N. & Forwick, M., 2010.** Holocene climate variations at the entrance to a warm Arctic fjord: evidence from Kongsfjorden trough, Svalbard. *Geological Society, London, Special Publications*, Vol. **344**, pp. 289—304.

**Skogseth, R., Haugan, P. M. & Jakobsson, M., 2005.** Watermass transformations in Storfjorden. *Continental Shelf Research*, Vol. **25**, pp. 667–695.

**Ślubowska, M. A., Koç, N., Rasmussen, T. L. & Kristensen, D. K, 2005.** Changes in the flow of Atlantic water into the Arctic Ocean since the last deglaciation: Evidence from the northern Svalbard continental margin, 80°N. *Paleoceanography*, Vol. **20**, pp. 1–16.

**Ślubowska-Woldengen, M., Rasmussen, T. L., Koç, N., Kristensen, D. K, Nilsen, F. & Solheim, A., 2007.** Advection of Atlantic Water to the western and northern Svalbard shelf since 17,500 cal yr BP. *Quaternary Science Reviews*, Vol. **26**, pp. 463–478.

**Ślubowska-Woldengen, M., Koç, N., Rasmussen, T. L., Kristensen, D. K, Hald, M. & Jennings, A. E., 2008.** Time-slice reconstructions of ocean circulation changes on the continental shelf in the Nordic and Barents Seas during the last 16,000 cal yr B.P. *Quaternary Science Reviews*, Vol. **27**, pp. 1476– 1492.

**Smalley, P. C., Nordaa, A. & Råheim, A., 1986.** Geochronology and paleothermometry of Neogene sediments from the Vøring Plateau using Sr, C and O isotopes. *Earth and Planetary Science Letters,* Vol. **78**, pp. 368—378.

**Solheim, A., 1991.** The depositional environment of surging sub-polar tidewater glaciers. Norsk Polarinstitutt, Skrifter No. 194, Oslo.

**Steinsund, P. I. 1994.** Benthic foraminifera in surface sediments of the Barents and Kara Seas; modern and late Quaternary applications. *University in Tromsø*, Tromsø.

**Steinsund, P. I. & Hald, M., 1994.** Recent calcium carbonate dissolution in the Barents Sea: Paleoceanographic applications. *Marine Geology,* Vol. **117**, pp. 303–316.

**Steinsund, P. I., Polyak, L., Hald, M., Mikhailov, V. & Korsun, S., 1994.** Distribution of calcareous benthic foraminifera in recent sediments of the Barents and Kara Seas. *University in Tromsø*, Tromsø.

**Stuiver, M., Pearson, G. W. & Braziunas, T., 1986.** Radiocarbon age calibration of marine samples back to 9000 Cal. Yr. *Radiobarbon*, Vol. **28**, No. 2b, pp. 980–102.

**Stuiver, M. & Reimer, P. J., 1993.** Extended 14C database and revised CALIB radiocarbon calibration program. *Radiocarbon*, Vol. **35**, No. 1, pp. 215—230.

**Svendsen, J. I. & Mangerud, J., 1997.** Holocene glacial and climatic variations on Spitsbergen, Svalbard. *The Holocene*, Vol. **7**, pp. 45–57.

**Swift, J. H., 1986**. The Arctic Waters. In: B.G. Hurdle (Editor), The Nordic Seas. *Springer-Verlag, New York*, pp. 129–153.

**Vorren, T., Hald, M. & Thomsen, E., 1984.** Quatenary sediments and environments on the continental shelf off northern Norway. *Maine Geology*, Vol. **57,** pp. 229–257.

**Vorren, T. O., Lebesby, E., Andreassen, K. & Larsen, K. -B., 1989.** Glacigenic sediment on a passive sontinental margin as exemplified by the Barents Sea. *Marine Geology*, Vol. **85**, pp. 251–272.

**Wassmann, P., Ratkova, T., Andreassen, I., Vernet, M., Pedersen, G. & Rey, F., 1999**. Spring Bloom Development in the Marginal Ice Zone and the Central Barents Sea. Mar. *Ecology.* Vol. **20**, No. 3—4, pp. 321–346.

**Wollenburg, J. E. & Mackensen, A., 1998.** Living benthic foraminifers from the central Arctic Ocean: faunal composition, standing stock and diversity. *Marine Micropaleontology*, Vol. **34**, pp. 153–185.

**Zajaczkowski, M., Szczucinski, W., Plessen, B. & Jernas, P., 2010**. Benthic foraminifera in Hornsund, Svalbard: Implications for paleoenvironmental reconstructions. *Polish Polar Research,* Vol. **31**, No. 4, pp. 349–375.

# 9. References